Anomalous Hall effect

Naoto Nagaosa

Department of Applied Physics, University of Tokyo, Tokyo 113-8656, Japan and
Cross Correlated Research Materials Group (CMRG), ASI, RIKEN, Wako 351-0198, Saitama, Japan

Jairo Sinova

Department of Physics, Texas A&M University, College Station, Texas 77843-4242, USA and
Institute of Physics ASCR, Cukrovarnická 10, 162 53 Praha 6, Czech Republic

Shigeki Onoda

Condensed Matter Theory Laboratory, ASI, RIKEN, Wako 351-0198, Saitama, Japan

A. H. MacDonald

Department of Physics, University of Texas at Austin, Austin, Texas 78712-1081, USA

N. P. Ong

Department of Physics, Princeton University, Princeton, New Jersey 08544, USA

(Dated: February 3, 2022)

We present a review of experimental and theoretical studies of the anomalous Hall effect (AHE), focusing on recent developments that have provided a more complete framework for understanding this subtle phenomenon and have, in many instances, replaced controversy by clarity. Synergy between experimental and theoretical work, both playing a crucial role, has been at the heart of these advances. On the theoretical front, the adoption of Berry-phase concepts has established a link between the AHE and the topological nature of the Hall currents which originate from spin-orbit coupling. On the experimental front, new experimental studies of the AHE in transition metals, transition-metal oxides, spinels, pyrochlores, and metallic dilute magnetic semiconductors, have more clearly established systematic trends. These two developments in concert with first-principles electronic structure calculations, strongly favor the dominance of an intrinsic Berry-phase-related AHE mechanism in metallic ferromagnets with moderate conductivity. The intrinsic AHE can be expressed in terms of Berry-phase curvatures and it is therefore an intrinsic quantum mechanical property of a perfect cyrstal. An extrinsic mechanism, skew scattering from disorder, tends to dominate the AHE in highly conductive ferromagnets. We review the full modern semiclassical treatment of the AHE which incorporates an anomalous contribution to wavepacket group velocity due to momentum-space Berry curvatures and correctly combines the roles of intrinsic and extrinsic (skew scattering and side-jump) scattering-related mechanisms. In addition, we review more rigorous quantum-mechanical treatments based on the Kubo and Keldysh formalisms, taking into account multiband effects, and demonstrate the equivalence of all three linear response theories in the metallic regime. Building on results from recent experiment and theory, we propose a tentative global view of the AHE which summarizes the roles played by intrinsic and extrinsic contributions in the disorder-strength *vs.* temperature plane. Finally we discuss outstanding issues and avenues for future investigation.

arXiv:0904.4154v1 [cond-mat.mes-hall] 26 Apr 2009

Contents

I. Introduction 2
A. A brief history of the AHE and new perspectives 2
B. Parsing the AHE: 5
1. Intrinsic contribution to σ_{xy}^{AH} 6
2. Skew scattering contribution to σ_{xy}^{AH} 7
3. Side-jump contribution to σ_{xy}^{AH} 7

II. Experimental and theoretical studies on specific materials 8
A. Transition-metals 8
1. Early experiments 8
2. Recent experiments 9
3. Comparison to theories 11
B. Complex oxide ferromagnets 12
1. First-principles calculations and experiments on $SrRuO_3$ 12
2. Spin chirality mechanism of the AHE in manganites 14
3. Lanthanum cobaltite 16
4. Spin chirality mechanism in pyrochlore ferromagnets 17
5. Anatase and Rutile $Ti_{1-x}Co_xO_{2-\delta}$ 18
C. Ferromagnetic semiconductors 18
D. Other classes of materials 20
1. Spinel $CuCr_2Se_4$ 20
2. Heusler Alloy 21
3. $Fe_{1-y}Co_ySi$ 21
4. MnSi 22
5. Mn_5Ge_3 23
6. Layered dichalcogenides 24
E. Localization and AHE 24

III. Theoretical aspects of the AHE and early theories 25
A. Symmetry considerations and analogies between normal Hall effect and AHE 26
B. Topological interpretation of the intrinsic mechanism: relation between Fermi sea and Fermi surface

properties 29
C. Early theoretical studies of the AHE 30
1. Karplus-Luttinger theory and the intrinsic mechanism 30
2. Extrinsic mechanisms 31
3. Kohn-Luttinger theory formalism 34

IV. Linear Transport Theories of the AHE 36
A. Semiclassical Boltzmann approach 37
1. Equation of motion of Bloch states wave-packets 38
2. Scattering and the side-jump 38
3. Kinetic equation for the semiclasscial Boltzmann distribution 39
4. Anomalous velocities, anomalous Hall currents, and anomalous Hall mechanisms 40
B. Kubo formalism 41
1. Kubo technique for the AHE 41
2. Relation between the Kubo and the semiclassical formalisms 42
C. Keldysh formalism 43
D. Two-dimensional ferromagnetic Rashba model – a minimal model 45

V. Conclusions: Future problems and perspectives on AHE 47

Acknowledgements 50

References 50

I. INTRODUCTION

A. A brief history of the AHE and new perspectives

The anomalous Hall effect has deep roots in the history of electricity and magnetism. In 1879 Edwin H. Hall (Hall, 1879) made the momentous discovery that, when a current-carrying conductor is placed in a magnetic field, the Lorentz force "presses" its electrons against one side of the conductor. One year later, he reported that his "pressing electricity" effect was ten times larger in ferromagnetic iron (Hall, 1881) than in non-magnetic conductors. Both discoveries were remarkable, given how little was known at the time about how charge moves through conductors. The first discovery provided a simple, elegant tool to measure carrier concentration more accurately in non-magnetic conductors, and played a midwife's role in easing the birth of semiconductor physics and solid-state electronics in the late 1940's. For this role, the Hall effect was frequently called the queen of solid-state transport experiments.

The stronger effect that Hall discovered in ferromagnetic conductors came to be known as the anomalous Hall effect (AHE). The AHE has been an enigmatic problem that has resisted theoretical and experimental assault for almost a century. The main reason seems to be that, at its core, the AHE problem involves concepts based on topology and geometry that have been formulated only in recent times. The early investigators grappled with notions that would not become clear and well defined until much later, such as the concept of Berry-phase (Berry, 1984). What is now viewed as Berry phase curvature, later dubbed "anomalous velocity" by Luttinger, arose naturally in the first microscopic theory of the AHE by Karplus and Luttinger (Karplus and Luttinger, 1954). However, because understanding of these concepts, not to mention the odd intrinsic dissipationless Hall current they seemed to imply, would not be achieved for another 40 years, the AHE problem was quickly mired in a controversy of unusual endurance. Moreover, the AHE seems to be a rare example of a pure, charge-transport problem whose elucidation has not – to date – benefited from the application of complementary spectroscopic and thermodynamic probes.

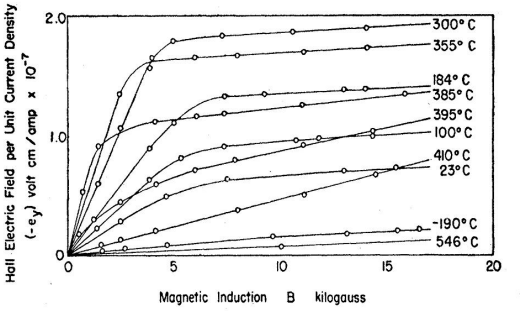


FIG. 1 The Hall effect in Ni [data from A. W. Smith, Phys. Rev. **30**, 1 (1910)]. [From Ref. Pugh and Rostoker, 1953.]

Very early on, experimental investigators learned that the dependence of the Hall resistivity ρ_{xy} on applied perpendicular field H_z is qualitatively different in ferromagnetic and non-magnetic conductors. In the latter, ρ_{xy} increases linearly with H_z, as expected from the Lorentz force. In ferromagnets, however, ρ_{xy} initially increases steeply in weak H_z, but saturates at a large value that is nearly H_z-independent (Fig. 1). Kundt noted that, in Fe, Co, and Ni, the saturation value is roughly proportional to the magnetization M_z (Kundt, 1893) and has a weak anisotropy when the field ($\hat{z}$) direction is rotated with respect to the cyrstal, corresponding to the weak magnetic anisotropy of Fe, Co, and Ni (Webster, 1925). Shortly thereafter, experiments by Pugh and coworkers (Pugh, 1930; Pugh and Lippert, 1932) established that an empirical relation between ρ_{xy}, H_z, and M_z,

$$\rho_{xy} = R_0 H_z + R_s M_z, \tag{1.1}$$

applies to many materials over a broad range of external magnetic fields. The second term represents the Hall effect contribution due to the spontaneous magnetization. This AHE is the subject of this review. Unlike R_0, which was already understood to depend mainly on the density of carriers, R_s was found to depend subtly on a variety of material specific parameters and, in particular, on the longitudinal resistivity $\rho_{xx} = \rho$.

In 1954, Karplus and Luttinger (KL) (Karplus and Luttinger, 1954) proposed a theory for the AHE that, in

hindsight, provided a crucial step in unraveling the AHE problem. KL showed that when an external electric field is applied to a solid, electrons acquire an additional contribution to their group velocity. KL's *anomalous velocity* was perpendicular to the electric field and therefore could contribute to Hall effects. In the case of ferromagnetic conductors, the sum of the *anomalous velocity* over all occupied band states can be non-zero, implying a contribution to the Hall conductivity σ_{xy}. Because this contribution depends only on the band structure and is largely independent of scattering, it has recently been referred to as the the *intrinsic* contribution to the AHE. When the conductivity tensor is inverted, the intrinsic AHE yields a contribution to $\rho_{xy} \approx \sigma_{xy}/\sigma_{xx}^2$ and therefore it is proportional to ρ^2. The anomalous velocity is dependent only on the perfect crystal Hamiltonian and can be related to changes in the phase of Bloch state wavepackets when an electric field causes them to evolve in crystal momentum space (Bohm *et al.*, 2003; Chang and Niu, 1996; Sundaram and Niu, 1999; Xiao and Niu, 2009). As mentioned, the KL theory anticipated by several decades the modern interest in Berry phase and Berry curvature effects, particularly in momentum-space.

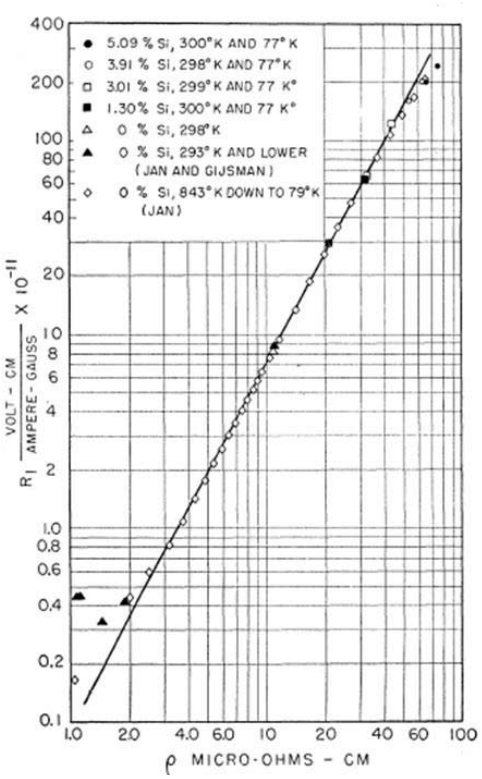


FIG. 2 Extraordinary Hall constant as a function of resistivity. The shown fit has the relation $R_s \sim \rho^{1.9}$. [From Ref. Kooi, 1954.]

Early experiments to measure the relationship between ρ_{xy} and ρ generally assumed to be of the power law form, *i.e.*, $\rho_{xy} \sim \rho^{\beta}$, mostly involved plotting ρ_{xy} (or R_s) vs. ρ, measured in a single sample over a broad interval of T (typically 77 to 300 K). As we explain below, competing theories in metals suggested either that $\beta = 1$ or $\beta = 2$. A compiled set of results was published by Kooi (Kooi, 1954) (Fig. 2). The subsequent consensus was that such plots do not settle the debate. At finite T, the carriers are strongly scattered by phonons and spin waves. These inelastic processes – difficult to treat microscopically even today – lie far outside the purview of the early theories. Smit suggested that, in the skew-scattering theory (see below), phonon scattering increases the value β from 1 to values approaching 2. This was also found by other investigators. A lengthy calculation by Lyo (Lyo, 1973) showed that skew-scattering at $T \gg \Theta_D$ (the Debye temperature) leads to the relationship $\rho_{xy} \sim (\rho^2 + a\rho)$, with a a constant. In an early theory by Kondo considering skew scattering from spin excitations (Kondo, 1962), it may be seen that ρ_{xy} also varies as ρ^2 at finite T.

The proper test of the scaling relation in comparison with present theories involves measuring ρ_{xy} and ρ in a set of samples at 4 K or lower (where impurity scattering dominates). By adjusting the impurity concentration n_i, one may hope to change both quantities sufficiently to determine accurately the exponent β and use this identification to tease out the underlying physics.

The main criticism of the KL theory centered on the complete absence of scattering from disorder in the derived Hall response contribution. The semi-classical AHE theories by Smit and Berger focused instead on the influence of disorder scattering in imperfect crystals. Smit argued that the main source of the AHE currents was asymmetric (*skew*) scattering from impurities caused by the spin-orbit interaction (SOI) (Smit, 1955, 1958). This AHE picture predicted that $R_s \sim \rho_{xx}$ ($\beta = 1$). Berger, on the other hand, argued that the main source of the AHE current was the *side-jump* experienced by quasiparticles upon scattering from spin-orbit coupled impurities. The side-jump mechanism could (confusingly) be viewed as a consequence of a KL anomalous velocity mechanism acting while a quasiparticle was under the influence of the electric field due to an impurity. The side-jump AHE current was viewed as the product of the side-jump per scattering event and the scattering rate (Berger, 1970). One puzzling aspect of this semiclassical theory was that all dependence on the impurity density and strength seemingly dropped out. As a result, it predicted $R_s \sim \rho_{xx}^2$ with an exponent β identical to that of the KL mechanism. The side-jump mechanism therefore yielded a contribution to the Hall conductivity which was seemingly independent of the density or strength of scatterers. In the decade 1970-80, a lively AHE debate was waged largely between the proponents of these two extrinsic theories. The three main mechanisms considered in this early history are shown schematically in Fig. 3.

Some of the confusion in experimental studies stemmed from a hazy distinction between the KL mechanism and the side-jump mechanism, a poor understanding of how the effects competed at a microscopic level, and a lack of systematic experimental studies in a diverse set of mate-

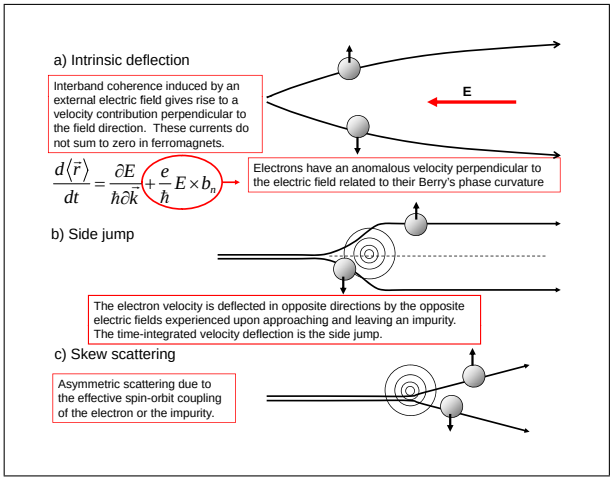


FIG. 3 Illustration of the three main mechanisms that can give rise to an AHE. In any real material all of these mechanisms act to influence electron motion.

rials.

One aspect of the confusion may be illustrated by contrasting the case of a high-purity mono-domain ferromagnet, which produces a spontaneous AHE current proportional to M_z, with the case of a material containing magnetic impurities (e.g. Mn) embedded in a non-magnetic host such as Cu (the dilute Kondo system). In a field H, the latter also displays an AHE current proportional to the induced $M = \chi H$, with χ the susceptibility (Fert and Jaoul, 1972). However, in *zero* H, time-reversal invariance (TRI) is spontaneously broken in the former, but not in the latter. Throughout the period 1960-1989, the two Hall effects were often regarded as a common phenomenon that should be understood microscopically on the same terms. It now seems clear that this view impeded progress.

By the mid-1980s, interest in the AHE problem had waned significantly. The large body of Hall data garnered from experiments on dilute Kondo systems in the previous two decades showed that $\rho_{xy} \sim \rho$ and therefore appeared to favor the skew-scattering mechanism. The points of controversy remained unsettled, however, and the topic was still mired in confusion.

Since the 1980's, the quantum Hall effect in two-dimensional (2D) electron systems in semiconductor heterostructures has become a major field of research in physics (Prange and Girvin, 1987). The accurate quantization of the Hall conductance is the hallmark of this phenomenon. Both the integer (Thouless *et al.*, 1982) and fractional quantum Hall effects can be explained in terms of the topological properties of the electronic wavefunctions. For the case of electrons in a two-dimensional crystal, it has been found that the Hall conductance is connected to the topological integer (Chern number) defined for the Bloch wavefunction over the first Brillouin zone (Thouless *et al.*, 1982). This way of thinking about the quantum Hall effect began to have a deep impact on the AHE problem starting around 1998. Theoretical interest in the Berry phase and in its relation to transport phenomena, coupled with many developments in the growth of novel complex magnetic systems with strong spin-orbit coupling (notably the manganites, pyrochlores and spinels) led to a strong resurgence of interest in the AHE and eventually to deeper understanding.

Since 2003 many systematics studies, both theoretical and experimental, have led to a better understanding of the AHE in the metallic regime, and to the recognition of new unexplored regimes that present challenges to future researchers. As it is often the case in condensed matter physics, attempts to understand this complex and fascinating phenomenon have motivated researchers to couple fundamental and sophisticated mathematical concepts to real-world materials issues. The aim of this review is to survey recent experimental progress in the field, and to present the theories in a systematic fashion. Researchers are now able to understand the links between different views on the AHE previously thought to be in conflict. Despite the progress in recent years, understanding is still incomplete. We highlight some intriguing questions that remain and speculate on the most promising avenues for future exploration. In this review we focus, in particular, on reports that have contributed significantly to the modern view of the AHE. For previous reviews, the reader may consult Pugh (Pugh and Rostoker, 1953) and Hurd (Hurd, 1972). For more recent short overviews focused on the topological aspects of the AHE, we point the reader to the reviews by Nagaosa (Nagaosa, 2006), and by Sinova *et al.*(Sinova *et al.*, 2004). A review of the modern semiclassical treament of AHE was recently written by Sinitsyn (Sinitsyn, 2008). The present review has been informed by ideas explained in the earlier works. Readers who are not familair with Berry phase concepts may find it useful to consult the elementary review by Ong and Lee (Ong and Lee, 2006) and the popular commentary by MacDonald and Niu (MacDonald and Niu, 2004).

Some of the recent advances in the understanding of the AHE that will be covered in this review are:

1. When σ_{xy}^{AH} is independent of σ_{xx}, the AHE can often be understood in terms of the geometric concepts of Berry phase and Berry curvature in momentum space. This AHE mechanism is responsible for the intrinsic AHE. In this regime, the anomalous Hall current can be thought of as the unquantized version of the quantum Hall effect. In 2D systems the intrinsic AHE is quantized in units of e^2/h at temperature $T = 0$ when the Fermi level lies between Bloch state bands.

2. Three broad regimes have been identified when surveying a large body of experimental data for diverse materials: (i) A high conductivity regime ($\sigma_{xx} > 10^6$ $(\Omega\text{cm})^{-1}$) in which a linear contribution to $\sigma_{xy}^{AH} \sim \sigma_{xx}$ due to skew scattering dominates σ_{xy}^{AH}. In this regime the normal Hall conductiv-

ity contribution can be significant and even dominate σ_{xy}, (ii) An intrinsic or scattering-independent regime in which σ_{xy}^{AH} is roughly independent of σ_{xx} (10^4 $(\Omega\text{cm})^{-1} < \sigma_{xx} < 10^6$ $(\Omega\text{cm})^{-1}$), (iii) A bad-metal regime ($\sigma_{xx} < 10^4$ $(\Omega\text{cm})^{-1}$) in which σ_{xy}^{AH} decreases with decreasing σ_{xx} at a rate faster than linear.

3. The relevance of the intrinsic mechanisms can be studied in-depth in magnetic materials with strong spin-orbit coupling, such as oxides and diluted magnetic semiconductors (DMS). In these systems a systematic non-trivial comparison between the observed properties of systems with well controlled materials properties and theoretical model calculations can be achieved.

4. The role of band (anti)-crossings near the Fermi energy has been identified using first-principles Berry curvature calculations as a mechanism which can lead to a large intrinsic AHE.

5. Semiclassical treatment by a generalized Boltzmann equation taking into account the Berry curvature and coherent inter-band mixing effects due to band structure and disorder has been formulated. This theory provides a clearer physical picture of the AHE than early theories by identifying correctly all the semiclassically defined mechanisms. This generalized semiclassical picture has been verified by comparison with controlled microscopic linear response treatments for identical models.

6. The relevance of non-coplanar spin structures with associated spin chirality and real-space Berry curvature to the AHE has been established both theoretically and experimentally in several materials.

7. Theoretical frameworks based on the Kubo formalism and the Keldysh formalism have been developed which are capable of treating transport phenomena in systems with multiple bands.

The review is aimed at experimentalists and theorists interested in the AHE. We have structured the review as follows. In the remainder of this section, we provide the minimal theoretical background necessary to understand the different AHE mechanisms. In particular we explain the scattering-independent Berry phase mechanism which is more important for the AHE than for any other commonly measured transport coefficient. In Sec. II we review recent experimental results on a broad range of materials, and compare them with relevant calculations where available. In Sec. III we discuss AHE theory from an historical perspective, explaining links between different ideas which are not always recognized, and discussing the physics behind some of the past confusion. The section may be skipped by readers who do not wish to be burdened by history. Section IV discusses the present understanding of the metallic theory based on a careful comparison of the different linear response theories which are now finally consistent. In Sec. V we present a summary and outlook.

B. Parsing the AHE:

The anomalous Hall effect is at its core a quantum phenomena which originates from quantum coherent band mixing effects by both the external electric field and the disorder potential. Like other coherent interference transport phenomena (e.g. weak localization), it cannot be satisfactorily explained using traditional semiclassical Boltzmann transport theory. Therefore, when parsing the different contributions to the AHE, they can be defined semiclassically only in a carefully elaborated theory.

In this section we identify three distinct contributions which sum up to yield the full AHE: *intrinsic, skew scattering, and side-jump contributions*. We choose this nomenclature to reflect the modern literature without breaking completely from the established AHE lexicon (see Sec. III). *However, unlike previous classifications, we base this parsing of the AHE on experimental and microscopic transport theory considerations, rather than on the identification of one particular effect which could contribute to the AHE.* The link to semiclassically defined processes is established after developing a fully generalized Boltzmann transport theory which takes inter-band coherence effects into account and is fully equivalent to microscopic theories (Sec. IV.A). In fact, much of the theoretical effort of the past few years has been expended in understanding this link between semiclassical and microscopic theory which has escaped cohesion for a long time.

A very natural classification of contributions to the AHE, which is guided by experiment and by microscopic theory of metals, is to separate them according to their dependence on the Bloch state transport lifetime τ. In the theory, disorder is treated perturbatively and higher order terms vary with a higher power of the quasiparticle scattering rate τ^{-1}. As we will discuss, it is relatively easy to identify contributions to the anomalous Hall conductivity, σ_{xy}^{AH}, which vary as τ^1 and as τ^0. In experiment a similar separation can sometimes be achieved by plotting σ_{xy} vs. the longitudinal conductivity $\sigma_{xx} \propto \tau$, when τ is varied by altering disorder or varying temperature. More commonly (and equivalently) the Hall resistivity is separated into contributions proportional to ρ_{xx} and ρ_{xx}^2.

This partitioning seemingly gives only two contributions to σ_{xy}^{AH}, one $\sim \tau$ and the other $\sim \tau^0$. The first contribution we *define* as the *skew-scattering* contribution, $\sigma_{xy}^{AH-skew}$. Note that in this parsing of AHE contributions it is the dependence on τ (or σ_{xx}) which defines it, not a particular mechanism linked to a microscopic or semiclassical theory. The second contribution proportional to τ^0 (or independent of σ_{xx}) we further

separate into two parts: *intrinsic* and *side-jump*. Although these two contributions cannot be separated experimentally by dc measurements, they *can* be separated experimentally (as well as theoretically) by defining the intrinsic contribution, σ_{xy}^{AH-int}, as the extrapolation of the ac-interband Hall conductivity to zero frequency in the limit of $\tau \to \infty$, with $1/\tau \to 0$ faster than $\omega \to 0$. This then leaves a unique definition for the third and last contribution, termed side-jump, as $\sigma_{xy}^{AH-sj} \equiv \sigma_{xy}^{AH} - \sigma_{xy}^{AH-skew} - \sigma_{xy}^{AH-int}$.

We examine these three contributions below (still at an introductory level). It is important to note that the above definitions have not relied on identifications of semiclassical processes such as side-jump scattering (Berger, 1970) or skew-scattering from asymmetric contributions to the semiclassical scattering rates (Smit, 1955) identified in earlier theories. Not surprisingly, the contributions defined above contain these semiclassical processes. However, it is now understood (see Sec. IV), that other contributions are present in the fully generalized semiclassical theory which were not precisely identified previously and which are necessary to be fully consitent with microscopic theories.

The ideas explained briefly in this section are substantiated in Sec. II by analyses of tendencies in the AHE data of several different material classes, and in Sec. III and Sec. IV by an extensive technical discussion of AHE theory. We assume throughout that the ferromagnetic materials of interest are accurately described by a Stoner-like mean-field band theory. In applications to real materials we imagine that the band theory is based on spin-density-functional theory (Jones and Gunnarsson, 1989) with a local-spin-density or similar approximation for the exchange-correlation energy functional.

1. Intrinsic contribution to σ_{xy}^{AH}

Among the three contributions, the easiest to evaluate accurately is the intrinsic contribution. We have defined the intrinsic contribution microscopically as the *dc* limit of the interband conductivity, a quantity which is not zero in ferromagnets when SOI are included. There is however a direct link to semiclassical theory in which the induced interband coherence is captured by a momentum-space Berry-phase related contribution to the anomalous velocity. We show this equivalence below.

This contribution to the AHE was first derived by KL (Karplus and Luttinger, 1954) but its topological nature was not fully appreciated until recently (Jungwirth *et al.*, 2002b; Onoda and Nagaosa, 2002). The work of Jungwirth *et al.* (Jungwirth *et al.*, 2002b) was motivated by the experimental importance of the AHE in ferromagnetic semiconductors and also by the thorough earlier analysis of the relationship between momentum space Berry phases and anomalous velocities in semiclassical transport theory by Niu *et al.* (Chang and Niu, 1996; Sundaram and Niu, 1999). The frequency-dependent inter-band Hall conductivity, which reduces to the intrinsic anomalous Hall conductivity in the *dc* limit, had been evaluated earlier for a number of materials by Mainkar *et al.* (Mainkar *et al.*, 1996) and Guo and Ebert (Guo and Ebert, 1995) but the topological connection was not recognized.

The intrinsic contribution to the conductivity is dependent only on the band structure of the perfect crystal, hence its name. It can be calculated directly from the simple Kubo formula for the Hall conductivity for an ideal lattice, given the eigenstates $|n,\boldsymbol{k}\rangle$ and eigenvalues $\varepsilon_n(\boldsymbol{k})$ of a Bloch Hamiltonian H:

$$\sigma_{ij}^{AH-int} = e^2\hbar \sum_{n\neq n'} \int \frac{d\boldsymbol{k}}{(2\pi)^3} [f(\varepsilon_n(\boldsymbol{k})) - f(\varepsilon_{n'}(\boldsymbol{k}))] \times \mathrm{Im} \frac{\langle n,\boldsymbol{k}|v_i(\boldsymbol{k})|n',\boldsymbol{k}\rangle\langle n',\boldsymbol{k}|v_j(\boldsymbol{k})|n,\boldsymbol{k}\rangle}{(\varepsilon_n(\boldsymbol{k}) - \varepsilon_{n'}(\boldsymbol{k}))^2}. \quad (1.2)$$

In Eq. (1.2) H is the $\boldsymbol{k}$-dependent Hamiltonian for the periodic part of the Bloch functions and the velocity operator is defined by

$$\boldsymbol{v}(\boldsymbol{k}) = \frac{1}{i\hbar}[\boldsymbol{r}, H(\boldsymbol{k})] = \frac{1}{\hbar}\boldsymbol{\nabla}_k H(\boldsymbol{k}). \quad (1.3)$$

Note the restriction $n \neq n'$ in Eq. (1.2).

What makes this contribution quite unique is that, like the quantum Hall effect in a crystal, it is directly linked to the topological properties of the Bloch states. (See Sec. III.B.) Specifically it is proportional to the integration over the Fermi sea of the Berry's curvature of each occupied band, or equivalently (Haldane, 2004; Wang *et al.*, 2007) to the integral of Berry phases over cuts of Fermi surface segments. This result can be derived by noting that

$$\langle n,\boldsymbol{k}|\boldsymbol{\nabla}_k|n',\boldsymbol{k}\rangle = \frac{\langle n,\boldsymbol{k}|\boldsymbol{\nabla}_k H(\boldsymbol{k})|n',\boldsymbol{k}\rangle}{\varepsilon_{n'}(\boldsymbol{k}) - \varepsilon_n(\boldsymbol{k})}. \quad (1.4)$$

Using this expression, Eq. (1.2) reduces to

$$\sigma_{ij}^{AH-int} = -\epsilon_{ij\ell}\frac{e^2}{\hbar}\sum_n \int \frac{d\boldsymbol{k}}{(2\pi)^d} f(\varepsilon_n(\boldsymbol{k}))\; b_n^\ell(\boldsymbol{k}), \quad (1.5)$$

where $\epsilon_{ij\ell}$ is the anti-symmetric tensor, $\boldsymbol{a}_n(\boldsymbol{k})$ is the Berry-phase connection $\boldsymbol{a}_n(\boldsymbol{k}) = i\langle n,\boldsymbol{k}|\boldsymbol{\nabla}_k|n,\boldsymbol{k}\rangle$, and $\boldsymbol{b}_n(\boldsymbol{k})$ the Berry-phase curvature

$$\boldsymbol{b}_n(\boldsymbol{k}) = \boldsymbol{\nabla}_k \times \boldsymbol{a}_n(\boldsymbol{k}) \quad (1.6)$$

corresponding to the states $\{|n,\boldsymbol{k}\rangle\}$.

This same linear response contribution to the AHE conductivity can be obtained from the semiclassical theory of wave-packets dynamics (Chang and Niu, 1996; Marder, 2000; Sundaram and Niu, 1999). It can be shown that the wavepacket group velocity has an additional contribution in the presence of an electric field: $\dot{\boldsymbol{r}}_c = \partial E_n(\boldsymbol{k})/\hbar\partial\boldsymbol{k} - (\boldsymbol{E}/\hbar)\times\boldsymbol{b}_n(\boldsymbol{k})$. (See Sec. IV.A.) The

intrinsic Hall conductivity formula, Eq. (1.5), is obtained simply by summing the second (anomalous) term over all occupied states.

One of the motivations for identifying the intrinsic contribution σ_{xy}^{AH-int} is that it can be evaluated accurately even for relatively complex materials using first-principles electronic structure theory techniques. In many materials which have strongly spin-orbit coupled bands, the intrinsic contribution seems to dominates the AHE.

2. Skew scattering contribution to σ_{xy}^{AH}

The skew scattering contribution to the AHE can be sharply defined; it is simply the contribution which is proportional to the Bloch state transport lifetime. It will therefore tend to dominate in nearly perfect crystals. It is the only contribution to the AHE which appears within the confines of traditional Boltzmann transport theory in which interband coherence effects are completely neglected. Skew scattering is due to chiral features which appear in the disorder scattering of spin-orbit coupled ferromagnets. This mechanism was first identified by Smit (Smit, 1955, 1958).

Treatments of semi-classical Boltzmann transport theory found in textbooks often appeal to the principle of detailed balance which states that the transition probability $W_{n\to m}$ from n to m is identical to the transition probability in the opposite direction ($W_{m\to n}$). Although these two transition probabilities are identical in a Fermi's golden-rule approximation, since $W_{n\to n'} = (2\pi/\hbar)|\langle n|V|n'\rangle|^2\delta(E_n - E_{n'})$, where V is the perturbation inducing the transition, detailed balance in this microscopic sense is not generic. In the presence of spin-orbit coupling, either in the Hamiltonian of the perfect crystal or in the disorder Hamiltonian, a transition which is right-handed with respect to the magnetization direction has a different transition probability than the corresponding left-handed transition. When the transition rates are evaluated perturbatively, asymmetric chiral contributions appear first at third order. (See Sec. IV.A). In simple models the asymmetric chiral contribution to the transition probability is often assummed to have the form (see Sec. III.C.2.a):

$$W^A_{\boldsymbol{k}\boldsymbol{k}'} = -\tau_A^{-1}\boldsymbol{k}\times\boldsymbol{k}'\cdot\boldsymbol{M}_s. \tag{1.7}$$

When this asymmetry is inserted into the Boltzmann equation it leads to a current proportional to the longitudinal current driven by $\boldsymbol{E}$ and perpendicular to both $\boldsymbol{E}$ and $\boldsymbol{M}_s$. When this mechanism dominates, both the Hall conductivity σ_H and the conductivity σ are proportional to the transport lifetime τ and the Hall resistivity $\rho_H^{skew} = \sigma_H^{skew}\rho^2$ is therefore proportional to the longitudinal resistivity ρ.

There are several specific mechanisms for skew scattering (see Sec.III.C.2 and Sec. IV.A). Evaluation of the skew scattering contribution to the Hall conductivity or resistivity requires simply that the conventional linearized Boltzmann equation be solved using a collision term with accurate transition probabilities, since these will generically include a chiral contribution. In practice our ability to accurately estimate the skew scattering contribution to the AHE of a real material is limited only by typically imperfect characterization of its disorder. We emphasize that skew scattering contributions to σ_H are present not only because of spin-orbit coupling in the disorder Hamiltonian, but also because of spin-orbit coupling in the perfect crystal Hamiltonain combined with purely scalar disorder. Either source of skew-scattering could dominate $\sigma_{xy}^{AH-skew}$ depending on the host material and also on the type of impurities.

We end this subsection with a small note directed to the reader who is more versed in the latest development of the full semiclassical theory of the AHE and in its comparison to the microscopic theory (see Sec. IV.A and IV.B.2). We have been careful above not to define the skew-scattering contribution to the AHE as the sum of *all* the contributions arising from the asymmetric scattering rate present in the collision term of the Boltzmann transport equation. We know from microscopic theory that this asymmetry also makes an AHE contribution or order τ^0. There exists a contribution from this asymmetry which is actually present in the microscopic theory treatment associated with the so called ladder diagram corrections to the conductivity, and therefore of order τ^0. In our experimentally practical parsing of AHE contributions we do not associate this contribution with skew-scattering but place it under the umbrella of side-jump scattering even though it does not physically originate from any side-step type of scattering.

3. Side-jump contribution to σ_{xy}^{AH}

Given the sharp defintions we have provided for the intrinsic and skew scattering contributions to the AHE conductivity, the equation

$$\sigma_{xy}^{AH} = \sigma_{xy}^{AH-int} + \sigma_{xy}^{AH-skew} + \sigma_{xy}^{AH-sj} \tag{1.8}$$

defines the side-jump contribution as the difference between the full Hall conductivity and the two-simpler contributions. In using the term side-jump for the remaining contribution, we are appealing to the historically established taxonomy outlined in the previous section. Establishing this connection mathematically has been the most controversial aspects of AHE theory, and the one which has taken the longest to clarify from a theory point of view. Although this classification of Hall conductivity contributions is often useful (see below), it is not generically true that the only correction to the intrinsic and skew contributions can be physically identified with the side-jump process defined as in the earlier studies of the AHE (Berger, 1964).

The basic semiclassical argument for a side-jump contribution can be stated straight-forwardly: when

considering the scattering of a Gaussian wavepacket from a spherical impurity with SOI ($H_{SO} = (1/2m^2c^2)(r^{-1}\partial V/\partial r)S_zL_z$), a wavepacket with incident wave-vector $\boldsymbol{k}$ will suffer a displacement transverse to $\boldsymbol{k}$ equal to $\frac{1}{6}k\hbar^2/m^2c^2$. This type of contribution was first noticed, but discarded, by Smit (Smit, 1958) and reintroduced by Berger (Berger, 1964) who argued that it was the key contribution to the AHE. This kind of mechanism clearly lies outside the bounds of traditional Boltzmann transport theory in which only the probabilities of transitions between Bloch states appears, and not microscopic details of the scattering processes. This contribution to the conductivity ends up being independent of τ and therefore contributes to the AHE at the same order as the intrinsic contribution in an expansion in powers of scattering rate. The separation between intrinsic and side-jump contributions, which cannot be distinquished by their dependence on τ, has been perhaps the most argued aspect of AHE theory since they cannot be distinquished by their dependence on scattering rate (see Sec. III.C.2.d).

As explained clearly in a recent review by Sinitsyn (Sinitsyn, 2008), side-jump and intrinsic contributions have quite different dependences on more specific system parameters, particularly in systems with complex band structures. Some of the initial controversy which surrounded side jump theories was associated with physical meaning ascribed to quantities which were plainly gauge dependent, like the Berry's connection which in early theories is typically identified as the definition of the side-step upon scattering. Studies of simple models, for example models of semiconductor conduction bands, also gave results in which the side-jump contribution seemed to be the same size but opposite in sign compared to the intrinsic contribution (Nozieres and Lewiner, 1973). We now understand (Sinitsyn *et al.*, 2007) that these cancellations are unlikely, except in models with a very simple band structure, *e.g.* one with a constant Berry's curvature. It is only through comparison between fully microscopic linear response theory calculations, based on equivalently valid microscopic formalisms such as Keldysh (non-equilibrium Grenn's function) or Kubo formalisms, and the systematically developed semiclassical theory that the specific contribution due to the side-jump mechanism can be separately identified with confidence (see Sec. IV.A).

Having said this, all the calculations comparing the intrinsic and side-jump contibutions to the AHE from a microscopic point of view have been performed for very simple models not immediately linked to real materials. A practical approch which is followed at present for materials in which σ^{AH} seems to be independent of σ_{xx}, is to first calculate the intrisic contribution to the AHE. If this explains the observation (and it appears that it usually does), then it is deemed that the intrinsic mechanism dominates. If not, we can take some comfort from understanding on the basis of simple model results, that there can be other contributions to σ^{AH} which are also independent of σ_{xx} and can for the most part be identified with the side jump mechanism. Unfortunately it seems extremelly challenging, if not impossible, to develop a predictive theory for these contributions, partly because they require many higher order terms in the perturbation theory that be summed, but more fundamentally because they depend sensitively on details of the disorder in a particular material which are normally unknown.

II. EXPERIMENTAL AND THEORETICAL STUDIES ON SPECIFIC MATERIALS

A. Transition-metals

1. Early experiments

Four decades after the discovery of the AHE, an empirical relation between magnetization and Hall resistivity was proposed independently by A. W. Smith and by E. M. Pugh (Pugh, 1930; Pugh and Lippert, 1932; Smith and Sears, 1929) (see Sec. I.A). Pugh investigated the AHE in Fe, Ni and Co and the alloys Co-Ni and Ni-Cu in magnetic fields up to 17 kG over large intervals in T (10-800 K in the case of Ni), and found that the Hall resistivity ρ_H is comprised of 2 terms, *viz.*

$$\rho_H = R_0 H + R_1 M(T,H), \tag{2.1}$$

where $M(T,H)$ is the magnetization averaged over the sample. Pugh defined R_0 and R_1 as the ordinary and extra-ordinary Hall coefficients, respectively. The latter $R_1 = R_s$ is now called the anomalous Hall coefficient (as in Eq. 1.1)).

On dividing Eq. (2.1) by ρ^2, we see that it just expresses the additivity of the Hall currents: the total Hall conductivity σ_{xy}^{tot} equals $\sigma_{xy}^{NH} + \sigma_{xy}^{AH}$, where σ_{xy}^{NH} is the ordinary Hall conductivity and σ_{xy}^{AH} is the AHE conductivity. A second implication of Eq. (2.1) emerges when we consider the role of domains. The anomalous Hall coefficient in Eq.(2.1) is proportional to the AHE in a single domain. As $H \to 0$, proliferation of domains rapidly reduces $\boldsymbol{M}(T,H)$ to zero (we ignore pinning). Cancellations of σ_{xy}^{AH} between domains result in a zero net Hall current. Hence the observed AHE term mimics the field profile of $M(T,H)$, as implied by Pugh's term R_1M. The role of $\boldsymbol{H}$ is simply to align the AHE currents by rotating the domains into alignment. The Lorentz force term σ_{xy}^{NH} is a "background" current with no bearing on the AHE problem.

The most interesting implication of Eq. (2.1) is that, in the absence of $\boldsymbol{H}$, a single domain engenders a spontaneous Hall current transverse to both $\boldsymbol{M}$ and $\boldsymbol{E}$. Understanding the origin of this spontaneous off-diagonal current has been a fundamental problem of charge transport in solids for the past 60 years. The AHE is also called the spontaneous Hall effect and the extraordinary Hall effect in the older literature.

2. Recent experiments

The resurgence of interest in the AHE motivated by the Berry-phase approach (Sec. I.B.1) has led to many new Hall experiments on $3d$ transition metals and their oxides. Both the recent and the older literature on Fe and Fe_3O_4 are reviewed in this section. An important finding of these studies is the emergence of three distinct regimes roughly delimited by the conductivity σ_{xx} and characterized by the dependence of σ_{xy}^{AH} on σ_{xx}. The three regimes are:

i) A high conductivity regime for $\sigma_{xx} \gtrsim 10^6$ $(\Omega\text{cm})^{-1}$ in which $\sigma_{xy}^{AH-skew} \sim \sigma_{xx}^1$ dominates σ_{xy}^{AH},

ii) A good metal regime for $\sigma_{xx}^{AH} \sim 10^4 - 10^6$ $(\Omega\text{cm})^{-1}$ in which $\sigma_{xy} \sim \sigma_{xx}^0$,

iii) A bad metal/hopping regime for $\sigma_{xx} < 10^4$ $(\Omega\text{cm})^{-1}$ in which $\sigma_{xy}^{AH} \sim \sigma_{xx}^{1.6-1.8}$.

We discuss each of these regimes below.

High conductivity regime – The Hall conductivity in the high-purity regime, $\sigma_{xx} > 0.5 \times 10^6$ $(\Omega\text{cm})^{-1}$, is dominated by the skew scattering contribution σ_{xy}^{skew}. The high-purity regime is one of the least studied experimentally. This regime is very challenging to investigate experimentally because the field H required for saturating M also yields a very large ordinary Hall effect (OHE) and R_0 tends to be of the order of R_s (Schad *et al.*, 1998). In the limit $\omega_c\tau \gg 1$, the OHE conductivity σ_{xy}^{NH} may be nonlinear in H (ω_c is the cyclotron frequency). Although σ_{xy}^{skew} increases as τ, the OHE term σ_{xy}^{NH} increases as τ^2 and therefore the latter ultimately dominates, and the AHE current may be unresolvable. Even though the anomalous Hall current can not always be cleanly separated from the normal Lorentz-force Hall effect in the high conductivity regime, the total Hall current invariably increases with σ_{xx} in a way which provides compelling evidence for a skew-scattering contribution.

In spite of these challenges several studies have managed to convincingly separate the competing contributions and have identifed a dominant linear relation between σ_{xy}^{AH} and σ_{xx} for $\sigma_{xx} \gtrsim 10^6$ $(\Omega\text{cm})^{-1}$ (Majumdar and Berger, 1973; Shiomi *et al.*, 2009). In an early study Majumdar *et al.* (Majumdar and Berger, 1973) grew highly pure Fe doped with Co. The resulting σ_{xy}^{AH}, obtained from Kohler plots extrapolation to zero field, show a clear dependence of $\sigma_{xy}^{AH} \sim \sigma_{xx}$ (Fig. 4 a). In a more recent study, a similar finding (linear dependence of $\sigma_{xy}^{AH} \sim \sigma_{xx}$) was observed by Shiomi *et al.* (Shiomi *et al.*, 2009) in Fe doped with Co, Mn, Cr, and Si. In these studies the high temperature contribution to σ_{xy}^{AH} (presumed to be intrinsic plus side jump) was substracted from σ_{xy} and a linear dependence of the resulting σ_{xy}^{AH} is observed (Fig. 4 a and b). In this recent study the conductivity is intentionally reduced by impurity doping to find the linear region and reliably exclude the Lorernz contribution. The results of these authors show, in particular, that the slope of σ_{xx} vs. σ_{xy}^{AH} depends on the species of the impurities as it is expected in the regime dominated by skew scattering. It is reassuring to note that the skewness parameters ($S_{skew} = \sigma^{AH}/\sigma_{xx}$) implied by the older and the more recent experiments are consistent, in spite of differences in the conductivity ranges studied. S_{skew} is independent of σ_{xx} (Majumdar and Berger, 1973; Shiomi *et al.*, 2009) as it should be when the skew scattering mechanism dominates. Further experiments in this regime are desirable to fully investiage the different dependence on doping, temperature, and impurity type. Also, new approaches to reliably disentangle the AHE and OHE currents will be needed to faicilitate such studies.

Good metal regime – Experiments re-examining the AHE in Fe, Ni, and Co have been performed by Miyasato *et al.* (Miyasato *et al.*, 2007). These experiments indicate a regime of σ_{xy} versus σ_{xx} in which σ_{xy} is insensitive to σ_{xx} in the range $\sigma_{xx} \sim 10^4$-10^6 $(\Omega\text{cm})^{-1}$ (see Fig. 5). This suggests that the scattering independent mechanisms (intrinsic and side-jump) dominates in this regime. However, in comparing this phenomenology to the discussion of AHE mechanisms in Sec. I.B, one must keep in mind that the temperature has been varied in the Hall data on Fe, Ni, and Co in order to change the resistivity, even though it is restricted to the range well below T_c (Fig. 5 upper panel). In the mechanisms discussed in Sec. I.B only elastic scattering was taken into account. Earlier tests of the ρ^2 dependence of ρ_{xy} carried by varying T were treated as suspect in the early AHE period (see Fig. 2) because the role of inelastic scattering was not fully understood. The effect of inelastic scattering from phonons and spin waves remains open in AHE theory and is not addressed in this review.

Bad metal/hopping regime– Several groups have measured σ_{xy} in Fe and Fe_3O_4 thin-film ferromagnets (Feng *et al.*, 1975; Fernandez-Pacheco *et al.*, 2008; Miyasato *et al.*, 2007; Sangiao *et al.*, 2009; Venkateshvaran *et al.*, 2008). (See Fig. 6.) Sangiao *et al.* (Sangiao *et al.*, 2009) studied epitaxial thin-films of Fe deposited by pulsed-laser deposition (PLD) on single-crystal MgO (001) substrates at pressures $< 5 \times 10^{-9}$ Torr. To vary σ_{xx} over a broad range, they varied the film thickness t from 1 to 10 nm. The ρ vs. T profile for the film with $t = 1.8$ nm displays a resistance minimum near 50 K, below which ρ shows an upturn which has been ascribed to localization or electron interaction effects (Fig. 7). The magnetization M is nominally unchanged from the bulk value (except possibly in the 1.3 nm film). AHE experiments were carried out from 2–300 K on these films and displayed as σ_{xy} vs. σ_{xx} plots together with previously published results (Fig. 6). In the plot, the AHE data from films with $t \leq 2$ nm fall in the weakly localized regime. The combined plot shows that Sangio *et al.*'s data are collinear (on a logarithmic scale) with those measured on 1 μm-thick films by Miyasato *et al.* (Miyasato *et al.*, 2007). For the three samples with $t = 1.3$–2 nm, the inferred exponent in the dirty regime is on average ~ 1.66. A concern is that

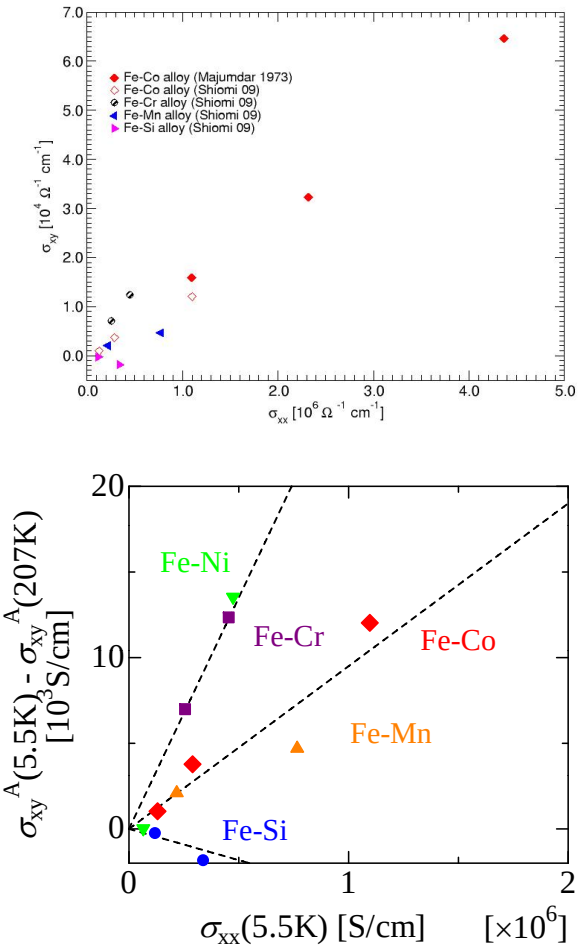


FIG. 4 σ_{xy}^{AH} for pure Fe film doped with Cr, Co, Mn and Si vs. σ_{xx} at low temperatures ($T = 4.2$ K and $T = 5.5$ K) (a). In many of the alloys, particularly in the Co doped system, the linear scaling in the higher conductivy sector, $\sigma_{xx} > 10^6$ $(\Omega\text{cm})^{-1}$, implies that skew scattering dominates σ_{xy}^{AH}. After Ref. Majumdar and Berger, 1973 and Ref. Shiomi *et al.*, 2009. The data from (Shiomi *et al.*, 2009), shown also at a larger scale in (b), is obtained by substracting the high temperature contribuiton to σ_{xy}. In the data shown the ordinary Hall contribution has been identified and substracted. [Panel (b) From Ref. Shiomi *et al.*, 2009.]

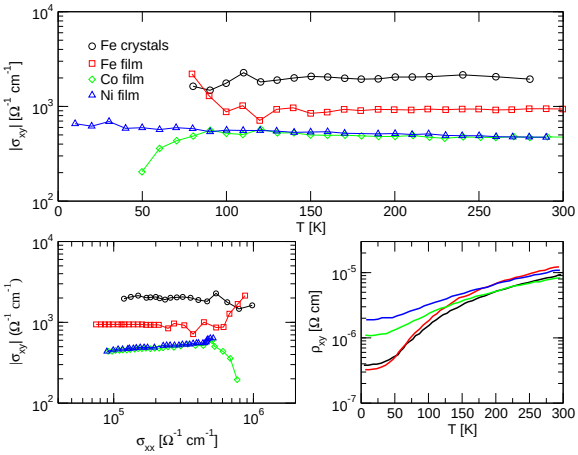


FIG. 5 Measurements of the Hall conductivity and resistivity in single-crystal Fe and in thin foils of Fe, Co, and Ni. The top and lower right panels show the T dependence of σ_{xy} and ρ_{xx}, respectively. The lower left panel plots $|\sigma_{xy}|$ against σ_{xx}. After Ref. Miyasato *et al.*, 2007.

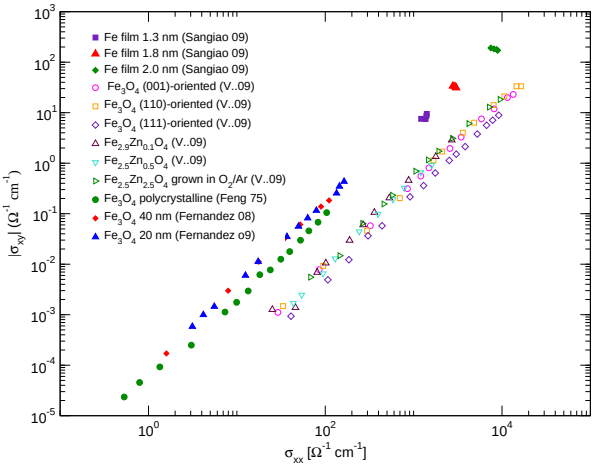


FIG. 6 Combined plot of the AHE conductivity $|\sigma_{xy}|$ versus the conductivity σ_{xx} in epitaxial films of Fe grown on MgO with thickness $t = 2.5$, 2.0, 1.8 and 1.3 nm (Sangiao *et al.*, 2009), in polycrystalline $Fe_{3-x}Zn_xO_4$ (Feng *et al.*, 1975), in thin-film $Fe_{3-x}Zn_xO_4$ between 90 and 350 K (Venkateshvaran *et al.*, 2008) and above the Verwey transition (Fernandez-Pacheco *et al.*, 2008).

the data from the 1.3 nm film was obtained by subtracting a $\ln T$ term from ρ (the subtraction procedure was not described). How localization affects the scaling plot is an open issue at present. In Sec. II.E, we discuss recent AHE measurements in disordered polycrystalline Fe films with $t < 10$ nm by Mitra *et al.* (Mitra *et al.*, 2007). Recent progress in understanding weak-localization corrections to the AHE is also reviewed there.

In magnetite, Fe_3O_4, scaling of $\sigma_{xy} \sim \sigma_{xx}^{\alpha}$ with $\alpha \sim 1.6 - 1.8$ was already apparent in early experiments on polycrystalline samples (Feng *et al.*, 1975). Recently, two groups have re-investigated the AHE in epitaxial thin films (data included in Fig. 6). Fernandez-Pacheco *et al.* (Fernandez-Pacheco *et al.*, 2008) measured a series of thin-film samples of Fe_3O_4 grown by PLD on MgO (001) substrates in ultra-high vacuum, whereas Venkateshvaran *et al.* (Venkateshvaran *et al.*, 2008) studied both pure Fe_3O_4 and Zn-doped magnetite $Fe_{3-x}Zn_xO_4$ deposited on MgO and Al_2O_3 substrates

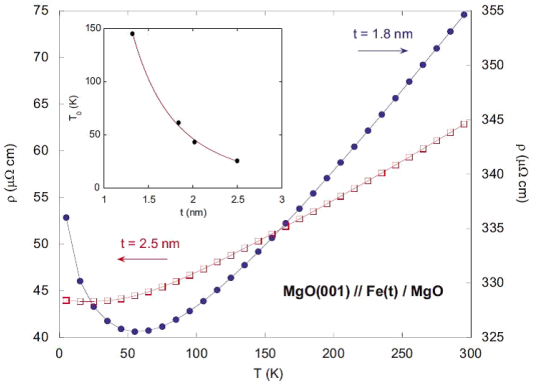


FIG. 7 The T dependence of ρ in epitaxial thin-films MgO(001)/Fe(t)/MgO with t = 1.8 nm and 2.5 nm. The inset shows how T_0, the temperature of the resistivity minimum, varies with t.[From Ref. Sangiao *et al.*, 2009.]

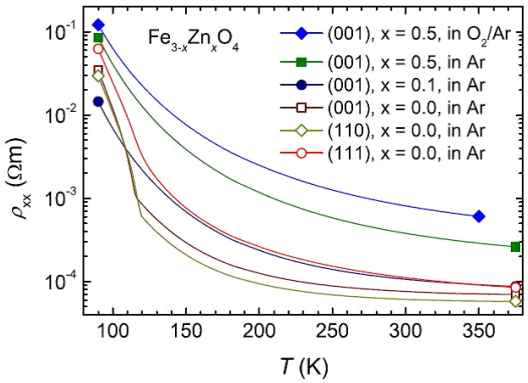


FIG. 8 Longitudinal resistivity ρ_{xx} vs. T for epitaxial $Fe_{3-x}Zn_xO_4$ films. The (001), (110) and (111) oriented films were grown on MgO(001), MgO(110) and Al_2O_3 substrates. [From Ref. Venkateshvaran *et al.*, 2008.]

grown by laser molecular-beam epitaxy under pure Ar or Ar/O mixture. In both studies, ρ increases monotonically by a factor of ∼10 as T decreases from 300 K to the Verwey transition temperature T_V = 120 K. Below T_V, ρ further increases by a factor of 10 to 100. The results for ρ vs. T from Venkateshvaran *et al.* (Venkateshvaran *et al.*, 2008) is shown in Fig. 8.

The large values of ρ and its insulating trend imply that magnetite falls in the strongly localized regime, in contrast to thin-film Fe which lies partly in the weak-localization (or incoherent) regime.

Both groups find good scaling fits extending over several decades of σ_{xx} with $\alpha \sim 1.6 - 1.8$ when varying T. Fernandez-Pacheco *et al.* (Fernandez-Pacheco *et al.*, 2008) plot σ_{xy} vs. σ_{xx} in the range 150< T <300 K for several thicknesses t and infer an exponent $\alpha = 1.6$. Venkateshvaran *et al.* (Venkateshvaran *et al.*, 2008) plot σ_{xy} vs. σ_{xx} from 90 to 350 K and obtain power-law fits with $\alpha = 1.69$, in both pure and Zn-doped magnetite (data shown in Fig. 6). Significantly, the 2 groups find that α is unchanged below T_V. There is presently no theory in the poorly conducting regime which predicts the observed scaling ($\sigma_{xx} < 10^{-1}$ $(\Omega\text{cm})^{-1}$).

3. Comparison to theories

Detailed first-principles calculations of the intrinsic contribution to the AHE conductivity have been performed for bcc Fe (Wang *et al.*, 2006; Yao *et al.*, 2004), fcc Ni, and hpc Co (Wang *et al.*, 2007). In Fe and Co, the values of σ_{xy} inferred from the Berry curvature $\Omega^z(\boldsymbol{k})$ are 7.5×10^2 and 4.8×10^2 $(\Omega\text{cm})^{-1}$, respectively, in reasonable agreement with experiment. In Ni, however, the calculated value -2.2×10^3 $(\Omega\text{cm})^{-1}$ is only 30% of the experimental value.

These calculations uncovered the crucial role played by avoided-crossings of band dispersions near the Fermi energy ε_F. The Berry curvature b_z is always strongly

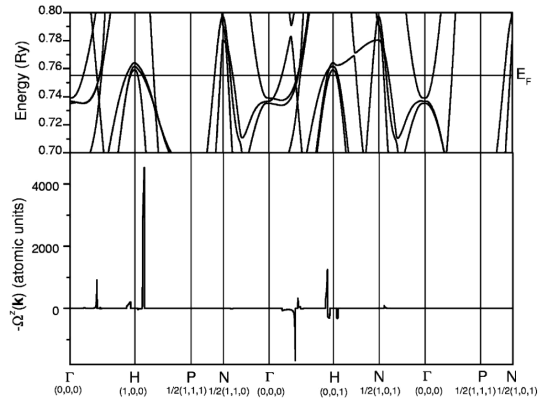


FIG. 9 First-principles calculation of the band dispersions and the Berry-phase curvature summed over occupied bands. [From Ref. Yao *et al.*, 2004.]

enhanced near avoided crossings, opposite direction for the upper and lower bands. A large contribution to σ_{xy}^{int} when the crossing is at the Fermi energy so that only one of the two bands is occupied, *e.g.* near the point H in Fig. 9. A map showing the contributions of different regions of the FS to $b^z(\boldsymbol{k})$ is shown in Fig. 10. The SOI can lift an accidental degeneracy at certain wavevectors $\boldsymbol{k}$. These points act as a magnetic monopole for the Berry curvature in $\boldsymbol{k}$-space (Fang *et al.*, 2003). In the parameter space of spin-orbit coupling, σ_{xy} is nonperturbative in nature. The effect of these "parity anomalies" (Jackiw, 1984) on the Hall conductivity was first discussed by Haldane (Haldane, 1988). A different conclusion on the role of topological enhancement in the intrinsic AHE was reported for a tight-binding calculation with the 2 orbitals d_{zx} and d_{yz} on a square lattice (Kontani *et al.*, 2007).

Motivated by the enhancement at the crossing points discussed above, Onoda *et al.* (Onoda *et al.*, 2006a, 2008) proposed a minimal model that focuses on the topological and resonantly enhanced nature of the intrinsic AHE

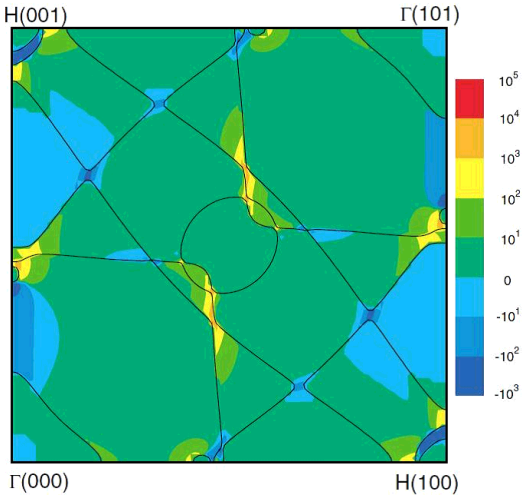


FIG. 10 First-principles calculation of the FS in the (010) plane (solid lines) and the Berry curvature in atomic units (color map). [From Ref. Yao *et al.*, 2004.]

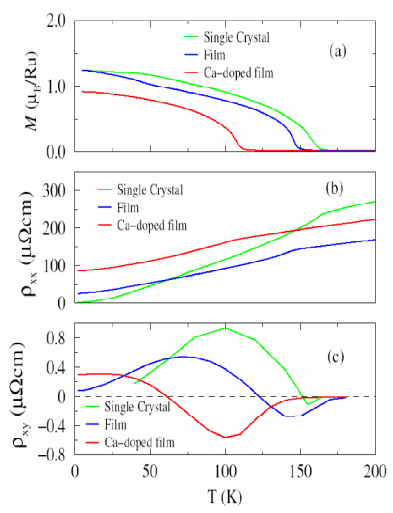


FIG. 11 Anomalous Hall effect in $SrRuO_3$. (A) The magnetization M, (B) longitudinal resistivity ρ_{xx}, and (C) transverse resistivity ρ_{xy} as functions of the temperature T for the single crystal and thin-film $SrRuO_3$, as well as for Ca-doped $Sr_{0.8}Ca_{0.2}RuO_3$ thin film. μ_B is the Bohr magneton. [From Ref. Fang *et al.*, 2003.]

arising from the sharp peak in $b^z(\boldsymbol{k})$ near avoided crossings. The minimal model is essentially a 2D Rashba model (Bychkov and Rashba, 1984) with an exchange field which breaks symmetries and accounts for the magnetic order and a random impurity potential to account for disorder. The model is discussed in Sec. IV.D. In the clean limit, σ_{xy} is dominated by the extrinsic skew-scattering contribution $\sigma_{xy}^{\rm skew}$, which almost masks the intrinsic contribution $\sigma_{xy}^{\rm int}$. Since $\sigma_{xy}^{\rm skew} \propto \tau$, it is suppressed by increased impurity scattering, whereas $\sigma_{xy}^{\rm int}$ – an interband effect – is unaffected. In the moderately dirty regime where the quasiparticle damping is larger than the energy splitting at the avoided crossing (typically, the SOI energy) but less than the bandwidth, $\sigma_{xy}^{\rm int}$ dominates $\sigma_{xy}^{\rm skew}$. As a result, one expects a crossover from the extrinsic to the intrinsic regime. When skew scattering is due to a spin-dependent scattering potential instead of spin-orbit coupling in the Bloch states, the skew to intrinsic crossover could be controlled by a different condition. In this minimal model, a well-defined plateau is not well-reproduced in the intrinsic regime unless a weak impurity potential is assumed (Onoda *et al.*, 2008). This crossover may be seen when the skew-scattering term shares the same sign as the intrinsic one (Kovalev *et al.*, 2009).

With further increase in the scattering strength, spectral broadening leads to the scaling relationship $\sigma_{xy} \propto \sigma_{xx}^{1.6}$, as discussed above (Kovalev *et al.*, 2009; Onoda *et al.*, 2006b, 2008). In the strong-disorder regime, σ_{xx} is no longer linear in the scattering lifetime τ. A different scaling, $\sigma_{xy} \propto \sigma_{xx}^2$, attributed to broadening of the electronic spectrum in the intrinsic regime, has been proposed by Kontani *et al.* (Kontani *et al.*, 2007).

As discussed above, there is some experimental evidence that this scaling prevails not only in the dirty metallic regime, but also deep into the hopping regime. Sangio *et al.* (Sangiao *et al.*, 2009), for e.g., obtained the exponent $\alpha \simeq 1.7$ in epitaxial thin-film Fe in the dirty regime. In manganite, scaling seems to hold, with the same nominal value of α, even below the Verwey transition where charge transport is deep in the hopping regime (Fernandez-Pacheco *et al.*, 2008; Venkateshvaran *et al.*, 2008). These regimes are well beyond the purview of either the minimal model, which considers only elastic scattering, or the theoretical approximations used to model its properties (Onoda *et al.*, 2006b, 2008).

Nonetheless, the experimental reports have uncovered a robust scaling relationship with α near 1.6, which extends over a remarkably large range of σ_{xx}. The origin of this scaling is an open issue at present.

B. Complex oxide ferromagnets

1. First-principles calculations and experiments on $SrRuO_3$

The perovskite oxide $SrRuO_3$ is an itinerant ferromagnet with a critical temperature T_c of 165 K. The electrons occupying the $4d$ t_{2g} orbitals in Ru^{4+} have a SOI energy much larger than that for $3d$ electrons. Early transport investigations of this material were reported in Refs. Allen *et al.*, 1996 and Izumi *et al.*, 1997. The latter authors also reported results on thin-film $SrTiO_3$. Recently, the Berry-phase theory has been applied to account for its AHE (Fang *et al.*, 2003; Mathieu *et al.*, 2004a,b), which

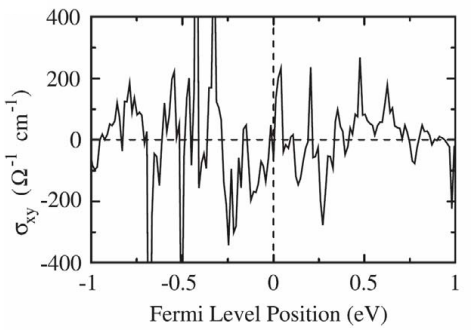


FIG. 12 The calculated transverse conductivity σ_{xy} as a function of the chemical potential μ for $SrRuO_3$. The chaotic behavior is the fingerprint of the Berry curvature distribution illustrated in Fig. 13. [From Ref. Fang *et al.*, 2003.]

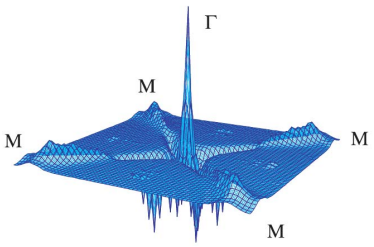


FIG. 13 The Berry curvature $b_z(\boldsymbol{k})$ for a band as a function of $\boldsymbol{k}_\perp = (k_x, k_y)$ with the fixed $k_z = 0$. [From Ref. Fang *et al.*, 2003.]

is strongly T dependent (Fig.11c). Neither the KL theory nor the skew-scattering theory seemed adequate for explaining the T dependence of the inferred AHE conductivity σ_{xy} (Fang *et al.*, 2003).

The experimental results motivated a detailed first-principles, band-structure calculation that fully incorporated the SOI. The AHE conductivity σ_{xy} was calculated directly using the Kubo formula Eq. (1.2) (Fang *et al.*, 2003). To handle numerical instabilities which arise near certain critical points, a fictitious energy broadening δ = 70 meV was introduced in the energy denominator. Fig. 12 shows the dependence of $\sigma_{xy}(\mu)$ on the chemical potential μ. In sharp contrast to the diagonal conductivity σ_{xx}, $\sigma_{xy}(\mu)$ fluctuates strongly, displaying sharp peaks and numerous changes in sign. The fluctuations may be understood if we map the momentum dependence of the Berry curvature $b_z(\boldsymbol{k})$ in the occupied band. For example, Fig. 13 displays $b_z(\boldsymbol{k})$ plotted as a function of $\boldsymbol{k}_\perp = (k_x, k_y)$, with k_z fixed at 0. The prominent peak at $\boldsymbol{k}_\perp = \boldsymbol{0}$ corresponds to the avoided crossing of the energy band dispersions, which are split by the SOI. As discussed in Sec. I.B, variation of the exchange splitting caused by a change in the spontaneous magnetization M strongly affects σ_{xy} in a nontrivial way.

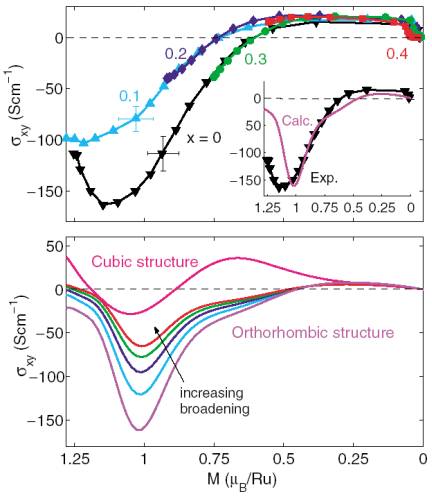


FIG. 14 (Upper panel) Combined plots of the Hall conductivity σ_{xy} vs. magnetization M in 5 samples of the ruthenate $Sr_{1-x}Ca_xRuO_3$ ($0 \leq x \leq 0.4$). The inset compares data σ_{xy} at $x = 0$ (triangles) with calculated values (solid curve). (Lower panel) First-principles calculations of σ_{xy} vs. M for cubic and orthorhombic structures. The effect of broadening on the curves is shown for the orthorhombic case. [From Ref. Mathieu *et al.*, 2004b.]

From the first-principles calculations, one may estimate the temperature dependence of σ_{xy} by assuming that it is due to the temperature-dependence of the Bloch state exchange splitting and that this splitting is proportional to the temperature-dependent magnetization. The new insight is that the T-dependence of $\sigma_{xy}(T)$ simply reflects the M dependence of σ_{xy}: at a finite temperature T', the magnitude and sign of σ_{xy} may be deduced by using the value of $M(T')$ in the zero-T curve. This proposal was tested against the results on both the pure material and the Ca-doped material $Sr_{1-x}Ca_xRuO_3$. In the latter, Ca doping suppresses both T_c and M systematically (Mathieu *et al.*, 2004a,b). As shown in Fig. 14 (upper panel), the measured values of M and σ_{xy}, obtained from 5 samples with Ca content $0.4 \leq x \leq 0$, fall on 2 continuous curves. In the inset, the curve for the pure sample ($x = 0$) is compared with the calculation. The lower panel of Fig. 14 compares calculated curves of σ_{xy} for cubic and orthorhombic lattice structures. The sensitivity of σ_{xy} to the lattice symmetry reflects the dominant contribution of the avoided crossing near ε_F. The sensitivity to broadening is shown for the orthorhombic case.

Kats *et al.* (Kats *et al.*, 2004) also have studied the magnetic field dependence of ρ_{xy} in an epitaxial film of $SrRuO_3$. They have observed sign-changes in ρ_{xy} near a magnetic field $B = 3$ T at $T = 130$ K and near $B = 8$ T at 134 K. This seems to be qualitative consistent with the Berry-phase scenario. On the other hand the authors suggest that the intrinsic-dominated picture is likely incomplete (or incorrect) near Tc (Kats *et al.*, 2004).

In the manganites, e.g. $La_{1-x}Ca_xMnO_3$ (LCMO), the three t_{2g} electrons on each Mn ion form a core local moment of spin $S = \frac{3}{2}$. A large Hund energy J_H aligns the core spin $\mathbf{S}$ with the $s = \frac{1}{2}$ spin of an itinerant electron that momentarily occupies the e_g orbital. Because this Hund coupling leads to an extraordinary magnetoresistance in weak H, the manganites are called colossal magnetoresistance (CMR) materials (Tokura and Tomioka, 1999). The double exchange theory summarized by Eq. (2.2) (below) is widely adopted to describe the onset of ferromagnetism in the CMR manganites.

As T decreases below the Curie temperature $T_C \simeq 270$ K in LCMO, the resistivity ρ falls rapidly from $\sim$15 mΩ cm to metallic values <2 mΩcm. CMR is observed over a significant interval of temperatures above and below T_C, where charge transport occurs by hopping of electrons between adjacent Mn ions (Fig. 15a). At each Mn site i, the Hund energy tends to align the carrier spin $\mathbf{s}$ with the core spin $\boldsymbol{S}_i$.

Early theories of hopping conductivity (Holstein, 1961) predicted the existence of a Hall current produced by the phase shift (Peierls factor) associated with the magnetic flux ϕ piercing the area defined by 3 non-collinear atoms. However, the hopping Hall current is weak. The observation of a large ρ_{xy} in LCMO that attains a broad maximum in modest H (Fig. 15b) led Matl *et al.* (Matl *et al.*, 1998) to propose that the phase shift is geometric in origin, arising from the solid angle described by $\boldsymbol{s}$ as the electron visits each Mn site ($\boldsymbol{s}||\boldsymbol{S}_i$ at each site i as shown in Fig. 16). To obtain the large ρ_{xy} seen, one requires $\boldsymbol{S}_i$ to define a finite solid angle Ω. Since $\boldsymbol{S}_i$ gradually aligns with $\mathbf{H}$ with increasing field, this effect should disappear along with $\langle\Omega\rangle$, as observed in the experiment. This appears to be the first application of a geometric-phase mechanism to account for an AHE experiment.

Subsequently, Ye *et al.* (Ye *et al.*, 1999) considered the Berry phase due to the thermal excitations of the Skyrmion (and anti-Skyrmion). They argued that the SOI gives rise to a coupling between the uniform magnetization $\boldsymbol{M}$ and the gauge field $\boldsymbol{b}$ by the term $\lambda \boldsymbol{M} \cdot \boldsymbol{b}$. In the ferromagnetic state, the spontaneous uniform magnetization $\boldsymbol{M}$ leads to a finite and uniform $\boldsymbol{b}$, which acts as a uniform magnetic field. Lyanda-Geller *et al.* (Lyanda-Geller *et al.*, 2001) also considered the AHE due to the spin chirality fluctuation in the incoherent limit where the hopping is treated perturbatively. This approach, applicable to the high-T limit, complements the theory of Ye *et al.* (Ye *et al.*, 1999).

The Berry phase associated with non-coplanar spin configurations, the scalar spin chirality, was first considered in theories of high-temperature superconductors in the context of the flux distribution generated by the complex order parameter of the resonating valence bond (RVB) correlation defined by χ_{ij}, which acts as the transfer integral of the "spinon" between the sites i and j (Lee *et al.*, 2006). The complex transfer integral also appears

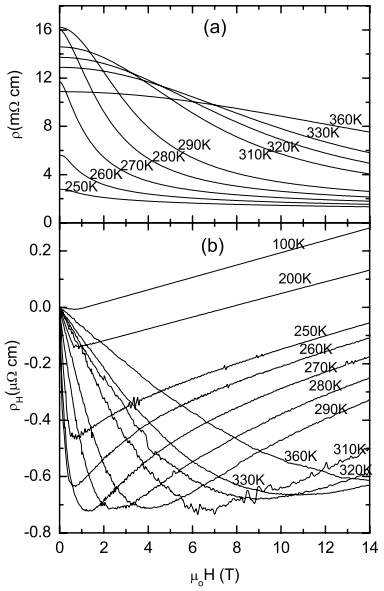


FIG. 15 (a) The colossal magnetoresistance ρ vs. H in $La_{1-x}Ca_xMnO_3$ ($T_C = 265$ K) at selected T. (b) The Hall resistivity ρ_{xy} vs. H at temperatures 100 to 360 K. Above T_C, ρ_{xy} is strongly influenced by the MR and the susceptibility χ. [From Ref. Matl *et al.*, 1998.]

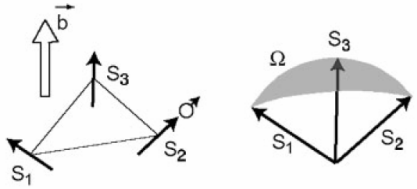


FIG. 16 Schematic view of spin chirality. When circulates among three spins to which it is exchange-coupled, it feels a fictitious magnetic field $\vec{b}$ with flux given by the half of the solid angle Ω subtended by the three spins. [From Ref. Lee *et al.*, 2006.]

in the double-exchange model specified by

$$H = -\sum_{ij,\alpha} t_{ij}(c^\dagger_{i\alpha}c_{j\alpha} + h.c.) - J_H \sum_i \boldsymbol{S}_i \cdot c^\dagger_{i\alpha}\boldsymbol{\sigma}_{\alpha\beta}c_{i\beta}, \quad (2.2)$$

where J_H is the ferromagnetic Hund's coupling between the spin $\boldsymbol{\sigma}$ of the conduction electrons and the localized spins $\boldsymbol{S}_i$.

In the manganese oxides, $\boldsymbol{S}_i$ represents the localized spin in t_{2g}-orbitals, while $c^\dagger$ and c are the operators for e_g-electrons. (The mean-field approximations of Hubbard-like theories of magnetism, the localized spin may also be regarded as the molecular field created by

the conduction electrons themselves, in which case J_H is replaced by the on-site Coulomb interaction energy U.) In the limit of large J_H, the conduction electron spin $\boldsymbol{s}$ is forced to align with $\boldsymbol{S}_i$ at each site. The matrix element for hopping from $i \to j$ is then given by

$$t_{ij}^{\rm eff} = t_{ij}\langle\chi_i|\chi_j\rangle = t_{ij}e^{ia_{ij}}\cos\left(\frac{\theta_{ij}}{2}\right), \qquad (2.3)$$

where $|\chi_i\rangle$ is the two-component spinor spin wave function with quantization axis $||\boldsymbol{S}_i$. The phase factor $e^{ia_{ij}}$ acts like a Peierls phase and can be viewed as originating from a fictitious magnetic field which influences the orbital motion of the conduction electrons.

We next discuss how the Peierls phase leads to a gauge field, i.e. flux, in the presence of non-coplanar spin configurations. Let $\boldsymbol{S}_i$, $\boldsymbol{S}_j$, and $\boldsymbol{S}_k$ be the local spins at sites i, j, and k, respectively. The product of the three transfer integrals corresponding to the loop $i \to j \to k \to i$ is

$$\begin{aligned} & \langle\boldsymbol{n}_i|\boldsymbol{n}_k\rangle\langle\boldsymbol{n}_k|\boldsymbol{n}_j\rangle\langle\boldsymbol{n}_j|\boldsymbol{n}_i\rangle \\ = \; & (1+\boldsymbol{n}_i\cdot\boldsymbol{n}_j+\boldsymbol{n}_j\cdot\boldsymbol{n}_k+\boldsymbol{n}_k\cdot\boldsymbol{n}_j)+i\boldsymbol{n}_i\cdot(\boldsymbol{n}_j\times\boldsymbol{n}_k) \\ \propto \; & e^{i(a_{ij}+a_{jk}+a_{ki})} = e^{i\Omega/2} \end{aligned} \qquad (2.4)$$

where $|\boldsymbol{n}_i\rangle$ is the two-component spinor wavefunction of the spin state polarized along $\boldsymbol{n}_i = \boldsymbol{S}_i/|\boldsymbol{S}_i|$. Its imaginary part is proportional to $\boldsymbol{S}_i\cdot(\boldsymbol{S}_j\times\boldsymbol{S}_k)$, which corresponds to the solid angle Ω subtended by the three spins on the unit sphere, and is called the scalar spin chirality (Fig. 16). The phase acquired by the electron's wave function around the loop is $e^{i\Omega/2}$, which leads to the Aharonov-Bohm (AB) effect and, as a consequence, to a large Hall response.

In the continuum approximation, this phase factor is given by the flux of the "effective" magnetic field $\boldsymbol{b}\cdot d\boldsymbol{S} = \nabla\times\boldsymbol{a}\cdot d\boldsymbol{S}$ where $d\boldsymbol{S}$ is the elemental directed surface area defined by the three sites. The discussion implies that a large Hall current requires the unit vector $\boldsymbol{n}(\boldsymbol{x}) = \boldsymbol{S}(\boldsymbol{x})/|\boldsymbol{S}(\boldsymbol{x})|$ to fluctuate strongly as a function of $\boldsymbol{x}$, the position coordinate in the sample. An insightful way to quantify this fluctuation is to regard $\boldsymbol{n}(\boldsymbol{x})$ as a map from the x-y plane to the surface of the unit sphere (we take a 2D sample for simplicity). An important defect in a ferromagnet – the Skyrmion (Sondhi *et al.*, 1993) – occurs when $\boldsymbol{n}(\boldsymbol{x})$ points down at a point $\boldsymbol{x}'$ in a region $\mathcal{A}$ of the x-y plane, but gradually relaxes back to up at the boundary of $\mathcal{A}$. The map of this spin texture wraps around the sphere once as $\boldsymbol{x}'$ roams over $\mathcal{A}$. The number of Skyrmions in the sample is given by the topological index

$$N_s = \int_{\mathcal{A}} dxdy \;\; \boldsymbol{n}\cdot\left(\frac{\partial\boldsymbol{n}}{\partial x}\times\frac{\partial\boldsymbol{n}}{\partial y}\right) = \int_{\mathcal{A}} dxdy\; b_z, \qquad (2.5)$$

where the first integrand is the directed area of the image on the unit sphere. N_s counts the number of times the map covers the sphere as $\mathcal{A}$ extends over the sample. The gauge field $\boldsymbol{b}$ produces a Hall conductivity. Ye *et al.* (Ye *et al.*, 1999) derived in the continuum approximation the coupling between the field $\boldsymbol{b}$ and the spontaneuos magnetization $\boldsymbol{M}$ through the SOI. The SOI coupling produces an excess of thermally excited positive Skyrmions over negative ones. This imbalance leads to a net uniform "magnetic field" $\boldsymbol{b}$ (anti)parallel to $\boldsymbol{M}$, and the AHE. In this scenario, ρ_{xy} is predicted to attain a maximum slightly below T_c, before falling exponentially to zero as $T \to 0$.

The Hall effect in the hopping regime has been discussed by Holstein (Holstein, 1961) in the context of impurity conduction in semiconductors. Since the energies ε_j and ε_k of adjacent impurity sites may differ significantly, charge conduction must proceed by phonon-assisted hopping. To obtain a Hall effect, we consider 3 non-collinear sites (labelled as $i = 1$, 2 and 3). In a field H, the magnetic flux ϕ piercing the area enclosed by the 3 sites plays the key role in the Hall response. According to Holstein, the Hall current arises from interference between the direct hopping path $1 \to 2$ and the path $1 \to 3 \to 2$ going via 3 as an intermediate step. Taking into account the changes in the phonon number in each process, we have

$$\begin{aligned} (1, N_\lambda, N_{\lambda'}) \;&\to\; (1, N_\lambda \mp 1, N_{\lambda'}) \to (2, N_\lambda \mp 1, N_{\lambda'} \mp 1), \\ (1, N_\lambda, N_{\lambda'}) \;&\to\; (3, N_\lambda \mp 1, N_{\lambda'}) \to (2, N_\lambda \mp 1, N_{\lambda'} \mp 1), \end{aligned} \qquad (2.6)$$

where $N_\lambda, N_{\lambda'}$ are the phonon numbers for the modes λ, λ', respectively.

In a field H, the hopping matrix element from $\boldsymbol{R}_i$ to $\boldsymbol{R}_j$ includes the Peierls phase factor $\exp[-i(e/c)\int_{\boldsymbol{R}_i}^{\boldsymbol{R}_j} d\boldsymbol{r}\cdot\boldsymbol{A}(\boldsymbol{r})]$. When we consider the interference between the two processes in Eq. (2.6), the Peierls phase factors combine to produce the phase shift $\exp(i2\pi\phi/\phi_0)$ where $\phi_0 = hc/e$ is the flux quantum. By the Aharonov-Bohm effect, this leads to a Hall response.

As discussed, this idea was generalized for the manganites by replacing the Peierls phase factor with the Berry phase factor in Eq. (2.4) (Lyanda-Geller *et al.*, 2001). The calculated Hall conductivity is

$$\sigma_H = G(\{\varepsilon\})\cos(\theta_{ij}/2)\cos(\theta_{jk}/2)\cos(\theta_{ki}/2)\sin(\Omega/2), \qquad (2.7)$$

where $\{\varepsilon\}$ is the set of the energy levels ε_a $(a = i, j, k)$, and θ_{ij} is the angle between $\boldsymbol{n}_i$ and $\boldsymbol{n}_j$. When the average of σ_H over all directions of $\boldsymbol{n}_a$ is taken, it vanishes even for finite spontaneous magnetization m. To obtain a finite σ_{xy}, it is necessary to incorporate SOI.

Assuming the form of hopping integral with the SOI given by

$$V_{jk} = V_{jk}^{\rm orb}(1 + i\boldsymbol{\sigma}\cdot\boldsymbol{g}_{jk}), \qquad (2.8)$$

the Hall conductivity is proportional to the average of

$$[\boldsymbol{g}_{jk}\cdot(\boldsymbol{n}_j\times\boldsymbol{n}_k)][\boldsymbol{n}_1\cdot\boldsymbol{n}_2\times\boldsymbol{n}_3]. \qquad (2.9)$$

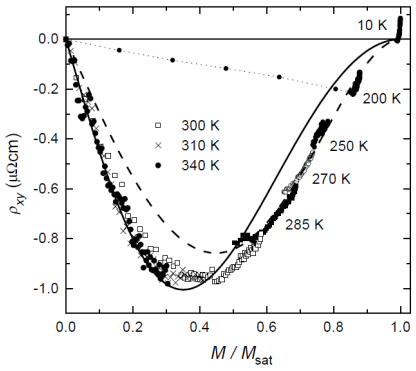


FIG. 17 Comparison between experiment and the theoretical prediction Eq.(2.10). Scaling behavior between the Hall resistivity ρ_H and the magnetization M is shown. The solid line is a fit to Eq.(2.10); the dashed line is the numerator of Eq.(2.10) only. There are no fitting parameters except the overall scale. [From Ref. Chun *et al.*, 2000.]

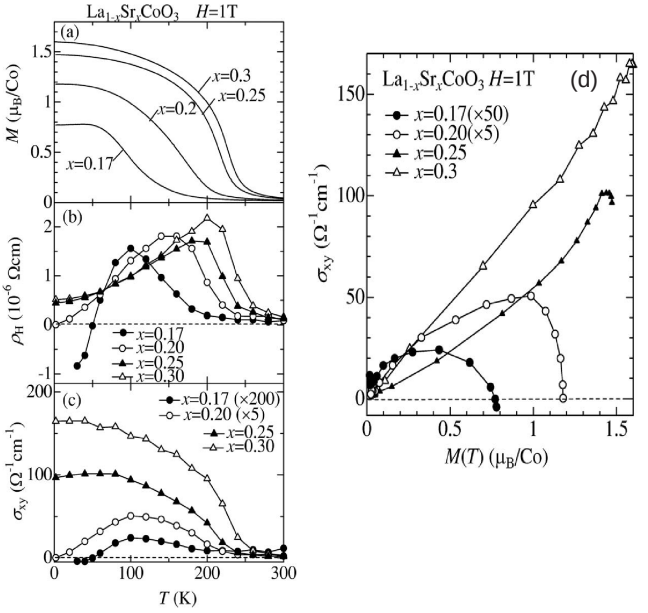


FIG. 18 Temperature dependence of the magnetization M (a), Hall resistivity ρ_{xy} (b), Hall conductivity σ_{xy} (c), in four crystals of $La_{1-x}Sr_xCoO_3$ ($0.17 \leq x \leq 0.30$) (all measured in a field $H = 1$ T). In Panels a, b and c, the data for $x = 0.17$ and 0.20 were multiplied by a factor of 200 and 50, respectively. (d) The Hall conductivity σ_{xy} at 1 T in the four crystals plotted against M. Results for $x = 0.17$ and 0.20 were multiplied by factors 50 and 5, respectively. [From Ref. Onose and Tokura, 2006.]

Taking the average of $\boldsymbol{n}$'s with $m = M/M_{sat}$ where M_{sat} is the saturated magnetization, we finally obtain

$$\rho_{xy} = \rho_{xy}^0 \frac{m(1-m^2)^2}{(1+m^2)^2}. \qquad (2.10)$$

This prediction has been tested by the experiment of Chun *et al.* (Chun *et al.*, 2000) shown in Fig. 17. The scaling law for the anomalous ρ_{xy} as a function of $|\mathbf{M}|$ obtained near T_C is in good agreement with the experiment.

Similar ideas have been used by Burkov and Balents (Burkov and Balents, 2003) to analyze the variable range hopping region in (Ga,Mn)As. The spin-chirality mechanism for the AHE has also been applied to CrO_2 (Yanagihara and Salamon, 2002, 2007), and the element Gd (Baily and Salamon, 2005). In the former case, the comparison between ρ_{xy} and the specific heat supports the claim that the critical properties of ρ_{xy} are governed by the Skyrmion density.

The theories described above assume large Hund coupling. In the weak-Hund coupling limit, a perturbative treatment in J_H has been developed to relate the AHE conductivity to the scalar spin chirality (Tatara and Kawamura, 2002). This theory has been applied to metallic spin-glass systems (Kawamura, 2007).

3. Lanthanum cobaltite

The subtleties and complications involved in analyzing the Hall conductivity of tunable ferromagnetic oxides are well illustrated by the cobaltites. Samoilov *et al.* (Samoilov *et al.*, 1998), and Baily and Salamon (Baily and Salamon, 2003) investigated the AHE in Ca-doped lanthanum cobaltite $La_{1-x}Ca_xCoO_3$, which displays a number of unusual magnetic and transport properties. They found an unusually large AHE near T_C as well as at low T, and proposed the relevance of spin-ordered clusters and orbital disorder scattering to the AHE in the low-T limit. Subsequently, a more detailed investigation of $La_{1-x}Sr_xCoO_3$ was reported by Onose and Tokura (Onose and Tokura, 2006). Figs. 18 a, b and c summarize the T dependence of M, ρ_{xy} and σ_{xy}, respectively in four crystals with $0.17 \leq x \leq 0.30$. The variation of ρ_{xx} vs. x suggests that a metal-insulator transition occurs between 0.17 and 0.19. Whereas the samples with $x \geq 0.2$ have a metallic ρ_{xx}-T profile, the sample with $x = 0.17$ is non-metallic (hopping conduction). Moreover, it displays a very large MR at low T and large hysteresis in curves of M vs. H, features that are consistent with a ferromagnetic cluster-glass state.

When the Hall conductivity is plotted vs. M (Fig. 18 d), σ_{xy} shows a linear dependence on M for the most metallic sample ($x = 0.30$). However, for $x = 0.17$ and 0.20, there is a pronounced downturn suggestive of the appearance of a different Hall term that is electron-like in sign. This is most apparent in the trend of the curves of ρ_{xy} vs. T in Fig. 18 b. Onose and Tokura (Onose and Tokura, 2006) propose that the negative term may arise from hopping of carriers between local moments which define a chirality that is finite, as discussed above.

4. Spin chirality mechanism in pyrochlore ferromagnets

In the examples discussed in the previous subsection, the spin-chirality mechanism leads to a large AHE at finite temperatures. An interesting question is whether or not there exist ferromagnets in which the spin chirality is finite in the ground state.

Ohgushi *et al.* (Ohgushi *et al.*, 2000) considered the ground state of the non-coplanar spin configuration in the Kagome lattice, which may be obtained as a projection of the pyrochlore lattice onto the plane normal to (1,1,1) axis. Considering the double exchange model Eq. (2.2), they obtained the band structure of the conduction electrons and the Berry phase distribution. Quite similar to the Haldane model (Haldane, 1988) or the model discussed in Eq. (3.21), the Chern number of each band becomes nonzero, and a quantized Hall effect results when the chemical potential is in the energy gap.

Turning to real materials, the pyrochlore ferromagnet $Nd_2Mo_2O_7$ (NMO) provides a test-bed for exploring these issues. Its lattice structure consists of two interpenetrating sublattices comprised of tetrahedrons of Nd and Mo atoms, respectively (the sublattices are shifted along the c-axis) (Taguchi *et al.*, 2001; Yoshii *et al.*, 2000). While the exchange between spins on either sublattice is ferromagnetic, the exchange coupling J_{df} between spins of the conducting d-electrons of Mo and localized f-electron spins on Nd is antiferromagnetic.

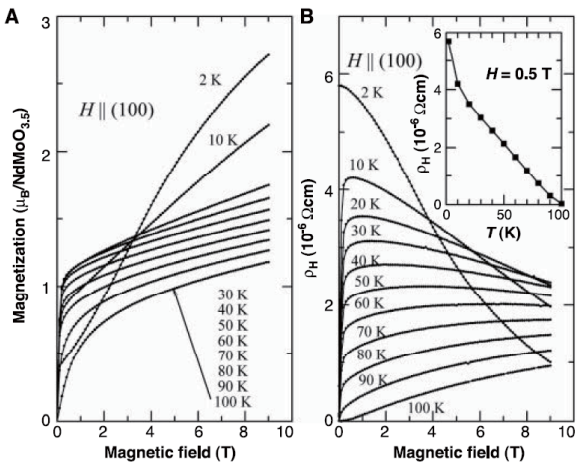


FIG. 19 Anomalous Hall effect in $Nd_2Mo_2O_7$. Magnetic field dependence of (A) the magnetization and (B) the transverse resistivity (ρ_{xy}) for different temperatures. [From Ref. Taguchi *et al.*, 2001.]

The dependences of the anomalous Hall resistivity ρ_{xy} on H at selected temperatures are shown in Fig. 19. The spins of Nd begin to align antiparallel to those of Mo below the crossover temperature $T^* \cong 40$ K. Each Nd spin is subject to a strong easy-axis anisotropy along the line from a vertex of the Nd tetrahedron to its center. The resulting noncoplanar spin configuration induces a transverse component of the Mo spins. Spin chirality is expected to be produced by the coupling J_{df}, which leads to the AHE of d-electrons. An analysis of the neutron scattering experiment has determined the magnetic structure (Taguchi *et al.*, 2001). The tilt angle of the Nd spins is close to that expected from the strong limit of the spin anisotropy, and the exchange coupling J_{fd} is estimated as $J_{fd} \sim 5$ K. This leads to a tilt angle of the Mo spins of $\sim 5^{\rm o}$. From these estimates, a calculation of the anomalous Hall conductivity in a tight-binding Hamiltonian of triply degenerate t_{2g} bands leads to $\sigma_H \sim 20\ (\Omega{\rm cm})^{-1}$, consistent with the value measured at low T. In a strong H, this tilt angle is expected to be reduced along with ρ_{xy}. This is in agreement with the traces displayed in Fig. 19.

The T dependence of the Hall conductivity has also been analyzed in the spin-chirality scenario by incorporating spin fluctuations (Onoda and Nagaosa, 2003). The result is that frustration of the Ising Nd spins leads to large fluctuations, which accounts for the large ρ observed. The recent observation of a sign-change in σ_{xy} in a field $\boldsymbol{H}$ applied in the $[1,1,1]$ direction (Taguchi *et al.*, 2003) is consistent with the sign-change of the spin chirality.

In the system $Gd_2Mo_2O_7$ (GMO), in which Gd^{3+} (d^7) has no spin anisotropy, the low-T AHE is an order-of-magnitude smaller than that in NMO. This is consistent with the spin-chirality scenario (Taguchi *et al.*, 2004). The effect of the spin chirality mechanism on the finite-frequency conductivity $\sigma_H(\omega)$ has been investigated (Kezsmarki *et al.*, 2005).

In another work, Yasui *et al.* (Yasui *et al.*, 2006, 2007) performed neutron scattering experiments over a large region in the (H,T)-plane with $\boldsymbol{H}$ along the $[0,\bar{1},1]$ and $[0,0,1]$ directions. By fitting the magnetization $M_{\rm Nd}(H,T)$ of Nd, the magnetic specific heat $C_{\rm mag}(H,T)$, and the magnetic scattering intensity $I_{\rm mag}(Q,H,T)$, they estimated $J_{dj} \cong 0.5$ K, which was considerably smaller than estimated previously (Taguchi *et al.*, 2001). Furthermore, they calculated the thermal average of the spin chirality $\langle \boldsymbol{S}_i \cdot \boldsymbol{S}_j \times \boldsymbol{S}_k \rangle$ and compared its value with that inferred from the AHE resistivity ρ_{xy}. They have emphasized that, when a 3-Tesla field is applied in the $[0,0,1]$ direction (along this direction H cancels the exchange field from the Mo spins), no appreciable reduction of ρ_{xy} is observed. These recent conclusions have cast doubt on the spin-chirality scenario for NMO.

A further puzzling feature is that, with $\boldsymbol{H}$ applied in the $[1,1,1]$ direction, one expects a discontinuous transition from the two-in, two-out structure (i.e. 2 of the Nd spins point towards the tetrahedron center while 2 point away) to the three-in, one-out structure for the Nd spins. However, no Hall features that might be identified with this cancellation have been observed down to very low T. This seems to suggest that quantum fluctuations of the Nd spins may play an important role, despite the large spin quantum number ($S = \frac{3}{2}$).

Machida has discussed the possible relevance of spin chirality to the AHE in the pyrochlore $Pr_2Ir_2O_7$

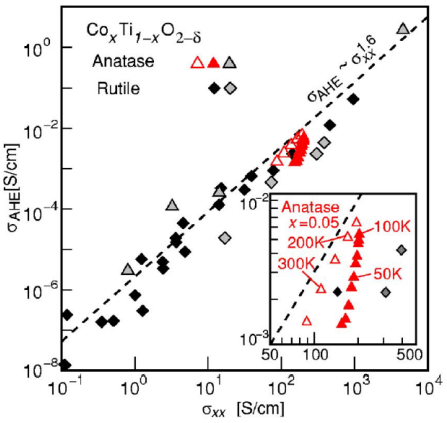


FIG. 20 Plot of AHE conductivity σ_{AHE} vs. conductivity σ for anatase $Ti_{1-x}Co_xO_{2-\delta}$ (triangles) and rutile $Ti_{1-x}Co_xO_{2-\delta}$ (diamonds). Grey symbols are data taken by other groups. The inset shows the expanded view of data for anatase with x= 0.05 (the open and closed triangles are for $T > 150$ K and $T < 100$ K, respectively. [From Ref. Ueno *et al.*, 2007.]

(Machida *et al.*, 2007a,b). In this system, a novel "Kondo effect" is observed even though the Pr^{3+} ions with $S = 1$ are subject to a large magnetic anisotropy. The magnetic and transport properties of $R_2Mo_2O_7$ near the phase boundary between the spin glass Mott insulator and ferromagnetic metal by changing the rare earth ion R has been studied (Katsufuji *et al.*, 2000).

5. Anatase and Rutile $Ti_{1-x}Co_xO_{2-\delta}$

In thin-film samples of the ferromagnetic semiconductor anatase $Ti_{1-x}Co_xO_{2-\delta}$, Ueno *et al.* (Ueno *et al.*, 2008) have reported scaling between the AHE resistance and the magnetization M. The AHE conductivity σ_{xy}^{AH} scales with the conductivity σ_{xx} as $\sigma_{xy}^{AH} \propto \sigma_{xx}^{1.6}$ (Fig. 20). A similar scaling relation was observed in another polymorph rutile. See also Ref. Ramaneti *et al.*, 2007 for related work on Co-doped TiO_2.

C. Ferromagnetic semiconductors

Ferromagnetic semiconductors combine semiconductor tunability and collective ferromagnetic properties in a single material. The most widely studied ferromagnetic semiconductors are diluted magnetic semiconductors (DMS) created by doping a host semiconductor with a transition metal which provides a localized large moment (formed by the d-electrons) and by introducing carriers which can mediate a ferromagnetic coupling between these local moments. The most extensively studied are the Mn based (III,Mn)V DMSs, in which substituting Mn for the cations in a (III,V) semiconductor can dope the system with hole carriers; (Ga,Mn)As becomes ferromagnetic beyond a concentration of 1%.

The simplicity of this basic but generally correct model hides within it a cornucopia of physical and materials science effects present in these materials. Among the phenomena which have been studied are metal-insulator transitions, carrier mediated ferromagnetism, disorder physics, magneto-resistance effects, magneto-optical effects, coupled magnetization dynamics, post-growth dependent properties, *etc.* A more in-depth discussion of these materials, both from the experimental and theoretical point of view, can be found in the recent review by Jungwirth *et al* (Jungwirth *et al.*, 2006).

The AHE has been one of the most fundamental characterization tools in DMSs, allowing, for example, direct electrical measurement of transition temperatures. The reliability of electrical measurement of magnetic properties in these materials has been verified by comparison with remnant magnetization measurements using a SQUID magnetometer (Ohno *et al.*, 1992). The relative simplicity of the effective band structure of the carriers in metallic DMSs, has made them a playing ground to understand AHE of ferromagnetic systems with strong spin-orbit coupling.

Experimentally, it has been established that the AHE in the archetypical DMS system (Ga,Mn)As is in the metallic regime dominated by a scattering-independent mechanism, i.e. $\rho_{xy}^{AH} \propto \rho_{xx}^2$ (Chun *et al.*, 2007; Edmonds *et al.*, 2002; Pu *et al.*, 2008; Ruzmetov *et al.*, 2004). The studies of Edmonds *et al.*, 2002 and Chun *et al.*, 2007 have established this relationship in the non-insulating materials by extrapolating the low temperature $\rho_{xy}(B)$ to zero field and zero temperature. This is illustrated in Fig. 21 where metallic samples, which span a larger range than the ones studied by Edmonds *et al.*, 2002, show a clear $R_S \sim \rho_{xx}^2$ dependence.

DMSs grown requires non-equilibrium (low temperature) conditions and the as-grown (often insulating) materials and post-grown annealed metallic materials show typically different behavior in the AHE response. A similar extrapolating procedure performed on insulating (Ga,Mn)As seems to exhibit a somewhat linear dependence of R_S on ρ_{xx}. On the other hand, considerable uncertainty is introduced by the extrapolation to low temperatures because ρ_{xx} diverges and the complicated magetoresistance of ρ_{xx} is a priori not known in the low T range.

A more recent study by Pu *et al.* (Pu *et al.*, 2008)of (Ga,Mn)As grown on InAs, such that the tensile strain creates a perpendicular anisotropic ferromagnet, has established the dominance of the intrinsic mechanism in metallic (Ga,Mn)As samples beyond any doubt. Measuring the longitudinal thermo-electric transport coefficients (ρ_{xx}, ρ_{xy}, α_{xy}, and α_{xx} where $\boldsymbol{J} = \sigma\boldsymbol{E} + \alpha(-\boldsymbol{\nabla}T)$), one can show that given the Mott relation $\alpha = \frac{\pi^2 k_B^2 T}{3e}(\frac{\partial\sigma}{\partial E})_{E_F}$ and the empirical relation $\rho_{xy}(B=0) = \lambda M_z \rho_{xx}^n$, the relation between the four separately measured transport

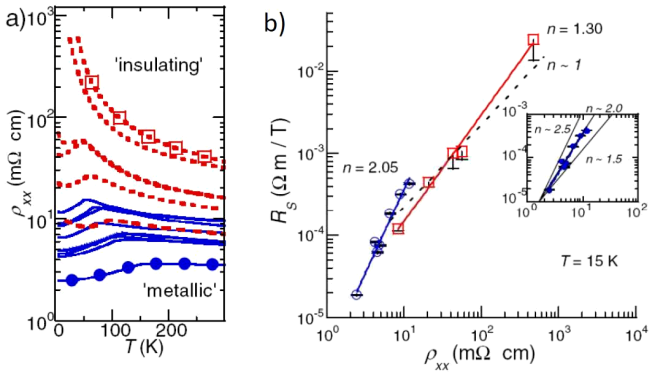


FIG. 21 (a) $Ga_{1-x}Mn_xAs$ samples that show insulating and metallic behavior defined by $\partial\rho_{xx}/\partial T$ near $T = 0$. (b) R_s vs. ρ_{xx} extrapolated from $\rho_{xy}(B)$ data to zero field and low temperatures. [From Ref. Chun *et al.*, 2007.]

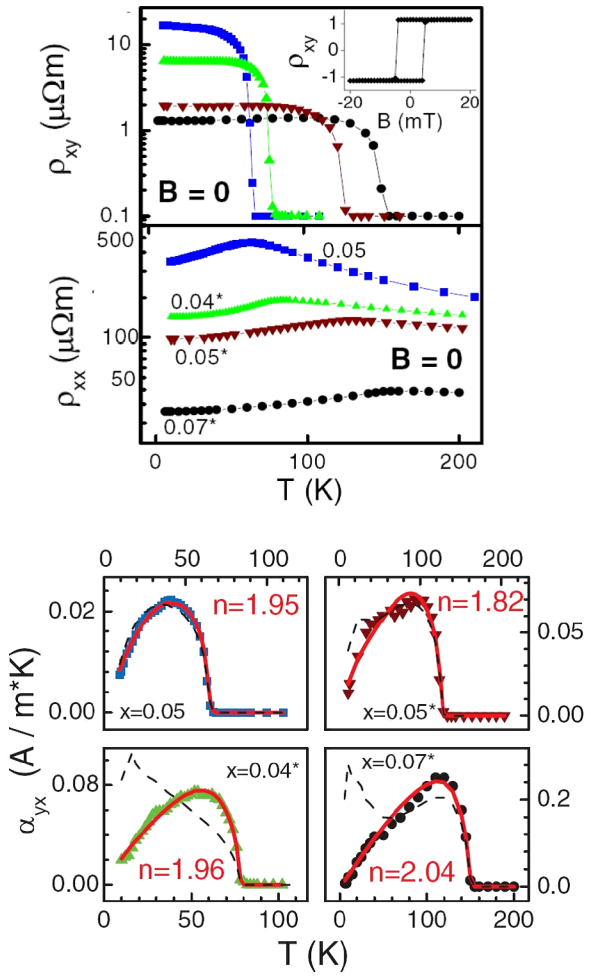


FIG. 22 (Top) Zero B field ρ_{xy} and ρ_{xx} for four samples grown on InAs substrates (i.e. perpendicular to plane easy axis). Annealed samples, which produce perpendicular to plane easy axes, are marked by a $*$. The inset indicates the B dependence of the 7% sample at 10 K. (Bottom) Zero-field Nerst coefficient α_{xy} for the four samples. The solid red curves indicate the best fit using Eq. (2.11) and the dashed curves the best fit setting n=1. [From Ref. Pu *et al.*, 2008.]

coefficients is:

$$\alpha_{xy} = \frac{\rho_{xy}}{\rho_{xx}^2}\left(\frac{\pi^2 k_B^2 T}{3e}\frac{\lambda'}{\lambda} - (n-2)\alpha_{xx}\rho xx\right). \qquad (2.11)$$

The fit to the $\frac{\lambda'}{\lambda}$ and n parameters are shown in Fig. 22. Fixing $n = 1$ does not produce any good fit to the data as indicated by the dashed lines in Fig. 22. These data excludes the possibility of a $n = 1$ type contribution to the AHE in metallic (Ga,Mn)As and further verify the validity the Mott relation in these materials.

Having established that the main contribution to the AHE in metallic (Ga,Mn)As is scattering-independent contributions, rather than skew-scattering contributions, DMSs are an ideal system to test our understanding of AHE. In the regime where the largest ferromagnetic critical temperatures are achieved (for doping levels above 1.5%), semi-phenomenological models that are built on Bloch states for the band quasiparticles, rather than localized basis states appropriate for the localized regime (Berciu and Bhatt, 2001), provide the natural starting point for a model Hamiltonian which reproduces many of the observed experimental effects (Jungwirth *et al.*, 2006; Sinova and Jungwirth, 2005). Recognizing that the length scales associated with holes in the DMS compounds are still long enough, a $\boldsymbol{k}\cdot\boldsymbol{p}$ envelope function description of the semiconductor valence bands is appropriate. To understand the AHE and magnetic anisotropy, it is necessary to incorporate intrinsic spin-orbit coupling in a realistic way.

A successful model for (Ga,Mn)As is specified by the effective Hamiltonian

$$\mathcal{H} = \mathcal{H}_{KL} + J_{pd}\sum_I \boldsymbol{S}_I \cdot \hat{\boldsymbol{s}}(\boldsymbol{r})\delta(\boldsymbol{r} - \boldsymbol{R}_I) + \mathcal{H}_{dis}, \quad (2.12)$$

where $\mathcal{H}_{KL}$ is the six-band Kohn-Luttinger (KL) $\boldsymbol{k}\cdot\boldsymbol{p}$ Hamiltonian (Dietl *et al.*, 2001), the second term is the short-range antiferromagnetic kinetic-exchange interaction between local spin $\boldsymbol{S}_I$ at site $\boldsymbol{R}_I$ and the itinerant hole spin (a finite range can be incorporated in more realistic models), and $\mathcal{H}_{dis}$ is the scalar scattering potential representing the difference between a valence band electron on a host site and a valence band electron on a Mn site and the screened Coulomb interaction of the itinerant electrons with the ionized impurities.

Several approximations can be used to vastly simplify the above model, namely, the virtual crystal approximation (replacing the spatial dependence of the local Mn moments by a constant average) and mean field theory in which quantum and thermal fluctuations of the local moment spin-orientations are ignored (Dietl *et al.*, 2001; Jungwirth *et al.*, 2006). In the metallic regime, disorder can be treated by a Born approximation or by more sophisticated, exact-diagonalization or Monte-Carlo methods (Jungwirth *et al.*, 2002a; Schliemann and MacDonald, 2002; Sinova *et al.*, 2002; Yang *et al.*, 2003).

Given the above simple model Hamiltonian the AHE can be computed if one assumes that the intrinsic

Berry's phase (or Karplus-Luttinger) contribution will most likely be dominan, because of the large SOI of the carriers and the experimental evidence showing the dominance of scattering-independent mechanisms. For practical calculations it is useful to use, as in the intrinsic AHE studies in the oxides (Fang *et al.*, 2003; Mathieu *et al.*, 2004a,b), the Kubo formalism given in Eq. (1.2) with disorder induced broadening, Γ, of the band-structure (but no side-jump contribution). The broadening is achieved by substituting one of the $(\varepsilon_n(\boldsymbol{k}) - \varepsilon_{n'}(\boldsymbol{k}))$ factors in the denominator by $(\varepsilon_n(\boldsymbol{k}) - \varepsilon_{n'}(\boldsymbol{k}) + i\Gamma)$. Applying this theory to metallic (III,Mn)V materials using both the 4-band and 6-band $\boldsymbol{k}\cdot\boldsymbol{p}$ description of the valence band electronic structure one obtains results in quantitative agreement with experimental data in (Ga,Mn)As and (In,Mn)As DMS (Jungwirth *et al.*, 2002b). In a follow up calculation Jungwirth *et al.* (Jungwirth *et al.*, 2003), a more quantitative comparison of the theory with experiments was made in order to account for finite quasiparticle lifetime effects in these strongly disorder systems. The effective lifetime for transitions between bands n and n', $\tau_{n,n'} \equiv 1/\Gamma_{n,n'}$, can be calculated by averaging quasiparticle scattering rates obtained from Fermi's golden rule including both screened Coulomb and exchange potentials of randomly distributed substitutional Mn and compensating defects as done in the dc Boltzman transport studies (Jungwirth *et al.*, 2002a; Sinova *et al.*, 2002). A systematic comparison between theoretical and experimental AHE data is shown in Fig. 23 (Jungwirth *et al.*, 2003). The results are plotted vs. nominal Mn concentration x while other parameters of the seven samples studied are listed in the figure legend. The measured σ_{AH} values are indicated by filled squares; triangles are theoretical results obtained for a disordered system assuming Mn-interstitial compensationg defects. The valence band hole eigenenergies $\varepsilon_{n\boldsymbol{k}}$ and eigenvectors $|n\boldsymbol{k}\rangle$ are obtained by solving the six-band Kohn-Luttinger Hamiltonian in the presence of the exchange field, $\boldsymbol{h} = N_{Mn}SJ_{pd}\hat{z}$ (Jungwirth *et al.*, 2006). Here $N_{Mn} = 4x/a_{DMS}^3$ is the Mn density in the $Mn_xGa_{1-x}As$ epilayer with a lattice constant a_{DMS}, the local Mn spin $S = 5/2$, and the exchange coupling constant $J_{pd} = 55$ meV nm^{-3}.

In general, when disorder is accounted for, the theory is in a good agreement with experimental data over the full range of Mn densities studied from $x = 1.5\%$ to $x = 8\%$. The effect of disorder, especially when assuming Mn-interstitial compensation, is particularly strong in the $x = 8\%$ sample shifting the theoretical σ_{AH} much closer to experiment, compared to the clean limit theory. The remaining quantitative discrepancies between theory and experiment have been attributed to the resolution in measuring experimental hole and Mn densities (Jungwirth *et al.*, 2003).

We conclude this section by mentioning the anomalous Hall effect in the non-metallic or insulating/hopping regimes. Experimental studies of (Ga,Mn)As digital ferromagnetic heterostructures, which consist of submonolayers of MnAs separated by spacer layers of GaAs,

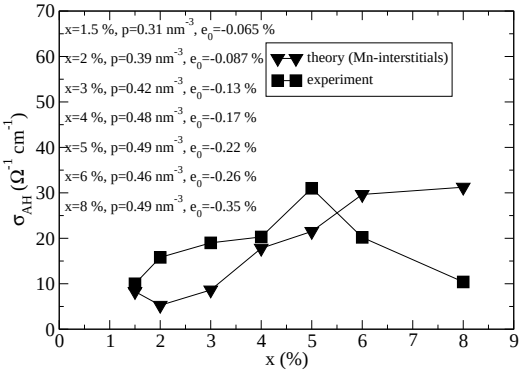


FIG. 23 Comparison between experimental and theoretical anomalous Hall conductivities. After Ref. Jungwirth *et al.*, 2003.

have shown longitudinal and Hall resistances of the hopping conduction type, $R_{xx} \propto T^{\alpha}\exp[(T_0/T)^{\beta}]$, and have shown that the anomalous Hall resistivity is dominated by hopping with a sublinear dependence of R_{AH} on R_{xx} (Allen *et al.*, 2004; Shen *et al.*, 2008), similar to experimental observations on other materials. Studies in this regime are still not as systematic as their metallic counterparts which clearly indicate a scaling power of 2. Experiments find a sublinear dependence of $R_{AH} \sim R_{xx}^{\beta}$, with $\beta \sim 0.2-1.0$ depending on the sample studies (Shen *et al.*, 2008). A theoretical understanding for this hopping regime remains to be worked out still. In previous theoretical calculations based on the hopping conduction with the Berry phase (Burkov and Balents, 2003) showed the insulating behavior $R_{AH} \to \infty$ as $R_{xx} \to \infty$ but failed to explain the scaling dependence of R_{AH} on R_{xx}.

D. Other classes of materials

1. Spinel $CuCr_2Se_4$

As mentioned in earlier sections, a key prediction of the KL theory (and its modern generalization, based on the Berry-phase approach) is that the AHE conductivity σ_{yx}^{AH} is independent of the carrier lifetime τ (dissipationless Hall current) in materials with moderate conductivity. This implies that the anomalous Hall resistivity ρ_{yx}^{AH} varies as ρ^2. Moreover, σ_{xy}^{AH} tend to be proportional to the observed magnetization M_z. We write

$$\sigma_{xy}^{AH} = S_H M_z, \tag{2.13}$$

with S_H a constant.

Previously, most tests were performed by comparing ρ_{yx} *vs.* ρ measured on the same sample over an extended temperature range. However, because the skew-scattering model can also lead to the same prediction $\rho_{yx} \sim \rho^2$ when inelastic scattering predominates, tests

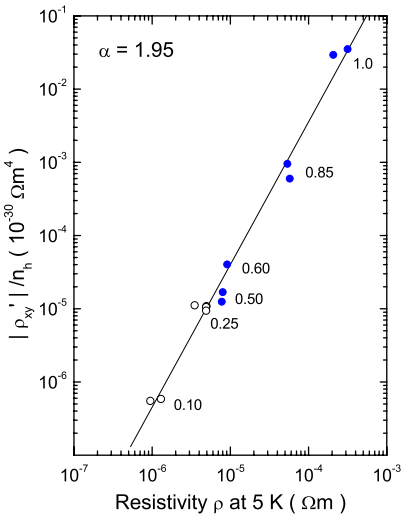


FIG. 24 Log-log plot of the quantity $|\rho'_{xy}|/n_h$ vs. ρ in twelve crystals of Br-doped spinel $CuCr_2Se_{4-x}Br_x$ with n_h the hole density (ρ is measured at 5 K; ρ_{xy} is measured at 2 and 5 K). Samples in which ρ_{yx} is electron-like (hole-like) are shown as open (closed) circles. The straight-line fit implies $|\rho'_{xy}|/n_h = A\rho^\alpha$ with $\alpha = 1.95 \pm 0.08$ and $A = 2.24\times10^{-25}$ (SI units). [From Ref. Lee *et al.*, 2004.]

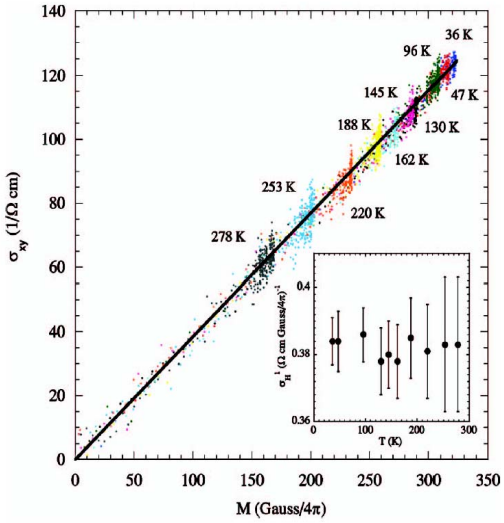


FIG. 25 Combined plots of σ_{xy} in the Heusler alloy Co_2CrAl versus the magnetization M at selected temperatures from 36 to 278 K. The inset shows the inferred values of $\sigma_{xy}^{AH} \equiv \sigma_{xy}/M$ at each T. [From Ref. Husmann and Singh, 2006.]

at finite T are inconclusive. The proper test requires a system in which ρ at 4 K can be varied over a very large range without degrading the exchange energy and magnetization M.

In the spinel $CuCr_2Se_4$, the ferromagnetic state is stabilized by 90° superexchange between the local moments of adjacent Cr ions. The charge carriers play only a weak role in the superexchange energy. The experimental proof of this is that when the carrier density n is varied by a factor of 20 (by substituting Se by Br), the Curie temperature T_C decreases by only 100 K from 380 K. Significantly, M at 4 K changes negligibly. The resistivity ρ at 4 K may be varied by a factor of 10^3 without weakening M. Detailed Hall and resistivity measurements were carried out by Lee *et al.* (Lee *et al.*, 2004) on twelve crystals of $CuCr_2Se_{4-x}Br_x$. They found that ρ_{yx} measured at 5 K changes sign (negative to positive) when x exceeds 0.4. At $x = 1$, ρ_{yx} attains very large values ($\simeq 700$ $\mu\Omega$cm at 5 K).

Lee *et al.* (Lee *et al.*, 2004) showed that the magnitude $|\rho_{yx}|/n$ varies as ρ^2 over 3 decades in ρ (Fig. 24), consistent with the prediction of the KL theory.

The AHE in the related materials $CuCr_2S_4$, $Cu_xZn_xCr_2Se_4$ ($x = \frac{1}{2}$) and Cu_3Te_4 has been investigated by Oda *et al.* (Oda *et al.*, 2001).

2. Heusler Alloy

The full Heusler alloy Co_2CrAl has the $L2_1$ lattice structure and orders ferromagnetically below 333 K. Several groups (Block *et al.*, 2004; Galanakis *et al.*, 2002) have argued that the conduction electrons are fully spin polarized ("half metal"). The absence of minority carrier spins is expected to simplify the analysis of the Hall conductivity. Hence this system is potentially an important system to test theories of the AHE.

The AHE has been investigated on single crystals with stoichiometry $Co_{2.06}Cr_{1.04}Al_{0.90}$ (Husmann and Singh, 2006). Below the Curie temperature $T_C = 333$ K, the magnetization M increases rapidly, eventually saturating to a low-T value that corresponds to 1.65 μ_B (Bohr magneton) per formula unit. Husmann and Singh show that, below ~310 K, $M(T)$ fits well to the form $[1-(T/T_C)^2]^{\frac{1}{2}}$. Assuming that the ordinary coefficient R_0 is negligible, they found that the Hall conductivity $\sigma_{xy} = \rho_{yx}/\rho^2$ is strictly linear in M (expressed as $\sigma_{xy} = \sigma_H^1 M$) over the T interval 36–278 K (Fig. 25). They interpret the linear variation as consistent with the intrinsic AHE theory. The value of $\sigma_H^1 = 0.383$ G/($4\pi\Omega$cm) inferred is similar to values derived from measurements on the dilute Ni alloys, half Heuslers and silicides.

3. $Fe_{1-y}Co_ySi$

The silicide FeSi is a non-magnetic Kondo insulator. Doping with Co leads to a metallic state with a low density p of holes. Over a range of Co doping ($0.05 < y < 0.8$) the ground state is a helical magnetic state with a peak Curie temperature $T_C \sim 50$ K. The magnetization corresponds to 1 μ_B (Bohr magneton) per Co ion. The tunability allows investigation of transport in a magnetic system with low p. Manyala *et al.* (Manyala *et al.*, 2004) observe that the Hall resistivity ρ_H increases to

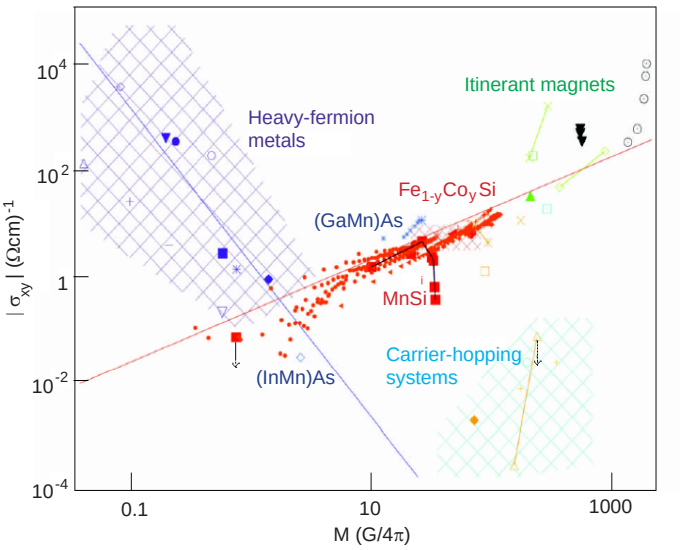


FIG. 26 Hall conductivity σ_{xy} of ferromagnetic metals and heavy fermion materials (collected at 1 kG and 5 K unless otherwise noted). Small solid circles represent $Fe_{1-y}Co_ySi$ for $5 < T < 75$ K and 500 G$< H <$ 50 kG with $y = 0.1$ (filled circles), 0.15 (filled triangles), $y = 0.2$ (+), and 0.3 (filled diamonds). MnSi data (5-35 K) are large, solid squares connected by black line. Small asterisks are (GaMn)As data for $5< T <$ 120 K. The rising line $\sigma_{xy} \sim M$ is consistent with the intrinsic AHE in itinerant ferromagnets while the falling line $\sigma_{xy} \sim M^{-3}$ applies to heavy fermions. [From Ref. Manyala *et al.*, 2004.]

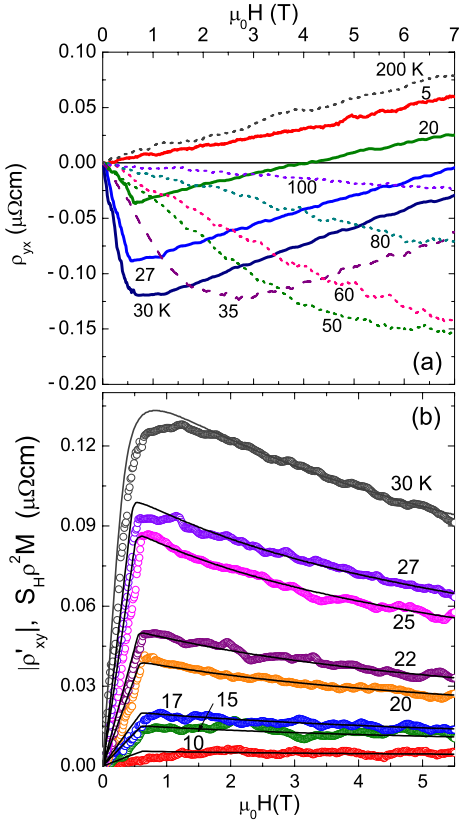


FIG. 27 (a) Hall resistivity ρ_{yx} vs. H in MnSi at selected T from 5 to 200 K. At high T, ρ_{yx} is linear in H, but gradually acquires an anomalous component $\rho'_{yx} = \rho_{yx} - R_0B$ with a prominent "knee" feature below $T_C = 30$ K. (b) Matching of the field profiles of the anomalous Hall resistivity ρ'_{yx} to the profiles of $\rho^2 M$, treating S_H and R_0 as adjustable parameters. Note the positive curvature of the high-field segments. [From Ref. Lee *et al.*, 2007.]

~1.5 $\mu\Omega$cm (at 5 K) at the doping y= 0.1. By plotting the observed Hall conductivity σ_{xy} against M, they find $\sigma_{xy} = S_H M$ with $S_H \sim 0.22$ G/(4$\pi\Omega$cm). In contrast, in heavy fermion systems (which include FeSi) $\sigma_{xy} \sim M^{-3}$.

4. MnSi

MnSi grows in the non-centrosymmetric B20 lattice structure which lacks inversion symmetry. Competition between the exchange energy J and Dzyaloshinsky-Moriya term D leads to a helical magnetic state with a long pitch λ (~180 Å). At ambient pressure, the helical state forms at the critical temperature $T_C = 30$ K. Under moderate hydrostatic pressure P, T_C decreases monotonically, reaching zero at the critical pressure P_c = 14 kbar. Although MnSi has been investigated for several decades, interest has been revived recently by a neutron scattering experiment which shows that, above P_c, MnSi displays an unusual magnetic phase in which the sharp magnetic Bragg spots at $P < P_c$ are replaced by a Bragg sphere (Pfleiderer *et al.*, 2004). Non-Fermi liquid exponents in the resistivity ρ vs. T are observed above P_c.

Among ferromagnets, MnSi at 4 K has a low resistivity ($\rho \sim$ 2-5 $\mu\Omega$cm). The unusually long carrier mean-free-path ℓ implies that the ordinary term $\sigma_{xy}^{NH} \sim \ell^2$ is greatly enhanced. In addition, the small ρ renders the total Hall voltage difficult to resolve. Both factors greatly complicate the task of separating σ_{xy}^{NH} from the AHE conductivity. However, the long ℓ in MnSi presents an opportunity to explore the AHE in the high-purity limit of ferromagnets. Using high-resolution measurements of the Hall resistivity ρ_{yx} (Fig. 27 a), Lee *et al.* (Lee *et al.*, 2007) recently accomplished this separation by exploiting the large longitudinal magnetoresistance (MR) $\rho(H)$. From Eq. (2.1) and (2.13), we have $\rho'_{yx}(H) = S_H \rho(H)^2 M(H)$, where $\rho'_{yx} = \rho^{AH}_{yx} = \rho_{yx} - R_0B$. At each T, the field profiles of $\rho'_{yx}(H)$ and $M(H)$ are matched by adjusting the two H-independent parameters S_H and R_0 (Fig. 27 b). The inferred parameters S_H and R_0 are found to be T independent below T_C (Fig. 28 a).

The Hall effect of MnSi under hydrostatic pressure (5–11.4 kbar) was measured recently (Lee *et al.*, 2008). In addition to the AHE and OHE terms σ_{xy}^{AH} and σ_{xy}^{NH}, Lee *et al.* observed a well-defined Hall term σ_{xy}^{C} with an unusual profile. As shown in Fig. 29 (note that in the figure σ_{xy}^{AH} and σ_{xy}^{NH} are labeled σ_{xy}^{A} and σ_{xy}^{N} respectively), the

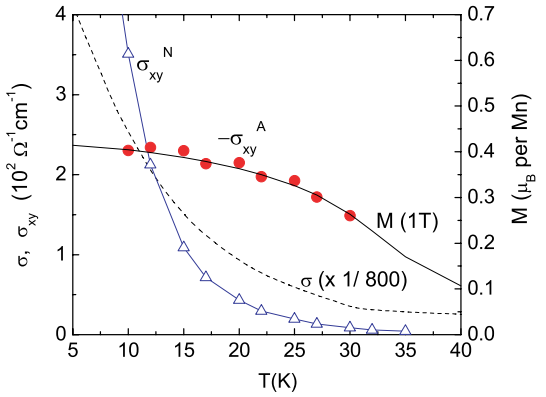


FIG. 28 Comparison of the anomalous Hall conductivity σ^A_{xy} and the ordinary term σ^N_{xy} measured in a 1-Tesla field in MnSi. σ^A_{xy}, inferred from the measured M (solid curve) and Eq. (2.13), is strictly independent of ℓ. Its T dependence reflects that of $M(T)$. $\sigma^N_{xy} \sim \ell^2$ is calculated from R_0. The conductivity at zero H, $\sigma \sim \ell$, is shown as a dashed curve. [From Ref. Lee *et al.*, 2007.]

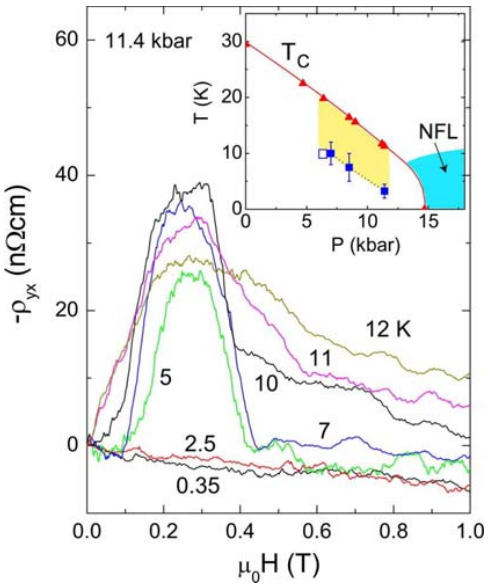


FIG. 29 (Main panel) $-\rho_{yx}$ vs. H in MnSi under hydrostatic pressure $P = 11.4$ kbar at several $T < T_C$, with $\boldsymbol{H}$ nominally along (111). The large Hall anomaly observed (electron-like in sign) arises from a new chiral contribution σ^C_{xy} to the total Hall conductivity. In the phase diagram (inset) the shaded region is where σ^C_{xy} is resolved. The non-Fermi liquid region is shaded blue. [From Ref. Lee *et al.*, 2008.]

new term appears abruptly at 0.1 T, rapidly rises to a large plateau value, and then vanishes at 0.45 T (curves at 5, 7 and 10 K). From the large magnitude of σ^C_{xy}, and its restriction to the field interval in which the cone angle is non-zero, the authors argue that it arises from the coupling of the carrier spin to the chiral spin textures in the helical magnetization, as discussed in Sec. II.B. The authors note that MnSi under pressure provides a very rare example in which the three Hall conductivities co-exist at the same T.

5. Mn_5Ge_3

The AHE in thin-film samples of Mn_5Ge_3 was investigated by Zeng *et al.* (Zeng *et al.*, 2006). They express the AHE resistivity ρ_{AH}, which is strongly T dependent (Fig. 30a), as the sum of the skew-scattering term $a(M)\rho_{xx}$ and the intrinsic term $b(M)\rho^2_{xx}$, viz.

$$\rho_{AH} = a(M)\rho_{xx} + b(M)\rho^2_{xx}. \qquad (2.14)$$

The quantity $b(M)$ is the intrinsic AHE conductivity σ_{AH-int}.

To separate the 2 terms, Zeng *et al.* plotted the quantity $\rho_{AH}/(M(T)\rho_{xx})$ against ρ_{xx} with T as a parameter. For $T < 0.8T_C$, the plot falls on a straight line with a small negative intercept (solid squares in Fig. 30b). The intercept yields the skew-scattering term $a(M)/M$ whereas the slope gives the intrinsic term $b(M)/M$. From the constant slope, they derive their main conclusion that σ_{AH-int} varies linearly with M.

To account for the linear-M dependence, Zeng *et al.* (Zeng *et al.*, 2006) identify the role of long-wavelength spin waves which cause fluctuations in the local direction of $\boldsymbol{M}(x)$ (and hence of $\boldsymbol{\Omega}$). They calculate the reduction in σ_{AH-int} and show that it varies linearly with M (Fig. 30 c).

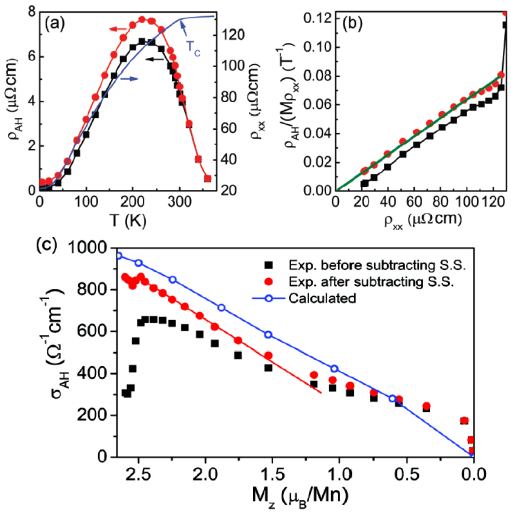


FIG. 30 (a) The T dependence of ρ_{AH} in Mn_5 Ge_3 before (solid squares) and after (solid circles) subtraction of the skew-scattering contribution. The thin curve is the resistivity ρ. (b) Plots of $\rho_{AH}/(M\rho_{xx})$ vs. ρ_{xx} before (solid squares) and after (solid circles) subtraction of skew-scattering term. (c) Comparison of calculated σ_{AH-int} vs. M_z (open circles) with experimental values before (squares) and after (solid circles) subtraction of skew-scattering term. [From Ref. Zeng *et al.*, 2006.]

6. Layered dichalcogenides

The layered transition-metal dichalcogenides are comprised of layers weakly bound by the van der Waals force. Parkin and Friend (Parkin and Friend, 1980) have shown that a large number of interesting magnetic systems may be synthesized by intercalating $3d$ magnetic ions between the layers.

The dichalcogenide Fe_xTaS_2 typically displays properties suggestive of a ferromagnetic cluster-glass state at low T for a range of Fe content x. However, at the composition $x = \frac{1}{4}$, the magnetic state is homogeneous. In single crystals of $Fe_{\frac{1}{4}}TaS_2$, the easy axis of $\boldsymbol{M}$ is parallel to $\hat{\mathbf{c}}$ (normal to the TaS_2 layers). Morosan *et al.* (Morosan *et al.*, 2007) observed that the curves of M vs. H display very sharp switching at the coercive field at all $T < T_C$ (160 K). In this system, the large ordinary term σ_{xy}^{NH} complicates the extraction of the AHE term σ_{xy}^{AH}. Converting the ρ_{yx}-H curves to σ_{xy}-H curves (Fig. 31), Checkelsky *et al.* (Checkelsky *et al.*, 2008) infer that the jump magnitude $\Delta\sigma_{xy}$ equals $2\sigma_{xy}^{AH}$ by assuming that Eq. (2.13) is valid. This method provides a direct measurement of σ_{xy}^{AH} without knowledge of R_0. As shown in Fig. 31 b, both the inferred σ_{xy}^{AH} and measured M are nearly T-independent below 50 K, but the former deviates sharply downwards above 50 K. Checkelsky *et al.* (Checkelsky *et al.*, 2008) propose that the deviation represents a large, negative inelastic-scattering contribution σ_{xy}^{in} that involves scattering from chiral textures of the spins which increase rapidly as T approaches T_C^-. In support, they show that the curve of $\sigma_{xy}^{in}/M(T)$ vs. T matches (within the resolution) that of $\Delta\rho(T)^2$ with $\Delta\rho(T) = \rho(T) - \rho(0)$.

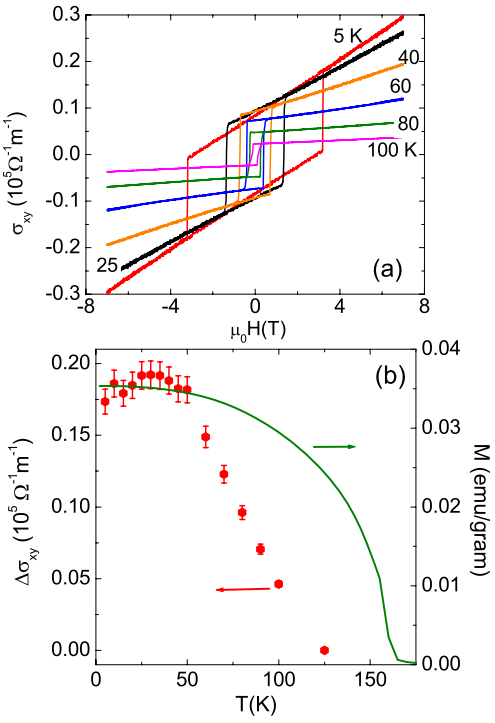


FIG. 31 (a) Hystersis loops of σ_{xy} vs. H in $Fe_{\frac{1}{4}}TaS_2$ calculated from the measured ρ and ρ_{yx} curves. The linear portions correspond to σ_{xy}^{NH} while the jump magnitude $\Delta\sigma_{xy}$ equals $2\sigma_{xy}^{AH}$. (b) Comparison of $\Delta\sigma_{xy}$ with the magnetization M measured at 0.1 T. Within the resolution, $\Delta\sigma_{xy}$ seems to be proportional to M below 50 K, but deviates sharply from M at higher temperatures, reflecting the growing dominance of a negative, inelastic-scattering term σ_{xy}^{in}. [From Ref. Checkelsky *et al.*, 2008.]

E. Localization and AHE

The role of localization in the anomalous Hall effect is an important issue, and there have been several works on this subject. (For a review of theoretical works, see Ref. Woelfle and Muttalib, 2006.) The weak localization effect on the normal Hall effect due to the external magnetic field has been studied by Fukuyama (Fukuyama, 1980), and the relation $\delta\sigma_{xy}^{WL}/\sigma_{xy} = 2\delta\sigma_{xx}^{WL}/\sigma_{xx}$ has been obtained where δO^{WL} represents the correction of the physical quantity O by the weak localization effect. This means that the Hall coefficient is not subject to the change due to the weak localization, *i.e.* $\delta\rho_{xy}^{NH} = 0$. An early experiment by Bergmann and Ye (Bergmann and Ye, 1991) on the anomalous Hall effect in the ferromagnetic amorphous metals showed almost no temperature dependence of the anomalous Hall conductivity, while the diagonal conductivity shows the logarithmic temperature dependence. Langenfeld and Woelfle (Langenfeld and Wolfle, 1991; Woelfle and Muttalib, 2006) studied theoretically the model

$$H = \sum_{\boldsymbol{k},\sigma} \varepsilon_{\boldsymbol{k}} c^\dagger_{\boldsymbol{k},\sigma} c_{\boldsymbol{k},\sigma} + \sum_i \sum_{\boldsymbol{k},\mathbf{k}',\sigma} e^{i(\boldsymbol{k}-\boldsymbol{k}')\cdot\boldsymbol{R}_i} [V + i(\boldsymbol{k}\times\boldsymbol{k}')\cdot\boldsymbol{J}_i] c^\dagger_{\boldsymbol{k}',\sigma'} c_{\boldsymbol{k},\sigma} \tag{2.15}$$

where $\boldsymbol{J}_i$ is proportional to the angular momentum of the impurity at $\boldsymbol{R}_i$, and the term containing it describes the spin-orbit scattering. They discussed the logarithmic correction to the anomalous Hall conductivity in this model, and found that Coulomb anomaly terms vanished identically, and the weak localization correction was cut-off by the phase-breaking lifetime τ_ϕ due to the skew scattering, explaining the experiment by Bergmann and Ye (Bergmann and Ye, 1991). Dugaev, Crepieux, and Bruno (Dugaev *et al.*, 2002) found that for the two-dimensional case the correction to the Hall conductivity was logarithmic in the ratio $\max(\tau_{\rm tr}/\tau_{SO}, \tau_{\rm tr}/\tau_\phi)$, with $\tau_{\rm tr}$ being the transport lifetime and τ_{SO} the lifetime due to the spin-orbit scattering. More recently, Mitra *et al.* (Mi-

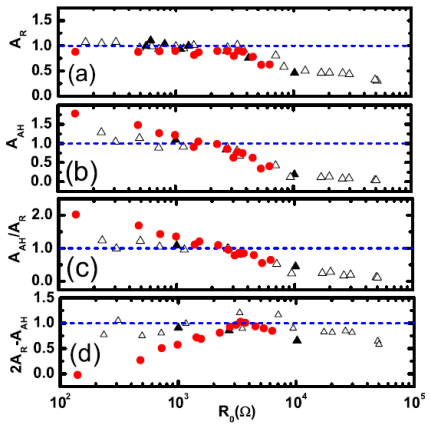


FIG. 32 The resistance (R_0)-temperature dependence of the coefficients A_R and A_{AH} defined in Eq. (2.16). Different symbols correspond to different methods of sample preparation. [From Ref. Mitra *et al.*, 2007.]

tra *et al.*, 2007) first observed the logarithmic temperature dependence of the anomalous Hall conductivity in the ultrathin film of polycrystalline Fe of sheet resistance R_{xx} less than ~ 3 kΩ. They defined the quantities $\Delta^N(Q) = (1/R_0 L_{00})(\delta Q/Q)$ for the physical quantity Q with respect to the reference temperature $T = T_0 = 5$ K by $\delta Q = Q(T) - Q(T_0)$, $R_0 = R_{xx}(T_0)$, and $L_{00} = e^2/\pi\hbar$. Defining the coefficients A_R and A_H by

$$\begin{aligned} \Delta^N(\sigma_{xx}) &= A_R \ln\left(\frac{T_0}{T}\right) \\ \Delta^N(\sigma_{xy}) &= (2A_R - A_{AH}) \ln\left(\frac{T_0}{T}\right) \end{aligned} \qquad (2.16)$$

Fig. 32 shows the R_0-dependence of the coefficients A_R and A_{AH} defined in the above Eq. (2.16).

The change in the interpretation comes from the fact that the phase-breaking lifetime τ_ϕ in the Fe film is mostly from scattering by the magnons and not from skew scattering, which allows a temperature regime where $\max(1/\tau_s, 1/\tau_{SO}, \omega_H) << \tau_\phi << 1/\tau_{tr}$ (τ_s: spin-flip scattering time, ω_H: internal magnetic field in the ferromagnet). In this region, they found that the weak localization effect can lead to coefficient of the logarithmic temperature dependence of σ_{xy} proportional to the factor $\sigma_{xy}^{SSM}/(\sigma_{xy}^{SSM} + \sigma_{xy}^{SJM})$ where $\sigma_{xy}^{SSM}(\sigma_{xy}^{SJM})$ is the contribution from the skew scattering (side jump) mechanism. Assuming that that ratio $\sigma_{xy}^{SJM}/\sigma_{xy}^{SSM}$ decreases as the sheet resistance R_0 increases, they were able to explain the sample-dependence of the logarithmic correction to the anomalous Hall conductivity (Mitra *et al.*, 2007). The absence of the logarithmic term in (Bergmann and Ye, 1991) is interpreted as being due to a large ratio of $\sigma_{xy}^{SJM}/\sigma_{xy}^{SSM}$ in their sample. It is interesting that the ratio $\sigma_{xy}^{SJM}/\sigma_{xy}^{SSM}$ can be estimated from the coefficient of the logarithmic term.

Up to now, we have discussed the weak localization effect. When the disorder strength increases, a metal-insulator transition will occur. For a normal metal under external magnetic field, the system belongs to the unitary class, and in 2D all the states are localized for any disorder (Lee and Ramakrishnan, 1985). In the quantum Hall system, however, the extended states can survive at discrete energies at the center of the broadened density of states at each Laudau level. This extended state carries the quantum Hall current. Field theoretical formulation of this localization problem has been developed (Prange and Girvin, 1987). In the presence of the external magnetic field, a Chern-Simons term appears in the non-linear sigma model whose coefficient is σ_{xy}. Therefore, the scaling variables are σ_{xx} and σ_{xy}, *i.e.*, the two-parameter scaling theory should be applied instead of the single-parameter scaling. It has been discussed that the scaling trajectory in the $\sigma_{xy} - \sigma_{xx}$ plane has the fixed point at $(\sigma_{xy}, \sigma_{xx}) = ((n+1/2)(e^2/h), \sigma_0)$ where σ_0 is some finite value, and σ_{xy} scales to the quantized value $n(e^2/h)$ when the initial value (given by the Boltzmann transport theory) lies in the range $(n-1/2)(e2/h) < \sigma_{xy}^{(0)} < (n+1/2)(e^2/h)$. In contrast to this quantum Hall system, there is no external magnetic field or the Landau level formation in the anomalous Hall system, and it is not trivial that the same two-parameter scaling theory applies to this case.

Onoda and Nagaosa (Onoda and Nagaosa, 2003) studied this problem using the generalized Haldane model (Haldane, 1988) which shows the quantum Hall effect without the external magnetic field. They calculated the scaling function of the localization length in the finite-width stripe sample in terms of the iterative transfer matrix method by MacKinnon (MacKinnon and Kramer, 1983), and found that two-parameter scaling holds even without an external magnetic field or Landau level formation. For the experimental realization of this quantized anomalous Hall effect, the $|\sigma_{xy}^{(0)}|$ given by Boltzmann transport theory (without the quantum correction) is larger than $e^2/(2h)$, and the temperature is lower than $T_{Loc} \sim \varepsilon_F e^{-c\sigma_{xx}^{(0)}/\sigma_{xy}^{(0)}}$, where ε_F is the Fermi energy and c is a constant of the order of unity. Therefore, the Hall angle $\sigma_{xy}^{(0)}/\sigma_{xx}^{(0)}$ should not be so small, hopefully of the order of 0.1. However, in the usual case, the Hall angle is at most 0.01, which makes the quantized anomalous Hall effect rather difficult to realize.

III. THEORETICAL ASPECTS OF THE AHE AND EARLY THEORIES

In this section, we review recent theoretical developments as well as the early theoretical studies of the AHE. First, we give a pedagogical discussion on the difference between the normal Hall effect due to the Lorentz force and the AHE (Sec. III.A). In Sec. III.B we discuss the topological nature of the AHE. In this Sec. III.C we present a wide survey of the early theories from a modern viewpoint in order to bring them into the context of the

present linear transport theory formalisms now used as a framework for AHE theories.

A. Symmetry considerations and analogies between normal Hall effect and AHE

Before describing these recent developments, we provide an elementary discussion that may facilitate understanding of the following sections.

The Hall effect is one of the fundamental transport phenomena in solid-state physics. Its occurrence is a direct consequence of broken time-reversal symmetry in the ferromagnetic state, $\mathcal{T}$. The charge current $\boldsymbol{J}$ is $\mathcal{T}$-odd,*i.e.*, it changes sign under time reversal. On the other hand, the electric field $\boldsymbol{E}$ is $\mathcal{T}$-even. Therefore, Ohm's law

$$\boldsymbol{J} = \sigma \boldsymbol{E} \tag{3.1}$$

relates two quantities with different $\mathcal{T}$-symmetries, which implies that the conductivity σ must be associated with diispative irreversible processes, and indeed we know that the Joule heating $Q = \sigma \boldsymbol{E}^2/2$ always accompanies the conductivity in Eq. (3.1). This irreversibility appears only when we consider macroscopic systems with continuous energy spectra.

Next, we consider the other aspect of the $\mathcal{T}$-symmetry, *i.e.*, the consequences of the $\mathcal{T}$-symmetry of the Hamiltonian which governs the microscopic dynamics of the system. This important issue has been formulated by Onsager, who showed that the response functions satisfy the following relation (Landau *et al.*, 1984)

$$K_{\alpha\beta}(\omega; , r, r'; B) = \varepsilon_\alpha \varepsilon_\beta K_{\beta\alpha}(\omega; , r', r; -B), \tag{3.2}$$

where $K_{\alpha\beta}(\omega; , r, r'; B)$ is the response of a physical quantity α at position r to the stimulus conjugate to the quantity β at position r' with frequency ω. Here $\varepsilon_\alpha(\varepsilon_\beta) = \pm 1$ specifies the symmetry property of α (β) with respect to the $\mathcal{T}$-operation. B suggests a magnetic field, but represents any time-reversal breaking field. In the case of a ferromagnet B can be associated with the magnetization M, the spontaneously generated time-reversal symmetry breaking field of a ferromagnet. The conductivity tensor σ_{ab} at a given frequency is proportional to the current-current response function. We can therefore make the identification $\alpha \to J_a$, $\beta \to J_b$, where J_i $(i = x, y, z)$ are the components of the current operator. Since, $\varepsilon_\alpha = \varepsilon_\beta = -1$, we can conlcude that

$$\sigma_{ab}(\omega; B) = \sigma_{ba}(\omega; -B). \tag{3.3}$$

Hence, we conclude that σ_{ab} is symmetric with respect to a and b in systems with $\mathcal{T}$-symmetry. The antisymmetric part $\sigma_{ab}(\omega) - \sigma_{ba}(\omega)$ is finite only if $\mathcal{T}$-symmetry is broken.

Now we turn back to irreversibility for the general form of the conductivity σ_{ab}, for which the dissipation is given by (Landau *et al.*, 1984)

$$\begin{aligned} Q &= \sum_{ab} \frac{1}{4}(\sigma^*_{ab} + \sigma_{ba}) E_a E^*_b \\ &= \frac{1}{4}\sum_{ab} [\mathrm{Re}(\sigma_{ab} + \sigma_{ba})\mathrm{Re}(E_a E^*_b) \\ &+ \mathrm{Im}(\sigma_{ab} - \sigma_{ba})\mathrm{Im}(E_a E^*_b)]. \end{aligned} \tag{3.4}$$

The real part of the symmetric combination $\sigma_{ab} + \sigma_{ba}$ and the imaginary part of the antisymmetric combination $\sigma_{ab} - \sigma_{ba}$ contribute to the dissipation, while the imaginary part of $\sigma_{ab} + \sigma_{ba}$ and the real part of $\sigma_{ab} - \sigma_{ba}$ represent the dispersive (dissipationless) responses. Therefore, $\mathrm{Re}(\sigma_{ab} - \sigma_{ba})$, which corresponds to the Hall response, does not produce dissipation. This means that the physical processes contributing to this quantity *can be* reversible, *i.e.*, dissipationless, even though they are not necessarily so. This point is directly related to the controversy between intrinsic and extrinsic mechanism for the AHE.

The origin of the ordinary Hall effect is the Lorentz force due to the magnetic field $\boldsymbol{H}$:

$$\boldsymbol{F} = -\frac{e}{c}\boldsymbol{v} \times \boldsymbol{H}, \tag{3.5}$$

which produces an acceleration of the electron perpendicular to its velocity $\boldsymbol{v}$ and $\boldsymbol{H}$. For free electrons this leads to circular cyclotron motion with frequency $\omega_c = eH/(mc)$. The Lorentz force leads to charge accumulations of opposite signs on the two edges of the sample. In the steady state, the Lorentz force is balanced by the resultant transverse electric field, which is observed as the Hall voltage V_H. In the standard Boltzmann-theory approach, the equation for the electron distribution function $f(\boldsymbol{p}, \boldsymbol{x})$ is given by (Ziman, 1967):

$$\frac{\partial f}{\partial t} + \boldsymbol{v} \cdot \frac{\partial f}{\partial \boldsymbol{x}} + \boldsymbol{F} \cdot \frac{\partial f}{\partial \boldsymbol{p}} = \left(\frac{\partial f}{\partial t}\right)_{\text{coll.}}, \tag{3.6}$$

where $\boldsymbol{p}$ and $\boldsymbol{x}$ are the momentum and real space coordinates, respectively. Putting $\boldsymbol{F} = -e(\boldsymbol{E} + \frac{\boldsymbol{v}}{c} \times \boldsymbol{H})$, and using the relaxatin time approximation for the collision term, $-\frac{1}{\tau}(f - f_{\text{eq}})$, with f_{eq} being the distribution function in thermal equilibrium, one can obtain the steady state solution to this Boltzmann equation as

$$f(\boldsymbol{p}) = f_{\text{eq}}(\boldsymbol{p}) + g(\boldsymbol{p}), \tag{3.7}$$

with

$$g(\boldsymbol{p}) = -\tau e \frac{\partial f_{\text{eq}}}{\partial \varepsilon} \boldsymbol{v} \cdot \left(\boldsymbol{E} - \frac{e\tau}{mc}\boldsymbol{H} \times \boldsymbol{E}\right), \tag{3.8}$$

where order H^2 terms have been neglected and the magnetic field H_z is assumed to be small, *i.e.* $\omega_c \tau \ll 1$. The current density $\boldsymbol{J} = -e\int \frac{d^3\boldsymbol{p}}{(2\pi)^3}\frac{\boldsymbol{p}}{m} f(\boldsymbol{p})$ is obtained from Eq. (3.8) to order $O(E)$ and $O(EH)$ as

$$\boldsymbol{J} = \sigma \boldsymbol{E} + \sigma_H \boldsymbol{H} \times \boldsymbol{E}, \tag{3.9}$$

where

$$\sigma = -\frac{1}{3}\int \frac{d^3\boldsymbol{p}}{(2\pi)^3} v^2 e^2 \tau \frac{\partial f_{\rm eq}}{\partial \varepsilon} \tag{3.10}$$

is the conductivity, while

$$\sigma_H = \frac{1}{3}\int \frac{d^3\boldsymbol{p}}{(2\pi)^3} v^2 e^2 \tau \frac{\partial f_{\rm eq}}{\partial \varepsilon}\frac{e\tau}{mc} \tag{3.11}$$

is the ordinary Hall conductivity.

Now let us fix the direction of the electric and magnetic fields as $\boldsymbol{E} = E_y \boldsymbol{e}_y$ and $\boldsymbol{H} = H_z \boldsymbol{e}_z$. Then the Hall current is along the x-direction and we write it as

$$J_x = \sigma_H E_y, \tag{3.12}$$

with the Hall conductivity $\sigma_H = ne^3\tau^2 H_z/m^2 c$ with n being the electron density. The Hall coefficient R_H is defined as the ratio $V_H/J_x H_z$, and from Eqs. (3.10) and (3.11), one obtains

$$R_H = -\frac{1}{nec}. \tag{3.13}$$

This result is useful to determine the electron density n experimentally, since it does not contain the relaxation time τ. Note here that for fixed electron density n, Eq. (3.13) means $\sigma_H \propto H\sigma_{xx}^2$ and that $\rho_H \propto H$, independent of the relaxation time τ (or equivalently σ_{xx}). In other words, the ratio $|\sigma_H|/\sigma_{xx} = \omega_c\tau \ll 1$. This relation will be compared with the AHE case below.

What happens in the opposite limit $\omega_c\tau \gg 1$? In this limit, the cyclotron motion is completed many times within the lifetime τ. This implies the closed cyclotron motion is repeated many times before being disrupted by scattering. When treated quantum mechanically the periodic classical motion leads to kinetic energy quantization and Landau level formation, which leads in turn to the celebrated quantum Hall effect. As is well known, in the 2D electron gas realized in semiconductor heterostructures, Landau-level quantization leads to the celebrated quantum Hall effect (Prange and Girvin, 1987). If we consider the free electrons, *i.e.* completely neglecting the potential (both periodic and random) and the interaction among electrons, one can show that σ_H is given by $\frac{e^2}{h}\nu$ where ν is the filling factor of the Landau levels. In combination with electron localization, gaps at integer filling factors lead to quantization of σ_H. For electrons in a two-dimensional cyrstal, the Hall quantization is still quantized, a property which can be traced to the topological properties of Bloch state wavefunctions discussed below. (Prange and Girvin, 1987).

Now let us consider the magnetic field effect for electrons under the influence of the periodic potential. For simplicity we study the tight-binding model

$$H = \sum_{ij} t_{ij} c_i^\dagger c_j. \tag{3.14}$$

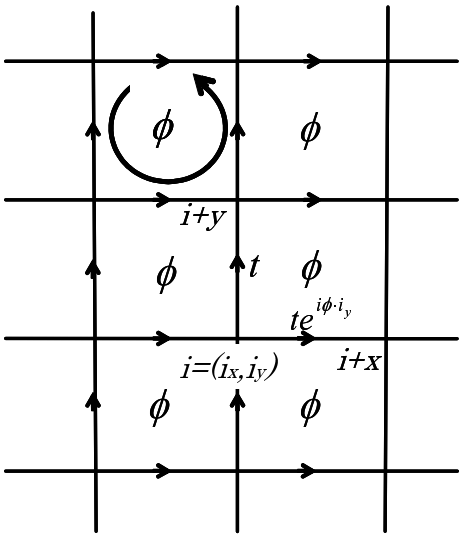


FIG. 33 Tight-binding model on a square lattice under the magnetic flux ϕ for each plaquette. We choose the gauge where the phase factor of the transfer integral along x-direction is given by $e^{-i\phi i_y}$ with i_y being the y-component of the lattice point position $i = (i_x, i_y)$.

The magnetic field adds the Peierls phase factor to the transfer integral t_{ij} between sites i and j, *viz.*

$$t_{ij} \to t_{ij}\exp[ia_{ij}], \tag{3.15}$$

with

$$a_{ij} = \frac{ie}{\hbar c}\int_i^j d\boldsymbol{r}\cdot\boldsymbol{A}(\boldsymbol{r}). \tag{3.16}$$

Note that the phase factor is periodic with the period 2π with respect to its exponent. Since the gauge transformation

$$c_i \to c_i \exp[i\theta_i] \tag{3.17}$$

together with the redefinition

$$a_{ij} \to a_{ij} + \theta_i - \theta_j \tag{3.18}$$

keeps the Hamiltonian invariant, a_{ij} itself is not a physical quantity. Instead, the flux $\phi = a_{ij} + a_{jk} + a_{kl} + a_{li}$ per square plaquette is the key quantity in the problem (see Fig.33)

For example, one may choose a gauge in which t_{ij} along the directions $\pm\hat{\mathbf{y}}$ is a real number t, while $t_{ii+x} = t\exp[-i\phi i_y]$ to produce a uniform flux distribution ϕ in each square plaquette. Here i_y is the y-component of the lattice point position $i = (i_x, i_y)$). The problem is that the i_y-dependence breaks the periodicity of the Hamiltonian along the y-axis, which invalidates the Bloch theorem. This corresponds to the fact that the vector potential $\boldsymbol{A}(\boldsymbol{r}) = (-Hy, 0)$ for the uniform magnetic field H is y-dependent, so that momentum component p_y is no longer conserved. However, when $\phi/(2\pi)$ is a rational

number n/m, where n and m are integers that do not share a common factor, one can enlarge the unit cell by m times along the y-direction to recover the periodicity, because $\exp[-i\phi(i_y+m)] = \exp[-i\phi i_y]$. Therefore, there appear m sub-bands in the 1st-Brillouin zone, each of which is characterized by a Chern number related to the Hall response as will be described in section III.B (Thouless *et al.*, 1982). The message here is that an external commensurate magnetic field leads to a multiband structure with an enlarged unit cell, leading to the quantized Hall response when the chemical potential is within the gap between the sub-bands. When $\phi/(2\pi)$ is an irrational number, on the other hand, one cannot define the Bloch wavefunction and the electronic structure is described by the Hofstadter butterfly (Hofstadter, 1976) .

Since flux 2π is equivalent to zero flux, a commensurate magnetic field can be equivalent to a magnetic field distribution whose average flux is zero. Namely, the total flux penetrating the m-plaquettes is $2\pi n$, which is equivalent to *zero*. Interestingly, spatially non-uniform flux distributions can also lead to quantum Hall effects. This possibility was first considered by Haldane (Haldane, 1988), who studied a tight-binding model on the honeycomb lattice. He introduced complex transfer integrals between the next-nearest neighbor sites in addition to the real one between the nearest-neighbor sites. The resultant Hamiltonian has translational symmetry with respect to the lattice vectors, and the Bloch wavefunction can be defined as the function of the crystal momentum $\boldsymbol{k}$ in the first Brillouin zone. The honeycomb lattice has two sites in the unit cell, and the tight-binding model produces two bands, separated by the band gap. The wavefunction of each band is characterized by the Berry phase curvature, which acts like a "magnetic field" in $\boldsymbol{k}$-space, as will be discussed in sections III.B and IV.A.

The quantum Hall effect results when the Fermi energy is within this band gap. Intuitively, this can be interpreted as follows. Even though the total flux penetrating the unit cell is zero, there are loops in the unit cells enclosing a nonzero flux. Each band picks up the flux distribution along the loops with different weight and contributes to the Hall response. The sum of the Hall responses from all the bands, however, is zero as expected. Therefore, the "polarization" of Hall responses between bands in a multiband system is a general and fundamental mechanism of the Hall response, which is distinct from the classical picture of the Lorentz force.

There are several ways to realize a flux distribution within a unit cell in momentum space. One is the relativistic spin-orbit interaction given by

$$H_{SOI} = \frac{\hbar e}{2m^2c^2}(\boldsymbol{s}\times\nabla V)\cdot\boldsymbol{p}, \tag{3.19}$$

where V is the potential, $\boldsymbol{s}$ the spin, and $\boldsymbol{p}$ the momentum of the electron. This Hamiltonian can be written as

$$H_{SOI} = \boldsymbol{A}_{SOI}\cdot\boldsymbol{p}, \tag{3.20}$$

with $\boldsymbol{A}_{SOI} = \frac{\hbar e}{2m^2c^2}(\boldsymbol{s}\times\nabla V)$ acting as the effective vector potential. Therefore, in the magnetically ordered state, *i.e.*, when $\boldsymbol{s}$ is ordered and can be regarded as a c-number, $\boldsymbol{A}_{SOI}$ plays a role similar to the vector potential of an external magnetic field. Note that the Bloch theorem is valid even in the presence of the spin-orbit interaction, since it preserves the translational symmetry of the lattice. However, the unit cell may contain more than two atoms and each atom may have multiple orbitals. Hence, the situation is very similar to that described above for the commensurate magnetic field or the Haldane model.

The following simple model is instructive. Let us consider the tight-binding model on a square lattice given by

$$\begin{aligned} H &= -\sum_{i,\sigma,a=x,y} t_s s^\dagger_{i,\sigma} s_{i+a,\sigma} + h.c. \\ &+ \sum_{i,\sigma,a=x,y} t_p p^\dagger_{i,a,\sigma} s_{i+a,a,\sigma} + h.c. \\ &+ \sum_{i,\sigma,a=x,y} t_{sp} s^\dagger_{i\sigma} p_{i+a,a,\sigma} + h.c. \\ &+ \lambda\sum_{i,\sigma}\sigma(p^\dagger_{i,x,\sigma} - i\sigma p^\dagger_{i,y,\sigma})(p_{i,x,\sigma} + i\sigma p_{i,y,\sigma}). \end{aligned} \tag{3.21}$$

On each site, we put the 3 orbitals s, p_x and p_y, associated with the corresponding creation and annihilation operators. The first three terms represent the transfer of electrons between the neighboring sites as shown by Fig. 34. The signs in front of t's are determined by the relative sign of the two orbitals connected by the transfer integrals, and all t's are assumed to be positive. The last term is a simplified SOI in which the z-component of the spin moment is coupled to that of the orbital moment. This 6-band model can be reduced to a 2-band model in the ferromagnetic state when only the $\sigma = +1$ component is retained. By the spin-orbit interaction, the p-orbitals are split into

$$|p\pm\rangle = \frac{1}{\sqrt{2}}(|p_x\rangle \pm i|p_y\rangle) \tag{3.22}$$

at each site, with the energy separation 2λ. Therefore, when only the lower energy state $|p-\rangle$ and the s-orbital $|s\rangle$ are considered, the tight-binding Hamiltonian becomes $H = \sum_{\boldsymbol{k}}\psi^\dagger(\boldsymbol{k})h(\boldsymbol{k})\psi(\boldsymbol{k})$ with $\psi(\boldsymbol{k}) = [s_{\boldsymbol{k},\sigma=1}, p_{\boldsymbol{k},-,\sigma=1}]^T$ and

$$h(\boldsymbol{k}) = \begin{bmatrix} \varepsilon_s - 2t_s(\cos k_x + \cos k_y) & \sqrt{2}t_{sp}(i\sin k_x + \sin k_y) \\ \sqrt{2}t_{sp}(-i\sin k_x + \sin k_y) & \varepsilon_p + t_p(\cos k_x + \cos k_y) \end{bmatrix}. \tag{3.23}$$

Note that the complex orbital $|p-\rangle$ is responsible for the complex off-diagonal matrix elements of $h(\boldsymbol{k})$. This produces the Hall response as one can easily see from the formula Eq. (1.5) and Eq. (1.6) in section I.B. When the Fermi energy is within the band gap, the Chern number for each band is ±1 when $\varepsilon_s - 4t_s < \varepsilon_p + 2t_p$, and they are zero otherwise. This can be understood by considering the effective Hamiltonian near $\boldsymbol{k} = \boldsymbol{0}$, which is given by

$$h(\boldsymbol{k}) = \bar{\varepsilon} + m\sigma_z + \sqrt{2}t_{sp}(k_y\sigma_x - k_x\sigma_y), \tag{3.24}$$

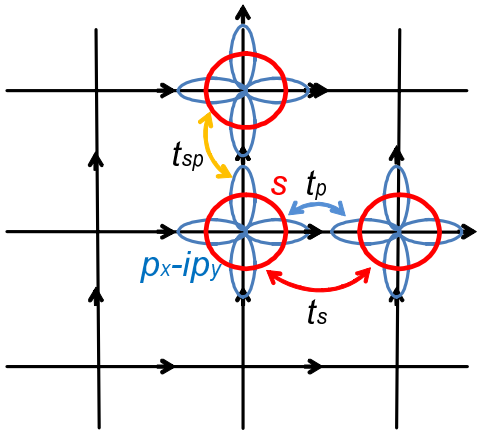


FIG. 34 Tight-binding model on a square lattice for a 3 band model made from s and $p_x - ip_y$ orbitals with polarized spins. The transfer integrals between s and $p_x - ip_y$ orbitals become complex along the y-direction in a way that is equivalent to effective magnetic flux

with $\bar{\varepsilon} = [(\varepsilon_s - 4t_s) + (\varepsilon_p + 2t_p)]/2$ and $m = (\varepsilon_s - 4t_s) - (\varepsilon_p + 2t_p)$, which is essentially the Dirac Hamiltonian in (2+1)D. One can calculate the Berry curvature $\boldsymbol{b}_\pm(\boldsymbol{k}) = \mp b_z(\boldsymbol{k}_\perp)\boldsymbol{e}_z$ defined in Eq. (1.6) for the upper(+) and lower (−) bands, respectively as

$$b_z(\boldsymbol{k}_\perp) = \frac{m}{2[\boldsymbol{k}_\perp^2 + m^2]^{3/2}}. \tag{3.25}$$

The integral over the two dimensional wavevector $\boldsymbol{k}_\perp = (k_x, k_y)$ leads to Hall conductance $\sigma_H = \frac{1}{2}\mathrm{sgn}(m)e^2/h$ in this continuum model when only the lower band is fully occupied (Jackiw, 1984). The distribution Eq. (3.25) indicates that the Berry curvature is enhanced when the gap m is small near this avoided band crossing. Note that the continuum model Eq. (3.24) cannot describe the value of the Hall conductance in the original tight-binding model since the information is not retained over all the first Brillouin zone. Actually, it has been proved that the Hall conductance is an integer multiple of e^2/h due to the single-valudeness of the Bloch wavefunction within the first Brillouin zone. However, the *change* of the Hall conductance between positive and negative m can be described correctly.

Onoda and Nagaosa (Onoda and Nagaosa, 2002) demonstrated that a similar scenario emerges also for a 6-band tight binding model of t_{2g}-orbitals with SOI. They showed that the Chern number of each band can be nonzero leading to a nonzero Hall response arising from the spontaneous magnetization. This suggests that the anomalous Hall effect can be of topological origin, a reinterpretation of the intrinsic contribution found by Karplus-Luttinger (Karplus and Luttinger, 1954). Another mechanism which can produce a flux is a non-coplanar spin structure with an associated spin chirality as has been discussed in section II.B.

The considerations explained here have totally neglected the finite lifetime τ due to the impurity and/or phonon scattering, a generalization of the parameter $\omega_c\tau$ which appeared in the case of the external magnetic field. A full understanding of disorder effects usually requires the full power of the detailed microscopic theories reviewed in Sec. IV. The ideas explained in this section though are sufficient to understand why the intrinsic Berry phase contribution to the Hall effect can be so important. The SOI produces an effective vector potential and a "magnetic flux distribution" within the unit cell. The strength of this flux density is usually much larger than the typical magnetic field strength available in the laboratory. In particular, the energy scale "$\hbar\omega_c$" related to this flux is that of the spin-orbit interaction for Eq. (3.20), and hence of the order of 30 meV in 3d transition metal elements. This corresponds to a magnetic field of the order of 300 T. Therefore, one can expect that the intrinsic AHE is easier to observe compared with the quantum Hall effect.

B. Topological interpretation of the intrinsic mechanism: relation between Fermi sea and Fermi surface properties

The discovery and subsequent investigation of the quantum Hall effect led to numerous important conceptual advances (Prange and Girvin, 1987). In particular, the utility of topological considerations in understanding electronic transport in solids was first appreciated. In this section, we provide an introduction to the application of topological notions such as the Berry phase and the Chern number to the AHE problem, and explain the long-unsuspected connections between these considerations and KL theory. A more elementary treatment is given in Ref. Ong and Lee, 2006.

The topological expression given in Eq. (1.5) was first obtained by Thouless, Kohmoto, Nightingale and Nijs (TKNN) (Thouless *et al.*, 1982) for Bloch electrons in a 2D insulating crystal lattice immersed in a strong magnetic field H. These authors showed that each band is characterized by a topological integer called the Chern number

$$C_n \equiv -\int \frac{dk_x dk_y}{(2\pi)^2} b_n^z(\boldsymbol{k}). \tag{3.26}$$

According to Eq. (1.5), the Chern number C_n gives the quantized Hall conductance of an ideal 2D insulator, *viz.* $\sigma_{xy} = e^2 C_n/h$. As mentioned in prior sections, these topological arguments were subsequently applied to semiclassical transport theory (Sundaram and Niu, 1999) and the AHE problem in itinerant ferromagnets (Jungwirth *et al.*, 2002b; Onoda and Nagaosa, 2002), and the equivalence to the KL expression (Karplus and Luttinger, 1954) for σ_H was established. (Note however, that in multiband systems, induced interband coherence among states with the same crystal momentum is a possibility.)

Although the intrinsic Berry-phase effect involves the entire Fermi sea, as is clear from Eq. (1.5), it is usually believed that transport properties of Fermi liquids

at low temperatures relative to the Fermi energy should be dependent only on Fermi-sruface properties. This is a simple consequence of the observation that at these temperatures only states near the Fermi surface can be excited to produce non-equillibirium transport.

The apparent contradiction between conventional Fermi liquid theory ideas and the Berry phase theory of the AHE was resolved by Haldane (Haldane, 2004), showed that the Berry phase contribution to the AHE could be viewed in an alternate way. Because of its topological nature, the intrinsic AHE, which is most naturally expressed as an integral over the occupied Fermi sea, can be rewritten as an integral over the Fermi surface. Let us start with the topological properties of the Berry phase. The Berry-phase curvature $\boldsymbol{b}_{n\boldsymbol{k}}$ is gauge-invariant and divergence-free except at quantized monopole and anti-monopole sources with the quantum $\pm 2\pi$, *i.e.*,

$$\boldsymbol{\nabla}_k \cdot \boldsymbol{b}_{n\boldsymbol{k}} = \sum_i q_{ni}\delta^3(\boldsymbol{k} - \boldsymbol{k}_{ni}), \quad q_{ni} = \pm 2\pi. \tag{3.27}$$

These monopoles and anti-monopoles appear at isolated $\boldsymbol{k}$ points in three dimensions. This is because in complex Hermitian eigenvalue problems, accidental degeneracy can occur by tuning the three parameters of $\boldsymbol{k}$.

To gain further insight on the topological nature of 3D systems, it is useful to rewrite Eq. (1.5) as

$$\sigma_{ij} = \epsilon_{ij\ell}\frac{e^2}{h}\frac{K^\ell}{2\pi}, \tag{3.28}$$

where

$$\boldsymbol{K} = \sum_n \boldsymbol{K}_n, \tag{3.29}$$

$$\boldsymbol{K}_n = -\frac{1}{2\pi}\int_{\text{F.B.Z.}} d^3\boldsymbol{k}\, f(\varepsilon_{n\boldsymbol{k}})\, \boldsymbol{b}_{n\boldsymbol{k}}. \tag{3.30}$$

We note that if the band dispersion $\varepsilon_{n\boldsymbol{k}}$ does not cross ε_F, K_n^ℓ is quantized in integer multiples (C_{na}) of a primitive reciprocal lattice vector $\boldsymbol{G}_a$ at $T = 0$. We have

$$\boldsymbol{K}_n = \sum_a C_{na}\boldsymbol{G}_a, \tag{3.31}$$

where the index a runs over the three independent primitive reciprocal lattice vectors (Kohmoto, 1985).

We next discuss the non-quantized part of the anomalous Hall conductivity. In a real material with multiple Fermi surface (FS) sheets indexed by α, we can describe each sheet by $\boldsymbol{k}_F^{(\alpha)}(\boldsymbol{s})$, where $\boldsymbol{s} = (s^1, s^2)$ is a parameterization of the surface. It is convenient to redefine the Berry-phase connection and curvature as

$$\tilde{a}^i(\boldsymbol{s}) = \boldsymbol{a}(\boldsymbol{k}(\boldsymbol{s}))\cdot\partial_{s^i}\boldsymbol{k}(\boldsymbol{s}), \tag{3.32}$$

$$\tilde{b}(\boldsymbol{s}) = \epsilon_{ij}\partial_{s^i}\tilde{a}^j(\boldsymbol{s}), \tag{3.33}$$

with ϵ_{ij} the rank-2 antisymmetric tensor.

By integrating Eq. (3.30) by parts, eliminating the integration over the Brillouin zone boundary for each band, and dropping the band indices, we may write (at $T = 0$) the vector $\boldsymbol{K}$ in Eq. (3.29) as

$$\boldsymbol{K} = \sum_a C_a\boldsymbol{G}_a + \sum_\alpha \boldsymbol{K}_\alpha, \tag{3.34}$$

$$\boldsymbol{K}_\alpha = \frac{1}{2\pi}\int_{S_\alpha} ds^1\wedge ds^2\ \tilde{b}(\boldsymbol{s})\boldsymbol{k}_F^{(\alpha)}(\boldsymbol{s}) + \frac{1}{4\pi}\sum_i \boldsymbol{G}_{\alpha i}\int_{\partial S_\alpha^i} ds\cdot\tilde{a}(\boldsymbol{s}). \tag{3.35}$$

Here, C_a is the sum of C_{na} over the fully occupied bands, α labels sheets of the Fermi surface S_α, and δS_α^i is the intersection of the Fermi surface S_α with the Brillouin zone boundary i where $\boldsymbol{k}_F^{(\alpha)}(\boldsymbol{s})$ jumps by $\boldsymbol{G}_{\alpha i}$. Note that the quantity

$$\frac{1}{2\pi}\int_{S_\alpha} ds^1\wedge ds^2\ \tilde{b}(\boldsymbol{s}) \tag{3.36}$$

gives an integer Chern number. Hence gauge invariance requires that

$$\sum_\alpha \frac{1}{2\pi}\int_{S_\alpha} ds^1\wedge ds^2\ \tilde{b}(\boldsymbol{s}) = 0. \tag{3.37}$$

The second term in Eq. (3.35) guarantees that $\boldsymbol{K}_\alpha$ is unchanged by any continuous deformation of the Brillouin zone into another primitive reciprocal cell.

C. Early theoretical studies of the AHE

1. Karplus-Luttinger theory and the intrinsic mechanism

The pioneering work of Karplus and Luttinger (KL) (Karplus and Luttinger, 1954) was the first theory of the AHE fully based on Bloch states $\psi_{n\boldsymbol{k}}$. As a matter of course, their calculations uncovered the important role played by the mere existence of bands and the associated overlap of Bloch states. The KL theory neglects all lattice disorder, so that the Hall effect it predicts is based on an intrinsic mechanism.

In a ferromagnet, the orbital motion of the itinerant electrons couples to spin ordering via the SOI. Hence all theories of the AHE invoke the SOI term, which, as we have mentioned, is described by the Hamiltonian given by Eq. 3.19, where $V(\boldsymbol{r})$ is the lattice potential. The SOI term preserves lattice translation symmetry and we can therefore define spinors which satisfy Bloch's theorem. When SO interactions are included the Bloch Hamiltonian acts in a direct product of orbital and spin-space. The total Hamiltonian H_T can be separated into contributions as follows:

$$H_T = H_0 + H_{SOI} + H_E \tag{3.38}$$

where H_0 is the Hamiltonian in the absence of SOI and H_E the perturbation due to the applied electric field $\boldsymbol{E}$. In simple models the consequences of magnetic order can

be represented by replacing the spin operator in Eq.(3.19) by the ordered magnetic moment $\boldsymbol{M}_s$ as $\boldsymbol{s} \to \frac{\hbar}{2}\frac{\boldsymbol{M}_s}{M_0}$, where M_0 is the magnitude of the saturated moment. The matrix element of $H_E = -eE_b x_b$ can be written as

$$\langle n\boldsymbol{k}|H_E|n'\boldsymbol{k}'\rangle = -eE_b\left(i\delta_{n,n'}\frac{\partial}{\partial k_b}\delta_{\boldsymbol{k},\boldsymbol{k}'} + i\delta_{\boldsymbol{k},\boldsymbol{k}'}J_b^{nn'}(\boldsymbol{k})\right), \tag{3.39}$$

where the "overlap" integral

$$J_b^{nn'}(\boldsymbol{k}) = \int_\Omega d\boldsymbol{r}\; u^*_{n\boldsymbol{k}}(\boldsymbol{r})\frac{\partial}{\partial k_b}u_{n'\boldsymbol{k}}(\boldsymbol{r}) \tag{3.40}$$

are regular functions of $\boldsymbol{k}$. In hindsight, $J_b^{nn'}(\boldsymbol{k})$ may be recognized as the Berry-phase connection $\boldsymbol{a}_n(\boldsymbol{k})$ discussed in Sec. I.B.1.

We next divide H_E into $H_E^r + H_E^a$, where H_E^a (H_E^r) corresponds to the first (second) term on the right hand side of Eq. (3.39). Absorbing H_E^r into the unperturbed Hamiltonian, *i.e.*, $H_p = H_0 + H_{SOI} + H_E^r$, KL treated the remaining term H_E^a as a perturbation. Accordingly, the density matrix ρ was written as

$$\rho = \rho_0(H_p) + \rho_1 \tag{3.41}$$

where $\rho_0(H_p)$ is the finite-temperature equilibrium density matrix and ρ_1 is the correction. KL assumed that ρ_1 gives only the ordinary conductivity, whereas the AHE arises solely from $\rho_0(H_p)$. Evaluating the average velocity $\bar{v}_a$ as $\bar{v}_a = \mathrm{Tr}[\rho_0 v_a]$, they found that

$$\bar{v}_a = -ieE_b\sum_{n,\boldsymbol{k}}\rho_0'(E^p_{n\boldsymbol{k}})J_a^{nn}(\boldsymbol{k}), \tag{3.42}$$

where ρ_0' is the derivative with respect to the energy. As it is clear here, this current is the dissipationless current in thermal equilibrium under the influence of the external electric field, *i.e.*, H_E^r. The AHE contribution arises from the interband coherence induced by an electronic field, and not from the more complicated rearrangements of states within the partially occupied bands.

A second assumption of KL is that, in $3d$ metals, the SOI energy $H_{SO} \ll \varepsilon_F$ (the Fermi energy) and W (the bandwidth), so that it suffices to consider H_{SO} to leading order. Using Eq. (3.19), the AHE response is then proportional to $|\boldsymbol{M}_s|$, consistent with the empirical relationship Eq. (2.1). More explicitly, to first-order in H_{SOI}, KL obtained

$$\bar{\boldsymbol{v}} = -\frac{e}{m\Delta^2}\sum_{\boldsymbol{k},n}\rho_0(\varepsilon_{n\boldsymbol{k}})[\boldsymbol{E}\cdot\boldsymbol{v}_{n\boldsymbol{k}}]\mathbf{F}_{\mathbf{nk}}, \tag{3.43}$$

where $\varepsilon_{n\boldsymbol{k}}$ is the energy of the Bloch state for H_0, Δ is the averaged value of interband energy separation, and $\mathbf{F}_{\mathbf{nk}}$ is the force $i\langle n\boldsymbol{k}|[H_{SOI},\boldsymbol{p}]|n\boldsymbol{k}\rangle$. This gives the anomalous Hall coefficient

$$R_s \cong \frac{2e^2H_{SO}}{m\Delta^2}\delta\left\langle\frac{m}{m^*}\right\rangle\rho^2, \tag{3.44}$$

where $|\boldsymbol{F}| \cong (e/c)H_{SO}v$, m^* is the effective mass, δ is the number of incompletely filled d-orbitals, and ρ is the resistivity.

Note that the ρ^2-dependence implies that the off-diagonal Hall conductivity σ_H is independent of the transport lifetime τ, *i.e.*, it is well-defined even in the absence of disorder, in striking contrast with the diagonal conductivity σ. The implication that $\rho_H = \sigma_H\rho^2$ varies as the square of ρ was immediately subjected to extensive experimental tests, as described in Sec. I.A.

An important finding in the KL theory is that interband matrix elements of the current operator contribute significantly to the transport currents. This contrasts with conventional Boltzmann transport theory, where the current arises solely from the group velocity $\boldsymbol{v}_{n,\boldsymbol{k}} = \partial\varepsilon_{n,\boldsymbol{k}}/\partial\boldsymbol{k}$.

In the Bloch basis

$$\langle\boldsymbol{r}|\psi_{n\boldsymbol{k}}\rangle = e^{i\boldsymbol{k}\cdot\boldsymbol{r}}\langle\boldsymbol{r}|u_{n\boldsymbol{k}}\rangle, \tag{3.45}$$

the N-orbital Hamiltonian (for a given $\boldsymbol{k}$) may be decomposed into the $2N\times 2N$ matrix $h(\boldsymbol{k})$, *viz.*

$$h(\boldsymbol{k}) = \sum_{n,m}\langle n\boldsymbol{k}|h(\boldsymbol{k})|m\boldsymbol{k}\rangle\; a_n^\dagger(\boldsymbol{k})a_m(\boldsymbol{k}). \tag{3.46}$$

The corresponding current operator for a given $\boldsymbol{k}$ is

$$J_\mu(t,\boldsymbol{k}) = \sum_{n,m}\langle n\boldsymbol{k}|\frac{\partial h(\boldsymbol{k})}{\partial\hbar k_\mu}|m\boldsymbol{k}\rangle\; a_n^\dagger(\boldsymbol{k})a_m(\boldsymbol{k}). \tag{3.47}$$

According to Hellman-Feynman's theorem

$$\langle n\boldsymbol{k}|\frac{\partial h(\boldsymbol{k})}{\partial k_\mu}|n\boldsymbol{k}\rangle = \frac{\partial\varepsilon_n(\boldsymbol{k})}{\partial\boldsymbol{k}}, \tag{3.48}$$

the diagonal contribution to the current is (with $n=m$)

$$J_\mu^{\mathrm{intra}}(t) = -e\sum_{n\boldsymbol{k}}v_g(\boldsymbol{k})N_n(\boldsymbol{k}), \tag{3.49}$$

where $N_n(\boldsymbol{k}) = a_n^\dagger(\boldsymbol{k})a_n(\boldsymbol{k})$ is the occupation number in the state $|n\boldsymbol{k}\rangle$. Eq. (3.49) corresponds to the expression in Boltzmann transport theory mentioned before. The inter-band matrix element $\langle n\boldsymbol{k}|\frac{\partial h(\boldsymbol{k})}{\partial k_\mu}|m\boldsymbol{k}\rangle$ with $n\neq m$ corresponds to inter-band transitions. As shown by KL, the inter-band matrix elements have profound consequences for the Hall current, as has become apparent from the Berry-phase approach.

2. Extrinsic mechanisms

a. Skew scattering

In a series of reports, Smit (Smit, 1955, 1958) mounted a serious challenge to the basic findings of KL. In the linear-response transport regime, the steady-state current balances the acceleration of electrons by $\boldsymbol{E}$

against momentum relaxation by scattering from impurities and/or phonons. Smit pointed out that this balancing was entirely absent from the KL theory, and purported to show that the KL term vanishes exactly. His reasoning wasa that the anomalous velocity central to KL's theory is proportional to the acceleration $\dot{\boldsymbol{k}}$ which must vanish on average at steady state because the force from $\boldsymbol{E}$ cancels that from the impurity potential.

More significantly, Smit proposed the skew-scattering mechanism (Fig. 3) as the source of the AHE (Smit, 1955, 1958). As discussed in Sec. I.B.2, in the presence of SOI, the matrix element of the impurity scattering potential reads

$$\langle \boldsymbol{k}' s|V|\boldsymbol{k}, s\rangle = \tilde{V}_{\boldsymbol{k},\boldsymbol{k}'}\left(\delta_{s,s'} + \frac{i\hbar^2}{4m^2c^2}\left(\langle s'|\boldsymbol{\sigma}|s\rangle \times \boldsymbol{k}'\right)\cdot\boldsymbol{k}\right). \tag{3.50}$$

Microscopic detailed balance would require that the transition probability $W_{n\to m}$ between states n and m is identical to that proceeding in the opposite direction ($W_{m\to n}$). It holds, for example, in the Fermi's golden-rule approximation

$$W_{n\to m} = \frac{2\pi}{\hbar}|\langle n|V|m\rangle|^2\delta(E_n - E_m), \tag{3.51}$$

where V is the perturbation inducing the transition. However, microscopic detailed balance is not generic. In calculations of the Hall conductivity, which involve the second Born approximation (third order in V), detailed balance already fails. In a simple N=1 model, skew scattering can be represented by an asymmetric part of the transition probability

$$W^A_{\boldsymbol{k}\boldsymbol{k}'} = -\tau_A^{-1}\boldsymbol{k}\times\boldsymbol{k}'\cdot\boldsymbol{M}_s. \tag{3.52}$$

When the asymmetric scattering processes is included (dubbed skew scattering), the scattering probability $W(\boldsymbol{k}\to\boldsymbol{k}')$ is distinct from $W(\boldsymbol{k}'\to\boldsymbol{k})$.

Physically, scattering of a carrier from an impurity introduces a momentum perpendicular to both the incident momentum $\boldsymbol{k}$ and the magnetization $\boldsymbol{M}$. This leads to a transverse current proportional to the longitudinal current driven by $\boldsymbol{E}$. Consequently, the Hall conductivity σ_H and the conductivity σ are both proportional to the transport lifetime τ. Equivalently, $\rho_H = \sigma_H\rho^2$ is proportional to the resistivity ρ.

As mentioned in Sec. I and in Sec. II, this prediction – qualitatively distinct from that in the KL theory – is consistent with experiments, especially on *dilute* Kondo systems. These are systems which are realized by dissolving magnetic impurities (Fe, Mn or Cr) in the non-magnetic hosts Au or Cu. (At higher concentrations, these systems become spin glasses.) Although these systems do not exhibit magnetic ordering even at T as low as 0.1 K, their Hall profiles ρ_H vs. H display an anomalous component derived from polarization of the magnetic local moments (Fig. 35 a).

Empirically, the Hall coefficient R_H has the form

$$R_H = R_0 + A/T \tag{3.53}$$

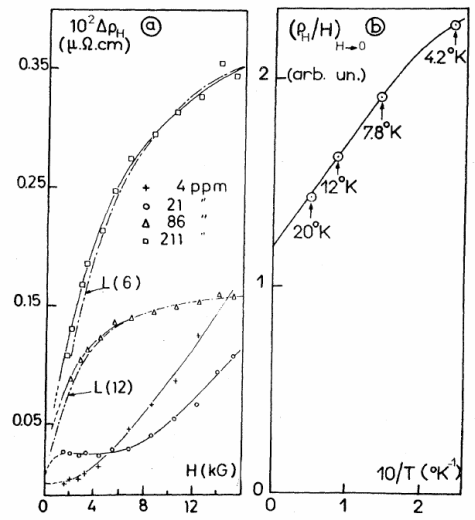


FIG. 35 The dependences of the Hall resistivity in AuFe on magnetic field (Panel a) and temperature (Panel b). [After Ref. Hurd, 1972.]

where R_0 is the nominally T-independent OHE coefficient and A is a constant (see Fig. 35 b). Identifying the second term with the paramagnetic magnetization $M = \chi H$, where $\chi(T) \propto 1/T$ is the Curie susceptibility of the local moments, we see that Eq. (3.53) is of the Pugh form Eq. (2.1).

Many groups have explored the case in which ρ and ρ_H can be tuned over a large range by changing the magnetic-impurity concentration c_i. Hall experiments on these systems in the period 1970-1985 by and large confirmed the skew-scattering prediction $\rho_H \propto \rho$. This led to the conclusion – often repeated in reviews – that the KL theory had been "experimentally disproved". As mentioned in Sec. I, this invalid conclusion ignores the singular role of TRI-breaking in ferromagnets. While Eq. (3.53) indeed describes skew scattering, the dilute Kondo system respects TRI in zero H. This essential qualitative differences between ferromagnets and systems with easily aligned local moments implies essential differences in the physics of their Hall effects.

b. Kondo theory

Kondo has proposed a finite-temperature skew-scattering model in which spin waves of local moments at finite T lead to asymmetric scattering (Kondo, 1962). In the KL theory, the moments of the ferromagnetic state are itinerant: the electrons carrying the transport current also produce the magnetization. Kondo has considered the opposite limit in which nonmagnetic s electrons scatter from spin-wave excitations of the ordered d-band local moments (with the interaction term $J\boldsymbol{S}_n\cdot\boldsymbol{s}$). Retaining terms linear in the spin-orbit coupling λ and cubic in J, Kondo derived an AHE current that arises from transition probabilities containing the skew-scattering term

$\sim \boldsymbol{k} \times \boldsymbol{k}'$. The T dependence of ρ_H matches well (especially near T_C) the ρ_H vs. T profiles measured in Ni (Jan, 1952; Jan and Gijsman, 1952; Lavine, 1961) and Fe (Jan, 1952) (Fig. 36).

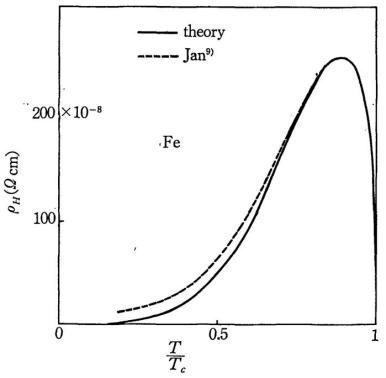


FIG. 36 Comparison of the curve of ρ_H vs. T measured in Fe by Jan with Kondo's calculation [From Ref. Kondo, 1962.]

Kondo has noted that a problem with his model is that it predicts that ρ_H should vanish when the d orbital angular momentum is quenched as in Gd (whereas ρ_H is observed to be large). A second problem is that the overall scale for ρ_H (fixed by the exchange energies F_0, F_1 and F_2) is too small by a factor of 100 compared with experiment. Kondo's model with the s-d spin-spin interaction replaced by a d(spin)-s(orbital) interaction has also been applied to antiferromagnets (Maranzana, 1967).

c. Resonant skew scattering

Resonant skew scattering arises from scattering of carriers from virtual bound states in magnetic ions dissolved in a metallic host. Examples are XM, where X = Cu, Ag and Au and M = Mn, Cr and Fe. The prototypical model is a $3d$ magnetic ion embedded in a broad s band, as described by the Anderson model (Hewson, 1993). As shown in Fig. 37, a spin-up s electron transiently occupies the spin-up bound state which lies slightly below ε_F. However, a second (spin-down) s electron cannot be captured because the on-site repulsion energy U raises its energy above ε_F. As seen in Fig. 37, the SOI causes the energies $E^m_{d\sigma}$ of the d orbitals (labelled by m) to be individually resolved. Here, $\sigma = \pm$ is the spin of the bound electron. The applied $\boldsymbol{H}$ merely serves to align spin $\sigma = +$ at each impurity.

The scattering of an incident wave $e^{i\boldsymbol{k}\cdot\boldsymbol{r}}$ is expressed by the phase shifts $\delta^m_{ls}(E)$ in the partial-wave expansion of the scattered wave. The phase shift is given by

$$\cot \delta^m_{ls}(E) = \frac{(E^m_{d\sigma} - E)}{\Delta}, \tag{3.54}$$

where Δ is the half-width of each orbital.

In the absence of SOI, $\delta^m_{ls}(E)$ is independent of m and there is no Hall current. The splitting caused by SOI

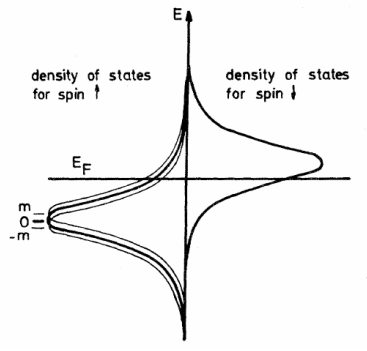


FIG. 37 Sketch of the broadened virtual bound states of a $3d$ magnetic impurity dissolved in a non-magnetic metallic host. The SOI lifts the degeneracy of the d levels indexed by m, the magnetic quantum number. [From Ref. Fert and Jaoul, 1972.]

results in a larger density of states at ε_F for the orbital m compared with $-m$ in the case where the up spin electron is more than half-filled as shown in Fig. 37. Because the phase shift is sensitive to occupancy of the impurity state (Friedel sum-rule), we have $\delta^m_{ls} \neq \delta^{-m}_{ls}$. This leads to a right-left asymmetry in the scattering, and a large Hall current ensues. Physically, a conduction electron incident with positive z-component of angular momentum m hybridizes more strongly with the virtual bound state than one with negative $-m$. This results in more electrons being scattered to the left than the right. When the up spin density of states are filled less than half, *i.e.*, $E^0_{d+} > 0$, the direction becomes the opposite, leading a sign change of the AHE.

Explicitly, the splitting of $E^m_{d\sigma}$ is given by

$$E^m_{d\pm} = E^0_{d\pm} \pm \frac{1}{2} m\lambda_{\pm}, \tag{3.55}$$

where λ_σ is the SOI energy for spin σ. Using Eq. (3.55) in (3.54), we have, to order $(\lambda_\sigma/\Delta)^2$,

$$\delta^m_{2\sigma} = \delta^0_{2\sigma} \sigma \frac{\lambda_\sigma m}{2\Delta} \sin^2 \delta^0_{2\sigma} + \frac{\lambda^2_\sigma m^2}{4\Delta^2} \sin^3 \delta^0_{2\sigma} \cos \delta^0_{2\sigma}. \tag{3.56}$$

Inserting the phase shifts into the Boltzmann transport equation, we find that the Hall angle $\gamma_\sigma \simeq \rho^\sigma_{xy}/\rho^\sigma_{xx}$ for spin σ is, to leading order in λ_σ/Δ,

$$\gamma_\sigma = \sigma \frac{3}{5} \frac{\lambda_\sigma}{\Delta} \sin(2\delta^0_{2\sigma} - \delta_1) \sin \delta_1, \tag{3.57}$$

where δ_1 is the phase shift of the p-wave channel which is assumed to be independent of m and s (Fert *et al.*, 1981; Fert and Jaoul, 1972). Thermal averaging over σ, we can obtain an estimate of the observed Hall angle γ. Its sign is given by the position of the energy level relative to ε_F. With the rough estimate $\lambda_\sigma/\Delta \simeq 0.1$, and $\sin \delta_1 \sim 0.1$, we have $|\gamma| \simeq 10^{-2}$. Without the resonant scattering enhancement, the typical value of γ is $\sim 10^{-3}$.

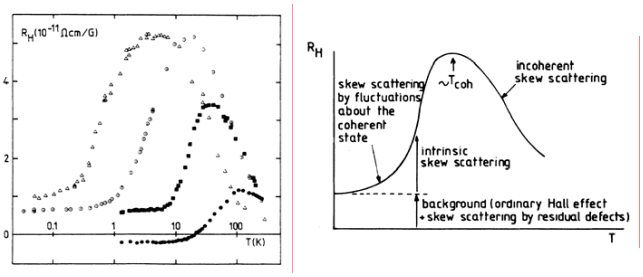


FIG. 38 The Hall coefficient R_H in heavy electron systems. Left panel: The T dependence of R_H in $CeAl_3$ (open triangle), UPt_3 (solid square), UAl_2 (solid circle), and a single crystal of $CeRu_2Si_2$ (circle dot symbol). The field $\boldsymbol{H}$ is along the c-axis. Right panel: Interpretation of the R_H-T curve based on skew scattering from local moments. After Ref. Hadzicleroux *et al.*, 1986 and Lapierre *et al.*, 1987. [From Ref. Fert and Levy, 1987.]

Heavy-electron systems are characterized by a very large resistivity ρ above a coherence temperature T_{coh} caused by scattering of carriers from strong fluctuations of the local moments formed by f-electrons at each lattice site. Below T_{coh}, the local-moment fluctuations decrease rapidly with incipient band-formation involving the f-electrons. At low T, the electrons form a Fermi liquid with a greatly enhanced effective mass. As shown in Fig. 38, the Hall coefficient R_H increases to a broad maximum at T_{coh} before decreasing sharply to a small value in the low-T coherent-band regime. Resonant skew scattering has also been applied to account for the strong T dependence of the Hall coefficient in $CeCu_2Si_2$, UBe_{13}, and UPt_3 (Coleman *et al.*, 1985; Fert *et al.*, 1981; Fert and Levy, 1987).

d. Side-jump

An extrinsic mechanism distinct from skew scattering is side-jump (Berger, 1970) (Fig. 3). Berger considered the scattering of a Gaussian wavepacket from a spherical potential well of radius R given by

$$\begin{aligned} V(r) &= \frac{\hbar^2}{2m}(k^2 - k_1^2) \quad (r < R) \\ V(r) &= 0 \qquad\qquad\qquad (r > R), \end{aligned} \tag{3.58}$$

in the presence of the SOI term $H_{SO} = (1/2m^2c^2)(r^{-1}\partial V/\partial r)S_zL_z$, where S_z (L_z) is the z-component of the spin (orbital) angular momentum. For a wavepacket incident with wavevector $\boldsymbol{k}$, Berger found that the wavepacket suffers a displacement Δy transverse to $\boldsymbol{k}$ given by

$$\Delta y = \frac{1}{6}k\lambda_c^2, \tag{3.59}$$

with $\lambda_c = \hbar/mc$ the Compton wavelength. For $k \cong k_F \cong 10^{10}\mathrm{m}^{-1}$ (in typical metals), $\Delta y \cong 3\times10^{-16}$ m is far too small to be observed.

In solids, however, the effective SOI is enhanced by band-structure effects by the factor (Fivaz, 1969)

$$\frac{2m^2c^2}{m^*\hbar}\tau_q \cong 3.4\times10^4, \tag{3.60}$$

with $\tau_q = (m^*/3\hbar^2)\sum_{m\neq n}(\chi\bar{\xi}\rho^2/\Delta E_{nm})|\langle m|\boldsymbol{q}\times\boldsymbol{p}|n\rangle|^2$. Here, $\Delta E_{nm} \cong 0.5$ eV is the gap between adjacent d-bands, $\chi \cong 0.3$ is the overlap integral, $\rho \cong 2.5\times10^{-10}$ m is the nearest-neighbor distance, and $\bar{\xi} = -(\hbar^2/2m^2c^2)\langle(r^{-1}\partial V/\partial r)\rangle \cong 0.1$ eV is the atomic SOI energy. The factor in Eq. (3.60) is essentially the ratio of the electron rest mass energy mc^2 to the energy gap ΔE_{nm}. With this enhancement, the transverse displacement is $\Delta y \simeq 0.8\times10^{-11}$ m, which renders the contribution relevant to the AHE.

However, because the side-jump contribution to σ_H is independent of τ, it is experimentally difficult to distinguish from the KL mechanism. We return to this issue in Sec. IV.A.

3. Kohn-Luttinger theory formalism

a. Luttinger theory

Partly motivated by the objections raised by Smit, Luttinger (Luttinger, 1958) revisited the AHE problem using the Kohn-Luttinger formalism of transport theory (Kohn and Luttinger, 1957; Luttinger and Kohn, 1958). Employing a systematic expansion in terms of the impurity potential $\bar{\varphi}$, he solved the transport equation for the density matrix and listed several contributions to the AHE current, including the intrinsic KL term, the skew-scattering term, and other contributions. They found that to zero-th order in $\bar{\varphi}$, the average velocity is obtained as the sum of the 3 terms $v_\beta^{(11)}$, u_β and $v_\beta^{(b)}$ defined by (Luttinger, 1958)

$$v_\beta^{(11)} = -ieE_\alpha\left(\frac{\partial J_\beta^\ell}{\partial k_\alpha} - \frac{\partial J_\alpha^\ell}{\partial k_\beta}\right)_{\boldsymbol{k}=\boldsymbol{0}}\left(\frac{\varepsilon_F}{3n_i\bar{\varphi}}\right), \tag{3.61}$$

$$u_\beta = -ieE_\alpha\left(\frac{\partial J_\beta^\ell}{\partial k_\alpha} - \frac{\partial J_\alpha^\ell}{\partial k_\beta}\right)_{\boldsymbol{k}=\boldsymbol{0}}, \tag{3.62}$$

and

$$v_\beta^{(b)} = ieE_\alpha\left[\left(\frac{\partial J_\beta^\ell}{\partial k_\alpha} - \frac{\partial J_\alpha^\ell}{\partial k_\beta}\right)C - \varepsilon_F T_{\alpha\beta}^{(0)}\right], \tag{3.63}$$

with n_i the impurity concentration. (For the definition of $T_{\alpha\beta}^{(0)}$, see Eq. (4.27) of Ref. Luttinger, 1958).

The first term $v_\beta^{(11)}$ is the skew-scattering contribution, while the second u_β is the velocity obtained by KL (Karplus and Luttinger, 1954). The third term $v_\beta^{(b)}$ is another term of the same order as u_β.

The issues raised by comparing intrinsic vs. extrinsic AHE mechanisms involve several fundamental issues in

the theory of transport and quantum systems away from equilibrium. Following Smit (Smit, 1955, 1958) and Luttinger (Luttinger, 1958), we consider the wavefunction expanded in terms of Bloch waves ψ_ℓ's, *viz.*

$$\psi(t) = \sum_\ell a_\ell(t)\psi_\ell, \tag{3.64}$$

where $\ell = (n, \boldsymbol{k})$ stands for the band index n and wavevector $\boldsymbol{k}$. The corresponding expectation value of the position operator $\bar{x}_\beta$ is given by

$$\bar{x}_\beta = i\sum_\ell \frac{\partial a_\ell}{\partial k_\beta} a_\ell^* + i\sum_{\ell,\ell'} a_{\ell'} a_\ell^* J_\beta^{\ell,\ell'} \tag{3.65}$$

where $J_\beta^{\ell,\ell'}$ was defined in Eq. (3.40). Taking the quantum-statistical average using the density matrix $(\rho_T)_{\ell',\ell} = \langle a_{\ell'} a_\ell^* \rangle$, the expectation value can be written as

$$\langle \bar{x}_\beta \rangle = i\sum_\ell \frac{\partial (\rho_T)_{\ell,\ell}}{\partial k_\beta}|_{\boldsymbol{k}=\boldsymbol{k}'} + i\sum_{\ell,\ell'} (\rho_T)_{\ell'\ell} J_\beta^{\ell,\ell'}. \tag{3.66}$$

It may be seen that the second term in Eq. (3.66) does not contribute to the current because it is a regular function of $\boldsymbol{k}$, and the expectation value of its time-derivative is zero. Finally, one obtains the expression

$$\langle \bar{v}_\beta \rangle = i\sum_\ell \frac{\partial (\dot{\rho}_T)_{\ell,\ell}}{\partial k_\beta}|_{\boldsymbol{k}=\boldsymbol{k}'} \tag{3.67}$$

by taking the time-derivative of Eq.(3.66).

Smit (Smit, 1955, 1958) assumed $a_\ell(t) = |a_\ell| e^{-i\varepsilon_{n\boldsymbol{k}} t}$ and obtained the diagonal part as

$$i(\dot{\rho}_T)_{\ell,\ell} = \frac{\partial \varepsilon_{n\boldsymbol{k}}}{\partial k_\beta} \langle |a_\ell|^2 \rangle, \tag{3.68}$$

while the off-diagonal part averages to zero because of the oscillatory factor $e^{-i(\varepsilon_\ell - \varepsilon_{\ell'})t}$. Inserting Eq. (3.68) in Eq. (3.67) and using $(\rho_T)_{\ell\ell} = \langle |a_\ell|^2 \rangle$, one obtains the usual expression for the velocity, *i.e.*,

$$\langle \bar{v}_\beta \rangle = \sum_\ell (\rho_T)_{\ell,\ell} \frac{\partial \varepsilon_{n\boldsymbol{k}}}{\partial k_\beta} \tag{3.69}$$

which involves the group velocity, but not the anomalous velocity. A subtlety in the expression Eq. (3.67) is clarified by writing $\rho = \rho_0 + f e^{st}$ where e^{st} is the adiabatic factor, and $\dot{\rho}_T = s f e^{st}$. This leads to the expression

$$\langle \bar{v}_\beta \rangle = is\sum_\ell \frac{\partial (f)_{n\boldsymbol{k},n\boldsymbol{k}'}}{\partial k_\beta}|_{\boldsymbol{k}=\boldsymbol{k}'}, \tag{3.70}$$

which approaches a finite value in the limit $s \to 0$. This means that $\frac{\partial (f)_{n\boldsymbol{k},n\boldsymbol{k}'}}{\partial k_\beta}|_{\boldsymbol{k}=\boldsymbol{k}'} \sim 1/s$, *i.e.*, a singular function of s. This is in sharp contrast to f itself, which is a regular function as $s \to 0$, which KL estimated. They considered the current or velocity operator instead of the position operator, the latter of which is unbounded and even ill-defined for periodic boundary conditions.

Luttinger (Luttinger, 1958) argued that the ratio $v_\beta^{(11)}/u_\beta$ equals $\varepsilon_F/(3n_i\bar{\varphi})$, which may become less than 1 for large impurity concentration n_i. However, if we assume $\bar{\varphi}$ is comparable to ε_F, the expansion parameter is $\varepsilon_F\tau/\hbar$, *i.e.*, $v_\beta^{(11)}/u_\beta = \varepsilon_F\tau/\hbar$.

The "metallicity" parameter $\varepsilon_F\tau/\hbar$ plays a key role in modern quantum-transport theory, especially in the weak localization and interaction theory (Lee and Ramakrishnan, 1985). Metallic conduction corresponds to $\varepsilon_F\tau/\hbar \gg 1$. More generally, if one assumes that the anomalous Hall conductivity σ_H is first order in the spin-orbit energy Δ, it can be written in a scaling form as

$$\sigma_H = \frac{e^2}{ha} \cdot \frac{\Delta}{\varepsilon_F} f\left(\frac{\hbar}{\varepsilon_F\tau}\right), \tag{3.71}$$

where the scaling function can be expanded as

$$f(x) = \sum_{n=-1}^{\infty} c_n x^n. \tag{3.72}$$

Here, c_n's are constants of the order of unity. The leading order term $c_{-1}x^{-1}$ corresponds to the skew-scattering contribution $\propto \tau$, while the second constant term c_0 is the contribution found by KL. If this expansion is valid, the intrinsic contribution by KL is always smaller than the skew scattering contribution in the metallic region with $\hbar/\varepsilon_F\tau \ll 1$. One should note however that the right hand side of this inequality should really have a smaller value to account for the weakness of the skew scattering amplitude. When both are comparable, *i.e.*, $\hbar/\varepsilon_F\tau \sim 1$, one needs to worry about the localization effect and the system is nearly insulating, with a conduction that is of the hopping type. This issue is discussed in more detail in Secs. II.A, II.E, and IV.D.

b. Adams-Blount formalism

Adams and Blount (Adams and Blount, 1959) expressed the KL theory in a way that anticipates the modern Berry-phase treatment by introducing the concept of "field-modified energy bands" and the "intracell" coordinate. They considered the diagonal part of the coordinate matrix in the band n as

$$x_c^\mu = i\hbar\frac{\partial}{\partial p_\mu} + X_\mu^{nn}(\boldsymbol{p}), \tag{3.73}$$

which is analogous to Eq. (3.39) obtained by KL. The first term is the Wannier coordinate identifying the lattice site, while the second term – the "intracell" coordinate – locates the wavepacket centroid *inside* a unit cell. Significantly, the *intracell* nature of X_μ^{nn} implies that it involves virtual interband transitions. Although the motion of the wavepacket is confined to the conduction band, its position inside a unit cell involves virtual

occupation of higher bands whose effects appear as a geometric phase (Ong and Lee, 2006). They found that the curl $\nabla_{\boldsymbol{k}} \times \boldsymbol{X}^{nn}$ acted like an effective magnetic field that lives in $\boldsymbol{k}$ space.

The application of an electric field $\boldsymbol{E}$ leads to an anomalous (Luttinger) velocity, which gives a Hall current that is manifestly dissipationless. This is seen by evaluating the commutation relationship of x_c^μ and x_c^ν. We have

$$\begin{aligned}[x_c^\mu, x_c^\nu] &= i\hbar\left[\frac{\partial X_\nu^{nn}}{\partial p_\mu} - \frac{\partial X_\mu^{nn}}{\partial p_\nu}\right] \\ &= i\hbar\varepsilon_{\mu\nu\lambda}\boldsymbol{B}_n(\boldsymbol{p})_\lambda, \end{aligned} \tag{3.74}$$

where we have defined the field $\boldsymbol{B}_n(\boldsymbol{p}) = \nabla_p \times \boldsymbol{X}^{nn}(\boldsymbol{p})$. This is analogous to the commutation relationship among the components of $\boldsymbol{\pi} = \boldsymbol{p} + (e/c)\boldsymbol{A}$ in the presence of the vector potential,*i.e.*, $[\pi_\mu, \pi_\nu] = i\hbar\varepsilon_{\mu\nu\lambda}[\nabla_r \times A(\boldsymbol{r})]_\lambda = i\hbar B_\lambda(\boldsymbol{r})$. The anomalous velocity arises from the fictitious "magnetic field" $\boldsymbol{B}_n(\boldsymbol{p})$ (which lives in momentum space), and non-commutation of the gauge-covariant coordinates x_c^μ's. This insight anticipated the modern idea of Berry phase curvature (see Secs. III.B and IV.A for details).

Taking the commutator between x_c^μ and the Hamiltonian $H_{nn} = E_n(\boldsymbol{p}) - F^\nu x_c^\nu$, we obtain

$$\boldsymbol{v}_{nn} = -i[\boldsymbol{x}_c, H_{nn}] = \frac{\partial E_n(\boldsymbol{p})}{\partial \boldsymbol{p}} - \boldsymbol{F} \times \boldsymbol{B}_n(\boldsymbol{p}). \tag{3.75}$$

The second term on the right hand side is called the anomalous velocity. Adams and Blount reproduced the results of Luttinger (Luttinger, 1958) and demonstrated it for the simple case of a uniform field $\boldsymbol{B}_n(\boldsymbol{p}) = \boldsymbol{D}$. As recognized by Smit (Smit, 1955, 1958), the currents associated with the anomalous velocities driven by $\boldsymbol{E}$ and by the impurity potential mutually cancel in steady state. However, $\boldsymbol{D}$ introduces corrections to the "driving term" and the "scattering term" in the transport equation. As a consequence, the current $\boldsymbol{J}$ is

$$\begin{aligned}\boldsymbol{J} &= ne^2 \sum_k \left(-\frac{2}{3} E \frac{df^{(0)}}{dE}\right) \\ &\times \left[\frac{\boldsymbol{F}\tau}{m} - \frac{\boldsymbol{F} \times \boldsymbol{D}}{\hbar} + \left(\frac{\tau^2 k^2}{3m\tau_A}\right)(\boldsymbol{F} \times \boldsymbol{D})\right]. \end{aligned} \tag{3.76}$$

Note that the current arises entirely from the average of the "normal current". However, the second term in Eq. (3.76) is similar to the anomalous velocity and is consistent with the conclusions of KL (Karplus and Luttinger, 1954) and Luttinger (Luttinger, 1958). The consensus now is that the KL contribution exists. However, in the clean limit $\tau \to \infty$, the leading contribution to the AHE conductivity comes from the skew-scattering term. A more complete discussion of the semiclassical treatment is in Sec. IV.A.

c. Nozieres-Lewiner theory

Adopting the premises of Luttinger's theory (Luttinger, 1958), Nozieres and Lewiner (Nozieres and Lewiner, 1973) investigated a simplified model comprised of one conduction and one valence band to derive all the possible contributions to the AHE. The Fermi level ε_F was assumed to lie near the bottom of the conduction band. Integrating over the valence band states, Nozieres and Lewiner derived an effective Hamiltonian for a state $\boldsymbol{k}$ in the conduction band. The derived position operator is $\boldsymbol{r}_{\text{eff}} = \boldsymbol{r} + \boldsymbol{\rho}$, where the new term $\boldsymbol{\rho}$ which involves the SOI parameter λ is given by

$$\boldsymbol{\rho} = -\lambda \boldsymbol{k} \times \boldsymbol{S}. \tag{3.77}$$

This polarization or effective shift modifies the transport equation to produce several contributions to σ_H. In their simple model, the anomalous Hall current $\boldsymbol{J}_{AHE}$ (besides that from the skew scattering) is

$$\boldsymbol{J}_{AHE} = 2Ne^2\lambda \boldsymbol{E} \times \bar{\boldsymbol{S}}, \tag{3.78}$$

where N is the carrier concentration, and $\bar{\boldsymbol{S}}$ is the averaged spin polarization. The sign is opposite to that of the intrinsic term $\boldsymbol{J}_{intrinsic} = -2Ne^2\lambda \boldsymbol{E} \times \bar{\boldsymbol{S}}$ obtained from the SOI in an ideal lattice. They identified all the terms as arising from the spin-orbit correction to the scattering potential, *i.e.*, in their theory there is no contribution from the intrinsic mechanism. However, one should be cautious about this statement because these cancellations occur among the various contributions and such cancellations can be traced back to the fact that the Berry curvature is independent of $\boldsymbol{k}$. In particular, it is often the case that the intrinsic contribution survives even when μ lies inside an energy gap, *i.e.*, $N = 0$ (the side-jump contribution is zero in this case). This issue lies at the heart of the discussion of the topological aspect of the AHE.

IV. LINEAR TRANSPORT THEORIES OF THE AHE

In this section we describe the three linear response theories now used to describe the AHE. All three theories are formally equivalent in the $\varepsilon_F\tau \gg 1$ limit. The three theories make nearly identical predictions; the small differences between the revised semiclassical theory and the two formalism of the quantum theory are thoroughly understood at least for several different toy model systems. The three different approaches have relative advantages and disadvantages. Considering all three provides a more nuanced picture of AHE physics. Their relative correspondence has been shown analytically in several simple models (Sinitsyn, 2008; Sinitsyn *et al.*, 2007). The generalized semiclassical Boltzmann transport theory which takes the Berry phase into account is reviewed in Sec. IV.A; this theory has the advantage of greater physical transparency, but it lacks the systematic character of the microscopic quantum-mechanical theories whose machinery deals automatically with the problems of interband coherence. Another limitation of the semiclassical

Boltzmann approach is that the "quantum correction" to the conductivities, *i.e.*, the higher order terms in $\hbar/\varepsilon_F\tau$, which lead to the Anderson localization and other interesting phenomena (Lee and Ramakrishnan, 1985) cannot be treated systematically.

The microscopic quantum-mechanical linear response theories based on the Kubo formalism and the Keldysh (non-equiliribrum Green's function) formalism are reviewed in Sec. IV.B.1 and Sec. IV.C, respectively. These formulations of transport theory are organized differently but are essentially equivalent in the linear regime. In the Kubo formalism, which is formulated in terms of the equilibrium Green's functions, the intrinsic contribution is more readily calculated, especially when combined with first-principles electronic structure theory in applications to complex materials. The Keldysh formalism can more easily account for finite lifetime quantum scattering effects and take account of the broadened quasiparticle spectral features due to the self-energy, while at the same time maintaining a structure more similar to that of semiclassical transport theory (Onoda *et al.*, 2006a). AWe contrast these techniques by comparing their applications to a common model, the ferromagnetic Rashba model in two-dimensions (2D) which has been studied intensively in recent years (Sec.IV.D).

A. Semiclassical Boltzmann approach

As should be clear from the complex phenomenology of the AHE in various materials classes discussed in Sec. II, it is not easy to establish a *one-size-fits-all* theory for this phenomenom. From a microscopic point of view the AHE is a formidable beast. In subsequent sections we outline systematic theories of the AHE in metallic systems which employ Keldysh and Kubo linear response theory formalisms and are organized around an expansion in disorder strength, characterized by the dimensionless quantity $\hbar/\varepsilon_F\tau$. A small value for this parameter may be taken as a definition of the *good metal*. We start with semiclassical theory, however, because of its greater physical transparency. In this section we outline the modern version (Sinitsyn, 2008; Sinitsyn *et al.*, 2007) of the semiclassical transport theory of the AHE. This theory augments standard semiclassical transport theory by accounting for coherent band-mixing by the external electric field (which leads to the anomalous velocity contribution) and by a random disorder potential (which leads to side jump). For simple models in which a comparison is possible, the two theories (*i.e.* (i) the Boltzmann theory with all side-jump effects (formulated now in a proper gauge-invariant way) and the anomalous velocity contribution included and (ii) the metallic limit of the more systematic Keldysh and Kubo formalism treatments) give identical results for the AHE. This section provides a more compact version of the material presented in the excellent review by Sinitsyn (Sinitsyn, 2008), to which we refer readers interested in further detail. Below we take $\hbar = 1$ to simplify notation.

In semiclassical transport theory one retreats from a microscopic description in terms of delocalized Bloch states to a formulation of transport in terms of the dynamics of wavepackets of Bloch states with a well defined band momentum and position $(n, \boldsymbol{k}_c, \boldsymbol{r}_c)$ and scattering between Bloch states due to disorder. The dynamics of the wavepackets between collisions can be treated by an effective Lagrangian formalism. The wavepacket distribution function is assummed to obey a classical Boltzmann equation which in a spatially uniform system takes the form (Sundaram and Niu, 1999):

$$\frac{\partial f_l}{\partial t} + \hbar\dot{\boldsymbol{k}}_c \cdot \frac{\partial f_l}{\partial \boldsymbol{k}_c} = -\sum_{l'}(\omega_{l',l} f_l - \omega_{l,l'} f_{l'}). \qquad (4.1)$$

Here the label l is a composition of band and momenta $(n, \boldsymbol{k}_c)$ labels and $\Omega_{l',l}$, the disorder averaged scattering rate between wavepackets defined by states l and l', is to be evaluated fully quantum mechanically. The semiclassical description is useful in clarifying the physical meaning and origin of the different mechanism contributing to the AHE. However, as explained in this review, contributions to the AHE which are important in a relative sense often arise from inter-band coherence effects which are neglected in conventional transport theory. The traditional Boltzmann equation therefore requires elaboration in order to achieve a successful description of the AHE.

There is a substantial literature (Berger, 1970; Jungwirth *et al.*, 2002b; Smit, 1955) on the application of Boltzmann equation concepts to AHE theory (see Sec. III.C). However stress was often placed only on one of the several possible mechanisms, creating a lot of confusion. A cohesive picture has been lacking until recently (Sinitsyn, 2008; Sinitsyn *et al.*, 2006, 2005). In particular, a key problem with some prior theory was that it incorrectly ascribed physical meaning to gauge dependent quantities. In order to build the correct gauge-invariant semiclassical theory of AHE we must take the following steps (Sinitsyn, 2008):

i) obtain the equations of motion for a wavepacket constructed from spin-orbit coupled Bloch electrons,

ii) derive the effect of scattering of a wave-packet from a smooth impurity, yielding the correct gauge-invariant expression for the corresponding side-jump,

iii) use the equations of motion and the scattering rates in Eq. (4.1) and solve for the non-equillibirum distribution function, carefully accounting for the points at which modifications are required to account for side-jump,

iv) utilize the non-equilibrium distribution function to calculate the dc anomalous Hall currents, again accounting for the contribution of side-jump to the macroscopic current.

The validity of this approach is partially established in the following sections by direct comparison with fully microscopic calculations for simple model systems in which we are able to identify each semiclassically defined mechanisms with a specific part of the microscopic calculations.

1. Equation of motion of Bloch states wave-packets

We begin by defining a wavepacket centered at position $\boldsymbol{r}_c$ with average momentum $\boldsymbol{k}_c$:

$$\Psi_{\boldsymbol{k}_c,\boldsymbol{r}_c}(\boldsymbol{r},t)=\frac{1}{\sqrt{V}}\sum_{\boldsymbol{k}} w_{\boldsymbol{k}_c,\boldsymbol{r}_c}(\boldsymbol{k})e^{i\boldsymbol{k}\cdot(\boldsymbol{r}-\boldsymbol{r}_c)}u_{n\boldsymbol{k}}(\boldsymbol{r}). \quad (4.2)$$

A key aspect of this wavepacket is that the complex function, sharply peaked around $\boldsymbol{k}_c$, must have a very specific phase factor in order to have the wavepacket centered around $\boldsymbol{r}_c$. This can be shown to be (Marder, 2000; Sundaram and Niu, 1999):

$$w_{\boldsymbol{k}_c,\boldsymbol{r}_c}(\boldsymbol{k})=|w_{\boldsymbol{k}_c,\boldsymbol{r}_c}(\boldsymbol{k})|\exp[i(\boldsymbol{k}-\boldsymbol{k}_c)\cdot\boldsymbol{a}_n], \quad (4.3)$$

where $\boldsymbol{a}_n\equiv\langle u_{n\boldsymbol{k}}|i\partial_{\boldsymbol{k}}u_{n\boldsymbol{k}}\rangle$ is the Berry's connection of the Bloch state (see Sec. I.B). We can generate dynamics for the wavepacket parameters $\boldsymbol{k}_c$ and $\boldsymbol{r}_c$ by constructing a semiclassical Lagrangian from the quantum wavefunctions:

$$\begin{aligned}\mathcal{L} &= \langle\Psi_{\boldsymbol{k}_c,\boldsymbol{r}_c}|i\frac{\partial}{\partial t}-H_0+eV|\Psi_{\boldsymbol{k}_c,\boldsymbol{r}_c}\rangle \\ &= \hbar\boldsymbol{k}_c\cdot\dot{\boldsymbol{r}}_c+\hbar\dot{\boldsymbol{k}}_c\cdot\boldsymbol{a}_n(\boldsymbol{k}_c)-E(\boldsymbol{k}_c)+eV(\boldsymbol{r}_c). \quad (4.4)\end{aligned}$$

All the terms in the above Lagrangian are common to conventional semiclassical theory except for the second term, which is a geometric term in phase space depending only on the path of the trajectory in this space. This term is the origin of the momentum-space Berry phase (Berry, 1984) effects in anomalous transport in the semiclassical formalism. The corresponding Euler-Lagrange equations of motion are:

$$\begin{aligned}\hbar\dot{\boldsymbol{k}}_c &= -e\boldsymbol{E} \quad (4.5)\\ \dot{\boldsymbol{r}}_c &= \frac{\partial E_n(\boldsymbol{k}_c)}{\partial\boldsymbol{k}_c}-\hbar\dot{\boldsymbol{k}}_c\times\boldsymbol{b}_n(\boldsymbol{k}_c) \quad (4.6)\end{aligned}$$

where $\boldsymbol{b}_n(\boldsymbol{k}_c)=\boldsymbol{\nabla}\times\boldsymbol{a}_n$ is the Berry's curvature of the Bloch state. Compared to the usual dynamic equations for wave-packets formed by free electrons, a new term emerges due to the non-zero Berry's curvature of the Bloch states. This term, which is already linear in electric field $\boldsymbol{E}$, is of the Hall type and as such will give rise in the linear transport regime to a Hall current contribution from the entire Fermi sea, *i.e.*, $j^{int}_{Hall}=-e^2\boldsymbol{E}\times\frac{1}{V}\sum_{\boldsymbol{k}}f_0(E_{n\boldsymbol{k}})\boldsymbol{b}_n(\boldsymbol{k})$.

2. Scattering and the side-jump

From the theory of elastic scattering we know that the transition rate $\omega_{l,l'}$ in Eq. (4.1) is given by the T-matrix element of the disorder potential:

$$\omega_{l'l}\equiv 2\pi|T_{l'l}|^2\delta(\epsilon_{l'}-\epsilon_l). \quad (4.7)$$

The scattering T-matrix is defined by $T_{l'l}=\langle l'|\hat{V}|\psi_l\rangle$, where $\hat{V}$ is the impurity potential operator and $|\psi_l\rangle$ is the eigenstate of the full Hamiltonian $\hat{H}=\hat{H}_0+\hat{V}$ that satisfies the Lippman-Schwinger equation $|\psi_l\rangle=|l\rangle+(\epsilon_l-\hat{H}_0+i\eta)^{-1}\hat{V}|\psi_l\rangle$. $|\psi_l\rangle$ is the state which evolves adiabatically from $|l\rangle$ when the disorder potential is turned on slowly. For weak disorder one can approximate the scattering state $|\psi_l\rangle$ by a truncated series in powers of $V_{ll'}=\langle l|\hat{V}|l'\rangle$:

$$|\psi_l\rangle\approx|l\rangle+\sum_{l''}\frac{V_{l''l}}{\epsilon_l-\epsilon_{l''}+i\eta}|l''\rangle+\dots \quad (4.8)$$

Using this expression in the above definition of the T-matrix and substituting it into Eq. (4.7), one can expand the scattering rate in powers of the disorder strength

$$\omega_{ll'}=\omega^{(2)}_{ll'}+\omega^{(3)}_{ll'}+\omega^{(4)}_{ll'}\cdots, \quad (4.9)$$

where $\omega^{(2)}_{ll'}=2\pi\langle|V_{ll'}|^2\rangle_{dis}\delta(\epsilon_l-\epsilon_{l'})$,

$$\omega^{(3)}_{ll'}=2\pi\left(\sum_{l''}\frac{\langle V_{ll'}V_{l'l''}V_{l''l}\rangle_{dis}}{\epsilon_l-\epsilon_{l''}-i\eta}+c.c.\right)\delta(\epsilon_l-\epsilon_{l'}), \quad (4.10)$$

and so on.

We can always decompose the scattering rate into components that are symmetric and anti-symmetric in the state indices: $\omega^{(s/a)}_{l'l}\equiv(\omega_{ll'}\pm\omega_{l'l})/2$. In conventional Boltzmann theory the AHE is due solely to the anti-symmetric contribution to the scattering rate (Smit, 1955).

The physics of this contribution to the AHE is quite similar to that of the longitudinal conductivity. In particular, the Hall conductivity it leads to is proportional to the Bloch state lifetime τ. Since $\omega^{(2)}_{l'l}$ is symmetric, the leading contribution to $\omega^{(a)}_{l'l}$ appears at order V^3. Partly for this reason the skew scattering AHE conductivity contributions is always much smaller than the longitudinal conductivity. (It is this property which motivates the identification below of additional transport mechanism which contribute to the AHE and can be analyzed in semiclassical terms.) The symmetric part of $\omega^{(3)}_{ll'}$ is not essential since it only renormalizes the second order result for $\omega^{(2)}_{l'l}$ and the antisymmetric is given by

$$\omega^{(3a)}_{ll'}=-(2\pi)^2\sum_{l''}\delta(\epsilon_l-\epsilon_{l''})\mathrm{Im}\langle V_{ll'}V_{l'l''}V_{l''l}\rangle_{dis}\delta(\epsilon_l-\epsilon_{l'}). \quad (4.11)$$

This term is proportional to the density of scatterers, n_i. Skew scattering has usually been associated directly with $\omega^{(3a)}$, neglecting in particular the higher order term $\omega^{(4a)}_{ll'}$ which is proportional to n_i^2 and should not be disregarded because it gives a contribution to the AHE which is of

the same order as the side-jump contribution considered below. This is a common mistake in the semiclassical analyses of the anomalous Hall effect (Sinitsyn, 2008).

Now we come to the interesting side-jump story. Because the skew scattering conductivity is small, we have to include effects which are absent in conventional Boltzmann transport theory. Remarkably it is possible to provide a successful analysis of one of the main additional effects, the side-jump correction, by means of a careful semiclassical analysis. As we have mentioned previously *side jump* refers to the microscopic displacement $\delta \boldsymbol{r}_{l,l'}$ experienced by a wave-packets formed from a spin-orbit coupled Bloch states, when scattering from state l to state l' under the influence of a disorder potential. In the presence of an external electric field side jump leads to an energy shift $\Delta U_{l,l'} = -e\boldsymbol{E}\cdot\delta\boldsymbol{r}_{l,l'}$. Since we are assuming only elastic scattering, an upward shift in potential energy requires a downward shift in band energy and *vice-versa*. We therefore need to adjust Eq. (4.1) by adding $\sum_{l'}\omega^s_{l,l'}\frac{\partial f_0(\epsilon_l)}{\epsilon_l}e\boldsymbol{E}\cdot\delta\boldsymbol{r}_{l,l'}$ to the r.h.s.

But what about the side-jump itself? An expression for the side-jump $\delta\boldsymbol{r}_{l,l'}$ associated with a particular transition can be derived by integrating $\dot{\boldsymbol{r}}_c$ through a transition (Sinitsyn, 2008). We can write

$$\begin{aligned}\dot{\boldsymbol{r}}_c \;=\; & \frac{d}{dt}\langle\Psi_{\boldsymbol{k}_c,\boldsymbol{r}_c}(\boldsymbol{r},t)|\boldsymbol{r}|\Psi_{\boldsymbol{k}_c,\boldsymbol{r}_c}(\boldsymbol{r},t)\rangle = \frac{d}{dt}\Big\{\int\frac{d\boldsymbol{r}}{V}\int d\boldsymbol{k}\\ & \int d\boldsymbol{k}' w(\boldsymbol{k})w^*(\boldsymbol{k}')e^{-i\boldsymbol{k}'\cdot\boldsymbol{r}}\left(\boldsymbol{r}e^{i\boldsymbol{k}\cdot\boldsymbol{r}}\right)u^*_{n\boldsymbol{k}'}(\boldsymbol{r})\\ & u_{n\boldsymbol{k}}(\boldsymbol{r})e^{i(E(\boldsymbol{k}')-E(\boldsymbol{k}))t/\hbar}\Big\} = \frac{dE_n(\boldsymbol{k}_c)}{d\boldsymbol{k}_c} + \\ & \frac{d}{dt}\left\{\int_{cell}d\boldsymbol{r}\int d\boldsymbol{k}w^*(\boldsymbol{k})u_{n\boldsymbol{k}}(\boldsymbol{r})\left(i\frac{\partial}{\partial_{\boldsymbol{k}}}w(\boldsymbol{k})u_{n\boldsymbol{k}}(\boldsymbol{r})\right)\right\}\end{aligned} \tag{4.12}$$

This expression is equivalent to the equations of motion derived within the Lagrangian formalism; this form has the advantage of making it apparent that in scattering from state l to a state l' a shift in the center of mass coordinate will accompany the velocity deflection. From Eq. (4.12) it appears that the scattering shift will go approximately as:

$$\delta\boldsymbol{r}_{l',l} \approx \langle u_{l'}|i\frac{\partial}{\partial\boldsymbol{k}'}u_{l'}\rangle - \langle u_l|i\frac{\partial}{\partial\boldsymbol{k}}u_l\rangle. \tag{4.13}$$

This quantity has usually been associated with the side-jump, although it is gauge-dependent and therefore arbitrary in value. The correct expression for the side jump is similar to this one, at least for the smooth impurity potentials situation, but was derived only recently by Sinitsyn *et al.* (Sinitsyn *et al.*, 2006, 2005):

$$\delta\boldsymbol{r}_{l'l} = \langle u_{l'}|i\frac{\partial}{\partial\boldsymbol{k}'}u_{l'}\rangle - \langle u_l|i\frac{\partial}{\partial\boldsymbol{k}}u_l\rangle - \hat{\boldsymbol{D}}_{\boldsymbol{k}',\boldsymbol{k}}\arg[\langle u_{l'}|u_l\rangle], \tag{4.14}$$

where $\arg[a]$ is the phase of the complex number a and $\hat{\boldsymbol{D}}_{\boldsymbol{k}',\boldsymbol{k}} = \frac{\partial}{\partial\boldsymbol{k}'} + \frac{\partial}{\partial\boldsymbol{k}}$. The last term is essential and makes the expression for the resulting side-jump gauge invariant. Note that the side-jump is independent of the details of the impurity potential or of the scattering process. As this discussion shows, the side jump contribution to motion during a scattering event is analogous to the anomalous velocity contribution to wave-packet evolution between collisions, with the role of the disorder potential in the former case taken over in the latter case by the external electric field.

3. Kinetic equation for the semiclasscial Boltzmann distribution

Equations (4.7) and (4.14) contain the quantum mechanical information necessary to write down a semiclasscial Boltzmann equation that takes into account both the change of momentum and the coordinate shift during scattering in the presence of a driving electric field $\boldsymbol{E}$. Keeping only terms up to linear order in the electric field the Boltzmann equation reads (Sinitsyn *et al.*, 2006):

$$\frac{\partial f_l}{\partial t} + e\boldsymbol{E}\cdot\boldsymbol{v}_{0l}\frac{\partial f_0(\epsilon_l)}{\partial\epsilon_l} = -\sum_{l'}\omega_{ll'}[f_l - f_{l'} - \frac{\partial f_0(\epsilon_l)}{\partial\epsilon_l}e\boldsymbol{E}\cdot\delta\boldsymbol{r}_{l'l}], \tag{4.15}$$

where $\boldsymbol{v}_{0l}$ is the usual group velocity $\boldsymbol{v}_{0l} = \partial\epsilon_l/\partial\boldsymbol{k}$. Note that for elastic scattering we do not need to take account of the Pauli blocking which yields factors like $f_l(1-f_{l'})$ on the r.h.s. of Eq. (4.15), and that the collision terms are linear in f_l as a consequence. (For further discussion of this point see Appendix B in Ref. Luttinger and Kohn, 1955.) This Boltzmann equation has the standard form except for the coordinate shift contribution to the collision integral explained above. Because of the side-jump effect, the collision term does not vanish when the occupation probabilities f_l are replaced by their thermal equilibrium values when an external electric field is present: $f_0(\epsilon_l) - f_0(\epsilon_l - e\boldsymbol{E}\cdot\delta\boldsymbol{r}_{ll'}) \approx -\frac{\partial f_0(\epsilon_l)}{\partial\epsilon_l}e\boldsymbol{E}\cdot\delta\boldsymbol{r}_{l'l} \neq 0$. Note that the term containing $\omega_{l,l'}f_l$ should be written as $\omega^{(s)}_{l,l'}f_l - \omega^{(a)}_{l,l'}f_l$. In making this simplification we are imagining a typical simple model in which the scattering rate depends only on the angle between $\boldsymbol{k}$ and $\boldsymbol{k}'$. In that case, $\sum_{l'}\omega^{(a)}_{l,l'} = 0$ and we can ignore a complication which is primarily notational.

The next step in the Boltzmann theory is to solve for the non-equilibrium distribution function f_l to leading order in the external electric field. We linearize by writing f_l as the sum of the equilibrium distribution $f_0(\epsilon_l)$ and non-equilibrium corrections:

$$f_l = f_0(\epsilon_l) + g_l + g^{adist}_l, \tag{4.16}$$

where we split the non-equilibrium contribution into two terms g_l and $g^{\rm adist}$ in order to capture the skew scattering effect. g_l and $g^{\rm adist}$ solve independent self-consistent time-independent equations (Sinitsyn *et al.*, 2006):

$$e\boldsymbol{E}\cdot\boldsymbol{v}_{0l}\frac{\partial f_0(\epsilon_l)}{\partial\epsilon_l} = -\sum_{l'}\omega_{ll'}(g_l - g_{l'}) \tag{4.17}$$

and

$$\sum_{l'}\omega_{ll'}\left(g_l^{adist}-g_{l'}^{adist}-\frac{\partial f_0(\epsilon_l)}{\partial\epsilon_l}e\boldsymbol{E}\cdot\delta\boldsymbol{r}_{l'l}\right)=0. \tag{4.18}$$

In Eq. (4.14) we have noted that $\delta\boldsymbol{r}_{l'l}=\delta\boldsymbol{r}_{ll'}$. To solve Eq. (4.17) we further decompose $g_l=g_l^s+g_l^{a1}+g_l^{a2}$ so that

$$\sum_{l'}\omega_{ll'}^{(3a)}(g_l^s-g_{l'}^s)+\sum_{l'}\omega_{ll'}^{(2)}(g_l^{a1}-g_{l'}^{a1})=0, \tag{4.19}$$

$$\sum_{l'}\omega_{ll'}^{(4a)}(g_l^s-g_{l'}^s)+\sum_{l'}\omega_{ll'}^{(2)}(g_l^{a2}-g_{l'}^{a2})=0. \tag{4.20}$$

Here g_l^s is the usual diagonal non-equilibrium distributions function which can be shown to be proportional to n_i^{-1}. From Eq. (4.11) and $\omega_{ll'}^{(3a)}\sim n_i$, it follows that $g_l^{3a}\sim n_i^{-1}$. Finally, from $\omega_{ll'}^{(4a)}\sim n_i^2$ and Eq. (4.20), it follows that $g_l^{4a}\sim n_i^0$; illustrating the dangers of ignoring the $\omega_{ll'}^{(4a)}$ contribution to $\omega_{l,l'}$. One can also show from Eq. (4.18) that $g_l^{adist}\sim n_i^0$.

4. Anomalous velocities, anomalous Hall currents, and anomalous Hall mechanisms

We are now at the final stage where we use the non-equilibrium distribution function derived from Eqs. (4.17)-(4.20) to compute the anomalous Hall current. To do so we need first to account for all contributions to the velocity of semiclassical particles that are consistent with this generalized semiclassical Boltzmann analysis. In addition to the band state group velocity $\boldsymbol{v}_{0l}=\partial\epsilon_l/\partial\boldsymbol{k}$, we must also take into account the velocity contribution due to the accumulations of coordinate shifts after many scattering events, another way in which the side-jump effect enters the theory, and the velocity contribution from coherent band mixing by the electric field (the anomalous velocity effect) (Nozieres and Lewiner, 1973; Sinitsyn, 2008; Sinitsyn *et al.*, 2006):

$$\boldsymbol{v}_l=\frac{\partial\epsilon_l}{\partial\boldsymbol{k}}+\boldsymbol{b}_l\times e\boldsymbol{E}+\sum_{l'}\omega_{l'l}\delta\boldsymbol{r}_{l'l}. \tag{4.21}$$

Combining Eqs. (4.16) and (4.21) we obtain the total current

$$\begin{aligned}\boldsymbol{j} &= e\sum_l f_l\boldsymbol{v}_l=e\sum_l(f_0(\epsilon_l)+g_l^s+g_l^{a1}+g_l^{a2}+g_l^{adist})\\ &\times(\frac{\partial\epsilon_l}{\partial\boldsymbol{k}}+\vec{\Omega}_l\times e\boldsymbol{E}+\sum_{l'}\omega_{l'l}\delta\boldsymbol{r}_{l'l})\end{aligned} \tag{4.22}$$

This gives *five* non-zero contributions to the AHE up to linear order in $\boldsymbol{E}$:

$$\sigma_{xy}^{total}=\sigma_{xy}^{int}+\sigma_{xy}^{adist}+\sigma_{xy}^{sj}+\sigma_{xy}^{sk1}+\sigma_{xy}^{sk2-sj}. \tag{4.23}$$

The first term is the intrinsic contribution which should be by now familiar to the reader:

$$\sigma_{xy}^{int}=-e^2\sum_l f_0(\epsilon_l)b_{z,l}. \tag{4.24}$$

Next are the effects due to coordinate shifts during scattering events (for $\boldsymbol{E}$ along the y-axis):

$$\sigma_{xy}^{adist}=e\sum_l(g_l^{adist}/E_y)(v_{0l})_x \tag{4.25}$$

follows from the distribution function correction due to side jumps while

$$\sigma_{xy}^{sj}=e\sum_l(g_l/E_y)\sum_{l'}\omega_{l'l}(\delta\boldsymbol{r}_{l'l})_x \tag{4.26}$$

is the current due to the side-jump velocity, *i.e.*, due to the accumulation of coordinate shifts after many scattering events. Since coordinate shifts are responsible both for σ_{xy}^{adist} and for σ_{xy}^{sj}, there is, unsurprisingly, an intimate relationship between those two contributions. In most of the literature, σ_{xy}^{adist} is usually considered to be part of the side-jump contribution, *i.e.*, $\sigma_{xy}^{adist}+\sigma_{xy}^{sj}\to\sigma_{xy}^{sj}$. We distinguish between the two because they are physically distinct and appear as separate contributions in the microscopic formulation of the AHE theory.

Finally, σ_{xy}^{sk1} and σ_{xy}^{sk2-sj} are contributions arising from the asymmetric part of the collision integral (Sinitsyn, 2008):

$$\sigma_{yx}^{sk1}=-e\sum_l(g_l^{a1}/E_x)(v_{0l})_y\sim n_i^{-1}, \tag{4.27}$$

$$\sigma_{yx}^{sk2-sj}=-e\sum_l(g_l^{a2}/E_x)(v_{0l})_y\sim n_i^0. \tag{4.28}$$

According to the old definition of skew scattering both could be viewed as skew scattering contributions because they originate from the asymmetric part of the collision term (Smit, 1955). However, if instead we *define* skew-scattering as the contribution proportional to n_i^{-1}, *i.e.* linear in τ, as in Sec. I.B, it is only the first contribution, Eq. (4.27), which is the skew scattering (Leroux-Hugon and Ghazali, 1972; Luttinger, 1958). The second contribution, Eq. (4.28), was generally discarded in prior semiclassical theories, although it is parametrically of the same size as the side-jump conductivity. Explicit quantitative estimates of σ_{yx}^{sk2-sj} so far exist only for the massive 2D Dirac band (Sinitsyn *et al.*, 2007). In parsing this AHE contribution we will incorporate it within the family of side-jump effects due to the fact that it proportional to n_i^0, *i.e.* independent of σ_{xx}. However, it is important to note that this "side-jump" contribution has no phyiscal link to the side-step experienced by a semiclasscial quasiparticle upon scattering. An alternative terminology for this contribution is *intrinsic skew scattering* to distinguish its physical origin from side-jump

deflections (Sinitsyn, 2008), but, to avoid further confusion, we simply include it as a contribution to the Hall conductivity which is of the order of σ^0_{xx} and originates from scattering.

As we will see below, when connecting the microscopic formalism to the semiclasscial one, σ^{int}_{xy}, can be directly identified with the single bubble (Kubo formalism) contribution to the conductivity, $\sigma^{adist}_{xy} + \sigma^{sj}_{xy} + +\sigma^{sk2}_{xy}$ constitute the usually termed ladder-diagram vertex corrections to the conductivity due to scattering and therefore it is natural to group them together although their physical origins are distinct. σ^{sk1}_{xy} is identified directly with the three-scattering diagram used in the literature. This comparison has been made specifically for two simple models, the massive 2D Dirac band (Sinitsyn *et al.*, 2007) and the 2D Rashba with exchange model (Borunda *et al.*, 2007).

B. Kubo formalism

1. Kubo technique for the AHE

The Kubo formalism relates the conductivity to the quilibrium current-current correlation function (Kubo, 1957). It provides a fully quantum mechanical formally exact expression for the conductivity in linear response theory (Mahan, 1990). We do not review the formal machinery for this approach here since can be found in many textbooks. Instead, emphasize the key issues in studying the AHE within this formalism and how it relates to the semiclassical formalism described in the previous section.

For the purpose of studying the AHE it is best to reformulate the current-current Kubo formula for the conductivity in the form of the Bastin formula (see appendix A in (Crépieux and Bruno, 2001)) which can be manipulated into the more familiar form for the conductivity of the Kubo-Streda formula for the $T = 0$ Hall conductivity $\sigma_{xy} = \sigma^{I(a)}_{xy} + \sigma^{I(b)}_{xy} + \sigma^{II}_{xy}$ where:

$$\sigma^{I(a)}_{xy} = \frac{e^2}{2\pi V}\mathrm{Tr}\langle \hat{v}_x G^R(\epsilon_F)\hat{v}_y G^A(\epsilon_F)\rangle_c, \tag{4.29}$$

$$\sigma^{I(b)}_{xy} = -\frac{e^2}{4\pi V}\mathrm{Tr}\langle \hat{v}_x G^R(\epsilon_F)\hat{v}_y G^R(\epsilon_F) + \hat{v}_i G^A(\epsilon_F)\hat{v}_j G^A(\epsilon_F)\rangle_c, \tag{4.30}$$

$$\begin{aligned}\sigma^{II}_{xy} &= \frac{e^2}{4\pi V}\int_{-\infty}^{+\infty} d\epsilon f(\epsilon)\mathrm{Tr}[v_x G^R(\epsilon)v_y \frac{G^R(\epsilon)}{d\epsilon} \\ &\quad - v_x \frac{G^R(\epsilon)}{d\epsilon} v_y G^R(\epsilon) + c.c.].\end{aligned} \tag{4.31}$$

Here the subscript c indicates a disorder configuration average. The last contribution, σ^{II}_{xy}, was first derived by Streda in the context of studying the quantum Hall effect (Středa, 1982). In these equations $G^{R/A}(\epsilon_F) = (\epsilon_F - H \pm i\delta)^{-1}$ are the retarded and advanced Green's functions evaluated at the Fermi energy of the total Hamiltonian.

Looking more closely σ^{II}_{xy} we notice that every term depends on products of retarded Green's functions only or products of advanced Green's functions only. It can be shown that only the disorder free part of σ^{II}_{xy} is important in the weak disorder limit, *i.e.* , this contribution is zeroth order in the parameter $1/k_F l_{sc}$. The only effect of disorder on this contribution (for metals) is to broaden the Green's functions (see below) through the introduction of a finite lifetime (Sinitsyn *et al.*, 2007). It can therefore be shown by a similar argument that in general σ^{Ib}_{xy}, is of order $1/k_F l_{sc}$ and can be neglected in the weak scattering limit (Mahan, 1990). Thus, important disorder effects beyond simple quasiparticle lifetime broadening are contained only in σ^{Ia}_{xy}. For these reasons, it is standard within the Kubo formalism to neglect σ^{Ib}_{xy} and evaluate the σ^{II}_{xy} contribution with a simple lifetime broadening approximation to the Green's function.

Within this formalism the effect of disorder on the disorder-configuration averaged Green's function is captured by the use of the T-matrix, defined by the integral equation $T = W + WG_0T$, where $W = \sum_i V_0\delta(r - r_i)$ is a delta-scatterers potential and G_0 are the Green's function of the pure lattice. From this one obtains

$$\bar{G} = G_0 + G_0 T G_0 = G_0 + G_0\Sigma\bar{G}. \tag{4.32}$$

Upon disorder averaging we obtain

$$\Sigma = \langle W\rangle_c + \langle WG_0W\rangle_c + \langle WG_0WG_0W\rangle_c + ... \tag{4.33}$$

To linear order in the impurity concentration, n_i, this translates to

$$\Sigma(z, \boldsymbol{k}) = n_i V_{\boldsymbol{k},\boldsymbol{k}} + \frac{n_i}{V}\sum_{\boldsymbol{k}} V_{\boldsymbol{k},\boldsymbol{k}'} G_0(\boldsymbol{k}', z) V_{\boldsymbol{k}',\boldsymbol{k}} + \cdots, \tag{4.34}$$

with $V_{\boldsymbol{k},\boldsymbol{k}'} = V(\boldsymbol{k} - \boldsymbol{k}')$ being the Fourier transform of the single impurity potential, which in the case of delta scatterers is simply V_0 (see Fig. 41 for a graphical reprentation). Note that $\bar{G}$ and G_0 are diagonal in momentum but, due to the presence of spin-orbit coupling, non-diagonal in spin-index in the Pauli spin-basis. Hence, the blue lines depicted in Fig. 39 represent $\bar{G}$ and are in general matrices in band levels.

One effect of disorder on the anomalous Hall conductivity is taken into account by inserting the disorder averaged Green's function, $\bar{G}^{R/A}$, directly into the expressions for σ^{Ia}_{xy} and σ^{II}_{xy}, Eq. (4.29) and Eq. (4.31). This step captures the intrinsic contribution to the AHE and the effect of disorder on it, which is generally weak in metallic systems. This contribution is separately identified in Fig. 39 a.

The so-called ladder diagram vertex corrections, also separately identified in Fig. 39, contribute to the AHE at the same order in $1/k_F l$ as the intrinsic contribution. It is useful to define a ladder-diagram corrected velocty vertex $\tilde{v}_\alpha(\epsilon_F) \equiv v_\alpha + \delta\tilde{v}_\alpha(\epsilon_F)$, where

$$\delta\tilde{v}_\alpha(\epsilon_F) = \frac{n_i V_0^2}{V}\sum_{\boldsymbol{k}} \bar{G}^R(\epsilon_F)(v_\alpha + \delta\tilde{v}_\alpha(\epsilon_F))\bar{G}^A(\epsilon_F), \tag{4.35}$$

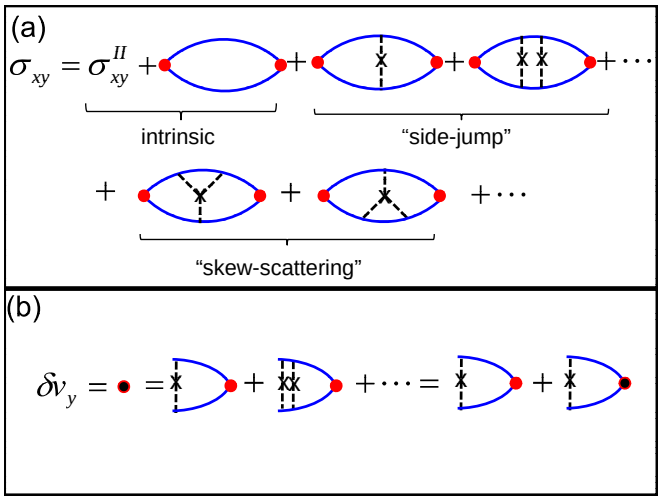


FIG. 39 Graphical representation of the Kubo formalism application to the AHE. The solid blue lines are the disorder averaged Green's function, $\bar{G}$, the red circles the bare velocity vertex $v_\alpha = \partial\hat{H}_0/\partial\hbar k_\alpha$, and the dashed lines with crosses represent disorder scattering ($n_i V_0^2$ for the delta-scatter model). (b) δv_y is the velocity vertex renormalized by vertex corrections.

as depicted in Fig. 39 b. Note again that $\tilde{v}_\alpha(\epsilon_F)$ and $v_\alpha = \partial\hat{H}_0/\partial\hbar k_\alpha$ are matrices in the spin-orbit coupled band basis. The skew scattering contributions are obtained by evaluating, without doing an infinite partial sum as in the case of the ladder diagrams, third order processes in the disorder scattering shown in Fig. 39.

As may seem obvious from the above machinery, calculating the intrinsic contribution is not very difficult, while calculating the full effects of the disorder in a systematic way (beyond calculating a few diagrams) is challenging for any disorder model beyond the simple delta-scattering model.

Next we illustrate the full use of this formalism for the simplest nontrivial model, massive 2D Dirac fermions, with the goals of illustrating the complexities present in each contribution to the AHE *and* the equivalence of quantum and semiclassical approaches. This model is of course not directly linked to any real material reviewed in Sec. II and its main merit is the possibility of obtaining full simple analytical expressions for each of the contributions. A more realistic model of 2D fermions with Rashba spin-orbit coupling will be discussed in Sec. IV.C. The ferromagnetic Rashba model has been used to propose a minimal model of AHE for materials in which band crossing near the Fermi surface dominate the AHE physics (Onoda *et al.*, 2008).

The massive 2D Dirac fermion model is specified by:

$$\hat{H}_0 = v(k_x\sigma_x + k_y\sigma_y) + \Delta\sigma_z + V_{dis}, \tag{4.36}$$

where $V_{dis} = \sum_i V_0\delta(\mathbf{r} - \mathbf{R}_i)$, σ_x and σ_y are Pauli matrices and the impurity free spectrum is $\epsilon^{\pm}_{\mathbf{k}} = \pm\sqrt{\Delta^2 + (vk)^2}$ where $k = |\mathbf{k}|$ and the labels $\pm$ distinguish bands with positive and negative energies. We ignore in this simple model spin-orbit coupled disorder contributions which can be directly incorporated through similar calculations as in Crepieux *et al* (Crépieux and Bruno, 2001). Within this model the disordered averaged Green's function is

$$\bar{G}^R = \frac{1}{1/G_0^R - \Sigma^R} = \frac{\epsilon_F + i\Gamma + v(k_x\sigma_x + k_y\sigma_y) + (\Delta - i\Gamma_1)\sigma_z}{(\epsilon_F - \epsilon^+ + i\Gamma^+)(\epsilon_F - \epsilon^- + i\Gamma^-)}\ , \tag{4.37}$$

where $\Gamma = \pi n_i V_0^2/(4v^2)$, $\Gamma_1 = \Gamma\cos(\theta)$, $\gamma^{\pm} = \Gamma_0 \pm \Gamma_1\cos(\theta)$, and $\cos\theta = \Delta/\sqrt{(vk)^2 + \Delta^2}$. Note that within this disorder model $\tau \propto 1/n_i$. Using the result in Eq. (4.37) one can calculate the ladder diagram correction to the bare velocity vertex given by Eq. (4.35):

$$\tilde{v}_y = 8v\Gamma\cos\theta\frac{(1+\cos^2\theta)}{\lambda(1+3\cos^2\theta)^2}\sigma_x + \left(v + v\frac{\sin^2\theta}{(1+3\cos^2\theta)}\right)\sigma_y, \tag{4.38}$$

where θ is evaluated at the Fermi energy. The details of the calculation of this vertex correction is described in Appendix A of Ref. Sinitsyn *et al.*, 2007. Incorporating this result in σ^{Ia}_{xy} we obtain the intrinsic and side-jump contributions to the conductivity for $\epsilon_F > \Delta$

$$\sigma^{int}_{xy} = \frac{e^2}{2\pi\hbar V}\sum_{\boldsymbol{k}}\mathrm{Tr}\left[v\sigma_x G v\sigma_y G\right] = -\frac{e^2\cos\theta}{4\hbar\pi}\ , \tag{4.39}$$

$$\begin{aligned}\sigma^{sj}_{xy} &= \frac{e^2}{2\pi\hbar V}\sum_{\boldsymbol{k}}\mathrm{Tr}\left[v\sigma_x G\delta\tilde{v}_y G\right] \\ &= -\frac{e^2\cos\theta}{4\pi\hbar}\left(\frac{3\sin^2\theta}{(1+3\cos^2\theta)} + \frac{4\sin^2\theta}{(1+3\cos^2\theta)^2}\right)\end{aligned}\ . \tag{4.40}$$

The direct calculation of the skew-scattering diagrams of Fig. 39 is $\sigma^{sk}_{xy} = -\frac{e^2}{2\pi\hbar n V_0}\frac{(vk_F)^4\Delta}{(4\Delta^2+(vk_F)^2)^2}$ and the final total result is given by

$$\begin{aligned}\sigma_{xy} \quad &= -\frac{e^2\Delta}{4\pi\hbar\sqrt{(vk_F)^2+\Delta^2}}[1 + \frac{4(vk_F)^2}{4\Delta^2+(vk_F)^2} \\ &+ \frac{3(vk_F)^4}{(4\Delta^2+(vk_F)^2)^2}] - \frac{e^2}{2\pi\hbar n V_0}\frac{(vk_F)^4\Delta}{(4\Delta^2+(vk_F)^2)^2}.\end{aligned} \tag{4.41}$$

2. Relation between the Kubo and the semiclassical formalisms

When comparing the semiclassical formalism to the Kubo formalism one has to keep in mind that in the semiclassical formalism the natural basis is the one that diagonalize the spin-orbit coupled Hamiltonian. In the case of the 2D massive Dirac model this is sometimes called chiral basis in the literature. On the other hand

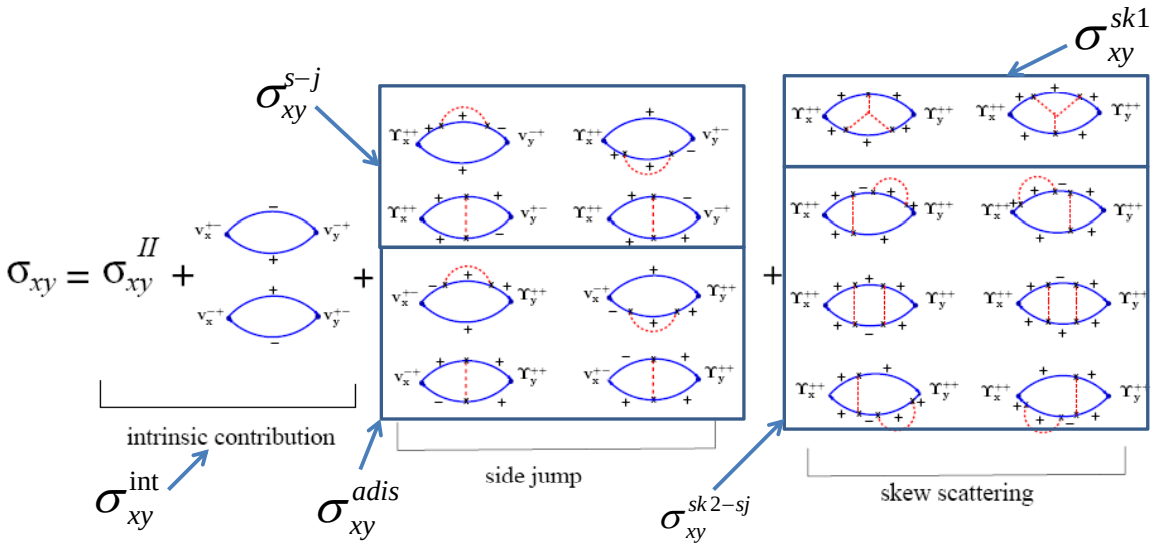


FIG. 40 Graphical representation of the AHE conductivity in the chiral (band eigenstate) basis. The two bands of the two-dimensional Dirac model are labeled "±". The subset of diagrams that correspond to specific terms in the semiclassical Boltzmann formalism are indicated.

in the application of the Kubo formalism it is simplest to compute the different Green's functions and vertex corrections in the Pauli basis and take the trace at the end of the calculation. In the case of the above model one can apply the formalism of Sec. IV.A and obtain the following results for the five distinct contributions: σ_{xy}^{int}, σ_{xy}^{adist}, σ_{xy}^{sj}, σ_{xy}^{sk2-sj} and σ_{xy}^{sk1}. Below we quote the results for the complicated semiclassical calculation of each term (see Sec. IV of Sinitsyn *et al.* (Sinitsyn *et al.*, 2007) for details):

$$\sigma_{xy}^{intr} = -\frac{e^2\Delta}{4\pi\hbar\sqrt{\Delta^2+(vk_F)^2}}; \tag{4.42}$$

$$\sigma_{xy}^{sj} = \sigma_{xy}^{adist} = -\frac{e^2\Delta k_F^2}{2\pi\hbar\sqrt{k_F^2+\Delta^2}(k_F^2+4\Delta^2)}; \tag{4.43}$$

$$\sigma_{xy}^{sk-sj} = -\frac{e^2 3\Delta(vk_F)^4}{4\pi\hbar\sqrt{(vk_F)^2+\Delta^2}[4\Delta^2+(vk_F)^2]^2}; \tag{4.44}$$

$$\sigma_{xy}^{sk} = -\frac{e^2}{2\pi\hbar n_i V_0}\frac{(vk_F)^4\Delta}{(4\Delta^2+(vk_F)^2)^2}. \tag{4.45}$$

The correspondance with the Kubo formalism results can be seen after a few algebra steps. The contributions σ_{xy}^{int} and σ_{xy}^{sk1} are equal in both cases (Eq. (4.39) and Eq. (4.41)). As expected, the intrinsic contribution, σ_{xy}^{intr}, is independent of disorder in the weak scattering limit and the skew scattering contribution is inversely proportional to the density of scatterers. However, recall that in Sec. I.B we have defined the side-jump contribution as the disorder contributions of zeroth order in n_i, *i.e.*, τ^0, as opposed to being directly linked to a side-step in the scattering process in the semiclassical theory. Hence, it is the sum of the three physically distinct processes $\sigma_{xy}^{adist}+\sigma_{xy}^{sj}+\sigma_{xy}^{sk2-sj}$ which can be shown to be identical to Eq. (4.40) after some algebraic manipulation. Therefore, the old notion of associating the skew scattering directly with the asymmetric part of the collision integral and the side-jump with the side-step scattering alone leads to contradictions with their usual association with respect to the dependence on τ (or equivalenty $1/n_i$). We also note, that unlike what happens in simple models where the Berry's curvature is a constant in momentum space, *e.g.*, the standard model for electrons in a 3D semiconductor conduction band (Nozieres and Lewiner, 1973), the dependence of the intrinsic and side-jump contributions are quite different with respect to parameters such as Fermi energy, exchange splitting, etc.

C. Keldysh formalism

Keldysh has developed a Green's function formalism applicable even to the nonequilibrium quantum states, for which the diagram techniques based on Wick's theorem can be used (Baym and Kadanoff, 1961; Kadanoff and Baym, 1962; Keldysh, 1965; Mahan, 1990; Rammer and Smith, 1986). Unlike with the thermal (Matsubara) Green's functions, the Keldysh Green's functions are de-

fined for any quantum state. The price for this flexibility is that one needs to introduce the path-ordered product for the contour from $t = -\infty \to t = \infty$ and back again from $t = \infty \to -\infty$. Correspondingly, four kinds of the Green's functions G^R, G^A, $G^<$ and $G^>$ need to be considered, although only three are independent (Baym and Kadanoff, 1961; Kadanoff and Baym, 1962; Keldysh, 1965; Mahan, 1990; Rammer and Smith, 1986). Therefore, the diagram technique and the Dyson equation for the Green's function have a matrix form.

In linear response theory, one can use the usual thermal Green's function and Kubo formalism. Since approximations are normally required in treating disordered systems, it is important to make them in a way which at least satisfies gauge invariance. In both formalisms this is an important theoretical requirement which requires some care. Roughly speaking, in the Keldysh formalism, G^R and G^A describe the single particle states, while $G^<$ represents the non-equilibrium particle occupation distribution and contains vertex corrections. Therefore, the self-energy and vertex corrections can be treated in a unified way by solving the matrix Dyson equation. This facilitates the analysis of some models especially when multiple bands are involved.

Another and more essential advantage of Keldysh formalism over the semiclassical formalism is that one can go beyond a finite order perturbative treatment of impurity scattering strength by solving a self-consistent equation, as will be discussed in the next subsection. In essence, we are assigning a finite spectral width to the semiclassical wave packet to account for an important consequence of quantum scattering effects. In the Keldysh formalism, the semiclassical limit corresponds to ignoring the history of scattering particles by keeping the two time labels in the Greens functions identical.

We restrict ourselves below to the steady and uniform solution. For more generic cases of electromagnetic fields, see Ref. Sugimoto *et al.*, 2007. Let $x = (t, \boldsymbol{x})$ be the time-space coordinate. Green's functions depend on two space-time points x_1 and x_2, and the matrix Dyson equation for the translationally invariant system reads (Rammer and Smith, 1986):

$$\begin{aligned}(\varepsilon - \hat{H}(\boldsymbol{p}) - \hat{\underline{\Sigma}}(\varepsilon, \boldsymbol{p})) \otimes \hat{\underline{G}}(\varepsilon, \boldsymbol{p}) &= 1, \\ \hat{\underline{G}}(\varepsilon, \boldsymbol{p}) \otimes (\varepsilon - \hat{H}(\boldsymbol{p}) - \hat{\underline{\Sigma}}(\varepsilon, \boldsymbol{p})) &= 1, \end{aligned} \tag{4.46}$$

where we have changed the set of variables $(x_1; x_2)$ to the center-of-mass and the relative coordinates, and then proceeded to the Wigner representation $(X; p)$ by means of the Fourier transformation of the relative coordinate;

$$(X, x) \equiv \left(\frac{x_1 + x_2}{2}, x_1 - x_2\right) \to \int dt \int d\boldsymbol{x}\, e^{i(\varepsilon t - \boldsymbol{p}\cdot\boldsymbol{x})/\hbar} \cdots , \tag{4.47}$$

with $p = (\varepsilon, \boldsymbol{p})$. In this Dyson equation, the product $\otimes$ iis reserved for matrix products in band indices, like those that also appear in the Kubo formalism.

In the presence of the external electromagnetic field A_μ, we must introduce the mechanical or kinetic energy-momentum variable

$$\pi_\mu(X; p) = p_\mu + eA_\mu(X). \tag{4.48}$$

replacing p as the argument of the Green's function, as shown by Onoda *et al* (Onoda *et al.*, 2006b). In this representation, $\hat{G}^<(X; \pi)/2\pi i$ is the quantum-mechanical generalization of the semi-classical distribution function. When an external electric field $\boldsymbol{E}$ is present, the equation of motion, or equivalently, the Dyson equation, retains the same form as Eq. (4.46) when the product $\otimes$ is replaced by the so-called Moyal product (Moyal, 1949; Onoda *et al.*, 2006b) given by

$$\otimes = \exp\left[\frac{i\hbar(-e)}{2}\boldsymbol{E}\cdot(\overleftarrow{\partial}_\varepsilon \overrightarrow{\boldsymbol{\nabla}}_p - \overleftarrow{\boldsymbol{\nabla}}_p \overrightarrow{\partial}_\varepsilon)\right]. \tag{4.49}$$

Henceforth, $\overrightarrow{\partial}$ and $\overleftarrow{\partial}$ denote the derivatives operating on the right-hand and left-hand sides, respectively, and the symbol $p = (\varepsilon, \boldsymbol{p})$ is used to represent the mechanical energy-momentum π. In this formalism, only gauge invariant quantities appear. For example, the electric field $\boldsymbol{E}$ appears instead of the vector potential $\boldsymbol{A}$.

Expanding Eq. (4.49) in $\boldsymbol{E}$ and inserting the result in Eq. (4.46), one obtains the Dyson equation to linear order in $\boldsymbol{E}$, corresponding to linear response theory. The linear order terms $\hat{G}^\alpha_{\boldsymbol{E}}$ and $\hat{\Sigma}^\alpha_{\boldsymbol{E}}$ in $\boldsymbol{E}$ are decomposed into two parts as

$$\hat{G}^<_{\boldsymbol{E}} = \hat{G}^<_{\boldsymbol{E},I}\partial_\varepsilon f(\varepsilon) + \left(\hat{G}^A_{\boldsymbol{E}} - \hat{G}^R_{\boldsymbol{E}}\right) f(\varepsilon), \tag{4.50}$$

$$\hat{\Sigma}^<_{\boldsymbol{E}} = \hat{\Sigma}^<_{\boldsymbol{E},I}\partial_\varepsilon f(\varepsilon) + \left(\hat{\Sigma}^A_{\boldsymbol{E}} - \hat{\Sigma}^R_{\boldsymbol{E}}\right) f(\varepsilon). \tag{4.51}$$

Here, $f(\varepsilon)$ represents the Fermi distribution function. In these decompositions, the first term on the r.h.s. corresponds to the nonequilibrium deviation of the distribution function due to the electric field $\boldsymbol{E}$. The second term, on the other hand, represents the change in quantum mechanical wavefunctions due to $\boldsymbol{E}$, and arises due to the multiband effect (Haug and Jauho, 1996) through the noncommutative nature of the matrices.

The corresponding separation of conductivity contributions is: $\sigma_{ij} = \sigma^I_{ij} + \sigma^{II}_{ij}$ with

$$\sigma^I_{ij} = e^2\hbar^2 \int \frac{d^{d+1}p}{(2\pi\hbar)^{d+1}i} \mathrm{Tr}\left[\hat{v}_i(\boldsymbol{p})\hat{G}^<_{E_j,I}(p)\right]\partial_\varepsilon f(\varepsilon), \tag{4.52}$$

$$\sigma^{II}_{ij} = e^2\hbar^2 \int \frac{d^{d+1}p}{(2\pi\hbar)^{d+1}i} \mathrm{Tr}\left[\hat{v}_i(\boldsymbol{p})\left(\hat{G}^A_{E_j}(p) - \hat{G}^R_{E_j}(p)\right)\right] f(\varepsilon). \tag{4.53}$$

This is in the same spirit as the Středa version (Středa, 1982) of the Kubo-Bastin formula (Bastin *et al.*, 1971; Kubo, 1957). The advantage here is that we can use the diagrammatic technique to connect the self-energy and the Green's function. For dilute impurities, one can take the series of diagrams shown in Fig. 41 corresponding to the T-matrix approximation. In this approximation,

the self-consistent integral equation for the self-energy and Green's function can be solved and the solution used to evaluate the first and second terms in Eq. (4.50) and Eq. (4.51).

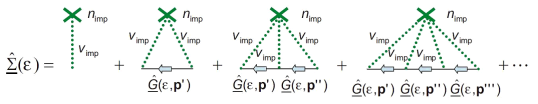


FIG. 41 Diagrammatic representation of the self-energy in the self-consistent T-matrix approximation in the Keldysh space, which is composed of the infinite series of multiple Born scattering amplitudes. [From Ref. Onoda *et al.*, 2008.]

In general, Eqs. (4.52) and (4.53), together with the self-consistent equations for G^R,G^A, and $G^<$ (Onoda *et al.*, 2008) defines a systematic diagrammatic method for calculating σ_{ij} in the Středa decomposition (Středa, 1982) of the Kubo-Bastin formula (Bastin *et al.*, 1971; Kubo, 1957).

D. Two-dimensional ferromagnetic Rashba model – a minimal model

A very useful model to study fundamental aspects of the AHE is the ferromagnetic two-dimensional (2D) Rashba model (Bychkov and Rashba, 1984):

$$\hat{H}(\boldsymbol{p})_{\rm tot} = \frac{\boldsymbol{p}^2}{2m} - \lambda \boldsymbol{p}\times\hat{\boldsymbol{\sigma}}\cdot\boldsymbol{e}^z - \Delta_0\hat{\sigma}^z + \hat{V}(\boldsymbol{x}). \quad (4.54)$$

Here m is the electron mass, λ is the Rashba spin-orbit interaction strength, Δ_0 is the mean field exchange splitting, $\hat{\boldsymbol{\sigma}} = (\hat{\sigma}_x, \hat{\sigma}_y, \hat{\sigma}_z)$ and $\hat{\sigma}^0$ are the Pauli and identity matrices, $\boldsymbol{e}^z$ is the unit vector in the z direction, and $\hat{V}(\boldsymbol{x}) = V_0\sum_i \delta(\boldsymbol{r}-\boldsymbol{r}_i)$ is a δ-scatterer impurity potential with impurity density n_i. Quantum transport properties of this simple but non-trivial model have been intensively studied in order to understand fundamental properties of the AHE in itinerant metallic ferromagnets. The metallic Rashba is a simple, but its AHE has both intrinsic and extrinsic contributions and both minority and majority spin Fermi surfaces. It therefore captures most of the features that are important in real materials with a minimum of complicating detail. The model has therefore received a lot of attention (Borunda *et al.*, 2007; Dugaev *et al.*, 2005; Inoue *et al.*, 2006; Kato *et al.*, 2007; Kovalev *et al.*, 2009, 2008; Nunner *et al.*, 2007; Onoda *et al.*, 2006b, 2008).

The bare Hamiltonian has the band dispersion:

$$\varepsilon_\sigma(\boldsymbol{p}) = \frac{\boldsymbol{p}^2}{2m} - \sigma\Delta_{\boldsymbol{p}}, \quad \Delta_{\boldsymbol{p}} = \sqrt{\lambda^2\boldsymbol{p}^2 + \Delta_0^2}, \quad (4.55)$$

illustrated in Fig. 42 a, and Berry-phase curvature

$$b^z_\sigma(\boldsymbol{p}) = \hbar^2\left[\boldsymbol{\nabla}_p\times(i\langle\boldsymbol{p},\sigma|\boldsymbol{\nabla}_p|\boldsymbol{p},\sigma\rangle)\right]^z = \frac{\lambda^2\hbar^2\Delta_0\sigma}{2\Delta^3_{\boldsymbol{p}}}, \quad (4.56)$$

where $\sigma = \pm$ labels the two eigenstates $|\boldsymbol{p},\sigma\rangle$ at momentum $\boldsymbol{p}$.

With this we can then obtain the intrisic contribution to the AHE by integrating over occupied states at zero temperature (Culcer *et al.*, 2003; Dugaev *et al.*, 2005):

$$\sigma^{\rm AH-int}_{xy} = \frac{e^2}{2h}\sum_\sigma \sigma\left[1 - \frac{\Delta_0}{\Delta_{p_\sigma}}\right]\theta(\mu - \varepsilon_\sigma(\boldsymbol{p}_\sigma)), \quad (4.57)$$

where $p_\pm$ denotes the Fermi momentum for the band $\sigma = \pm$.

An important feature of σ^{AH-int}_{xy} is its enhancement in the interval of $\varepsilon_{0,+} < \mu < \varepsilon_{0,-}$, where it approaches a maximum value close to $e^2/2h$, no matter how small Δ_0 is (provided that it is larger than $\hbar/\tau$). Near $\boldsymbol{p} = 0$ the Berry curvatures of the two bands are large and opposite in sign. The large Berry curvatures translate into large intrinsic Hall conductivities only when the chemical potential lies between the local maximum of one band and the local minimum of the other. This enhancement of the intrinsic AHE near avoided band crossings is illustrated in Fig. 42 b, where it is seen to survive moderate disorder broadening of several times Δ_0. This peaked feature arises from the topological nature of σ^{AH-int}_{xy}. As a consequence it is important to note that the result is non-perturbative in SOI; only a perturbative expansion on $\hbar/\varepsilon_F\tau$ is justified.

Cucler *et al.* (Culcer *et al.*, 2003) were the first to study this model, obtaining Eq. (4.57). They were was followed by Dugaev *et al.* (Dugaev *et al.*, 2005) where the intrinsic contribution was calculated within the Kubo formalism. Although these studies found a non-zero σ^{AH-int}_{xy}, they did not calculate all the contributions arising from disorder (some aspects of the disorder treatment in (Dugaev *et al.*, 2005) where corrected by these authors in (Sinitsyn *et al.*, 2007)). The intrinsic AHE σ^{AH-int}_{xy} comes form both σ^I_{xy} and σ^{II}_{xy}. The first part σ^I_{xy} contains the intra-band contribution $\sigma^{I(a)}_{xy}$ which is sensitive to the impurity scattering vertex correction.

The calculation of $\sigma^{I(a)}_{xy}$ incorporating the effects of disorder using the Kubo formalism, *i.e.*, incorporating the ladder vertex corrections ("side-jump") and the leading $O(V_0^3)$ skew-scattering contributions (Sec. IV.B.1), yields a vanishing σ^{AH}_{xy} for the case where ε_F is above the gap at $\boldsymbol{p} = \boldsymbol{0}$ (*i.e.* both subbands are occupied), irrespective of the strength of the spin-independent scattering amplitude (Borunda *et al.*, 2007; Inoue *et al.*, 2006; Nunner *et al.*, 2008). On the other hand, when only the majority band $\sigma = +$ is occupied, $\sigma^{I(a)}_{xy}$ is given by the skew-scattering contribution (Borunda *et al.*, 2007),

$$\sigma^{I(a)}_{xy} \approx -\frac{e^2}{h}\frac{1}{n_{\rm imp}u_{\rm imp}}\frac{\lambda^2 p_+^4 D_+(\mu)\Delta_0\Delta_{p_+}}{(3\Delta_0^2 + \Delta^2_{p_+})^2}, \quad (4.58)$$

in the leading-order in $(1/n_{\rm imp})$.

Some properties of the ferromagnetic Rashba model appear unphyiscal in the limit $\tau\to\infty$ (Onoda *et al.*,

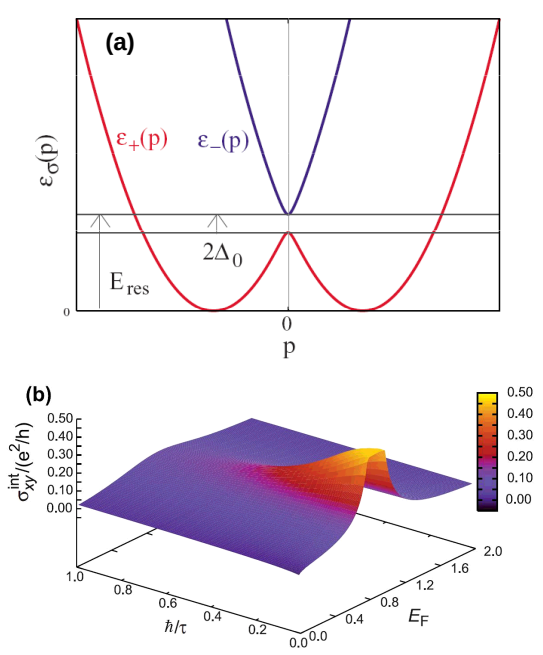


FIG. 42 (a) Band dispersion of the ferromagnetic 2D Rashba model in the clean limit. (b) The intrinsic anomalous Hall conductivity of the Hamiltonian Eq. (4.54) as functions of the Fermi level ε_F measured from the bottom of the majority band and $\hbar/\tau \equiv m n_{\rm imp} V_0^2/\hbar^2$, which is the Born scattering amplitude for $\lambda = \Delta_0 = 0$. This figure is for the parameter set $\Delta_0 = 0.1$, $2m\lambda = 3.59$, and $2mV_0/\hbar^2 = 0.6$, with energy unit has been taken as $\varepsilon_{0,-}$. [From Ref. Onoda *et al.*, 2006b.]

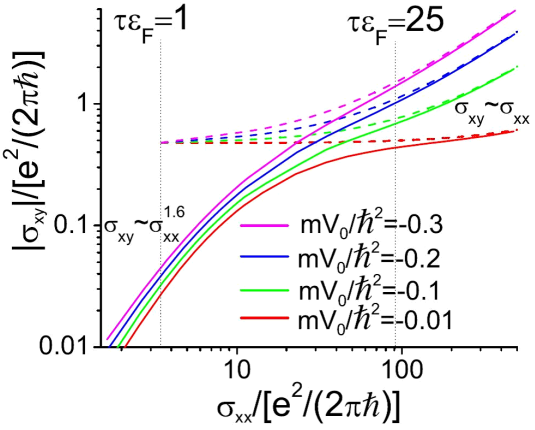


FIG. 43 Total anomalous Hall conductivity *vs.* σ_{xx} for the Hamiltonian Eq. (4.54) obtained in the self-consistent T-matrix approximation to the Keldysh approach (Kovalev *et al.*, 2009; Onoda *et al.*, 2006b, 2008). Curves are for a variety of disorder strengths. The same parameter values have been taken as in Fig. 42 with the chemical potential being located at the center of the two subbands. The dashed curves represent the corresponding semiclassical results. [After Ref. Kovalev *et al.*, 2009.]

2008): σ_{xy} vanishes discontinuously as the chemical potential μ crosses the edge $\varepsilon_{0,-}$ of the minority band which leads to a diverging anomalous Nernst effect at $\mu = \varepsilon_{0,-}$, irrespective of the scattering strength, if one assumes the Mott relation to be valid for anomalous transport (Smrčka and Středa, 1977). However, this unphysical property does not really hold, in fact, σ_{xy} does not vanish even when both subbands are occupied, as shown by including all higher-order Born scattering amplitudes as it is done automatically in the numerical Keldysh approach (Onoda *et al.*, 2006a). In particular, the skew-scattering contribution arises from the odd-order Born scattering (*i.e.*, even order in the impurity potential) beyond the conventional level of approximation, $O(V_0^3)$, that gives rise to the normal skew scattering contributions (Kovalev *et al.*, 2008). This yields the unconventional behavior $\sigma_{xy}^{AH-skew} \propto 1/n_{\rm imp}$ independent of V_0 (Kovalev *et al.*, 2008). The possible appearance of the AHE in the case where both subbands are occupied was also suggested in the numerical diagonalization calculation of the Kubo formula (Kato *et al.*, 2007). The influence of spin-dependent impurities has also been analyzed (Nunner *et al.*, 2008).

A numerical calculation of σ_{xy}^{AH} based on the Keldysh formalism using the self-consistent T-matrix approximation, shown in Fig. 43, suggests three distinct regimes for the AHE as a function of σ_{xx} at low temperatures (Onoda *et al.*, 2006a, 2008). In particular, it shows a crossover from the predominant skew-scattering region in the clean limit ($\sigma_{xy} \propto \sigma_{xx}$) to an intrinsic-dominated metallic region ($\sigma_{xy} \sim$ constant). In this simple model no well defined plateau is observed. These results also suggests another crossover to a regime, referred to as the *incoherent regime* by (Onoda *et al.*, 2008), where σ_{xy} decays with the disorder following the scaling relation of $\sigma_{xy} \propto \sigma_{xx}^n$ with $n \approx 1.6$. This scaling arises in the calculation due to the influence of finite-lifetime disorder broadening on σ_{xy}^{AH-int}, while the skew-scattering contribution is quickly dimished by disorder as expected. Kovalev *et al.* (Kovalev *et al.*, 2009) revisited the Keldysh calculations for this model, studying them numerically and analytically. In particular, their study extended the calculations to include the dependence of the skew-scattering contribution on the chemical potential μ both for $\mu < \varepsilon_{0,-}$ and for $\mu > \varepsilon_{0,-}$ (as shown in Fig. 43). These authors demonstrated that changing the sign of the impurity potential changes the sign of the skew-scattering contribution. The data collapse illustrated in Fig. 43 then fails, especially near the intrinsic-extrinsic crossover. Data collapse in σ^{xy} *vs.* σ_{xx} plots is therefore not a general property of 2D Rashba models and should not be expected in real materials. There is, however, a sufficient tendency in this direction to motivate analyzing experiments by plotting data in this way.

Minimal model– The above results have the following implications for the generic nature of the AHE (Onoda *et al.*, 2006b, 2008). The 2D ferromagnetic Rashba model can be viewed as a minimal model that takes into ac-

count both the "parity anomaly" (Jackiw, 1984) associated with an avoided-crossing of dispersing bands, as well as impurity scattering in a system with two Fermi surface sheets. Consider then a general 3D ferromagnet. When the SOI is neglected, majority and minority spin Fermi surfaces will intersect along lines in 3D. For a particular projection k_x of Bloch momentum along the magnetization direction, the Fermi surfaces will touch at points. SOI will generically lift the band degeneracy at these points. At the $\boldsymbol{k}$-point where the energy gap is a minimum the contribution to σ_{xy}^{AH-int} will be a maximum and therefore the region around this point should account for most of σ_{xy}^{AH}, as the first-principles calculations seem to indicate (Fang *et al.*, 2003; Wang *et al.*, 2007, 2006; Yao *et al.*, 2004, 2007). We emphasize that the Berry phase contributions from the two bands are nearly opposite, so that a large contribution from this region of k-space accrues only if the Fermi level lies between the split bands. Expanding the Hamiltonian at this particular $\boldsymbol{k}$-point, one can then hope to obtain an effective Hamiltonian of the form of the ferromagnetic Rashba model. Note that the gap Δ_0 in this effective model Hamiltonian, Eq. (4.54), comes physically from the SOI splitting at this particular $\boldsymbol{k}$-point, while the "Rashba SOI" λ is proportional to the Fermi velocity near this crossing point. In 3D, the anomalous Hall conductivity is then given by the 2D contribution integrated over p_z near this minimum gap region, and remains of order of e^2/ha (a the lattice constant) if no accidental cancellation occurs.

We point out that a key assumption made in the above reasoning is that the effective Hamiltonian obtained in this expansion is sufficiently similar to the ferromagnetic Rashba model. We note that in the Rashba model it is Δ_0 and not the SOI which opens the gap, so this is already one key difference. The SO interactions in any effective Hamiltonian of this type should in general contain at least Rashba-like and Dresselhaus-like contributions. Further studies examining the crossing points more closely near these minimum gap regions will shed further light on the relationship between the AHE in real materials and the AHE in simple models for which detailed perturbative studies are feasible.

The minimal model outlined above suggests the presence of three regimes: (i) the superclean regime dominated by the skew-scattering contribution over the intrinsic one, (ii) the intrinsic metallic regime where σ_{xy} becomes more or less insensitive to the scattering strength and σ_{xx}, and (iii) the dirty regime with $k_F\ell = 2\varepsilon_F\tau/\hbar \lesssim 1$ exhibiting a sublinear dependence of $\rho_{xy} \propto \rho_{xx}^{2-n}$, or equivalently $\sigma_{xy} \propto \sigma_{xx}^{n}$ with $n \approx 1.6$. It is important to note that this minimal model is based on elastic scattering and cannot explain the scaling observed in the localized hopping conduction regime as σ_{xx} is tuned by changing T. Nevertheless, if we multiply the 2D anomalous Hall conductivity by a^{-1} with the lattice constant $a \sim 5$ $\mathring{A}$ for comparison to the experimental results on three-dimensional bulk samples, then an enhanced σ_{xy}^{AH} of the order of the quantized value e^2/h in the intrinsic regime should be interpreted as $\sim e^2/ha \sim 10^3\ \Omega^{-1}\ \mathrm{cm}^{-1}$. This value compares well with the empirically observed cross over seen in the experimental findings on Fe and Co, as discussed in Sec. II.A.

V. CONCLUSIONS: FUTURE PROBLEMS AND PERSPECTIVES ON AHE

In this concluding section, we summarize what has been achieved by the recent studies of the AHE and what is not yet understood, pointing out possible directions for future research on this fascinating phenomenon. To keep this section brief, we exclude the historical summary presented in Sec. I.A and Sec. III.C which outline the early debate on the origin of the AHE. We avoid repeating all thel points highlighted already in Sec. I.A and focus on the most salient ones. Citations are kept to a minimum as well and we refer mostly to the sections in which the material was presented.

a. Recent developments

The renewed interest in the AHE, which has lead to a richer and more cohesive understanding of the problem, began in 1998 and was fueled by other connected developments in solid state physics. These were: i) the development of geometrical and topological concepts useful in understanding electronic properties such as quantum phase interference and the quantum Hall effect. (Lee and Ramakrishnan, 1985; Prange and Girvin, 1987), ii) the demostration of the close relation between the Hall conductance and the toplogical Chern number revealed by the TKNN formula (Thouless *et al.*, 1982), iii) the development of accurate first-principles band structure calculation which account realistically for SOI, and iv) the association of the Berry-phase concept (Berry, 1984) with the noncoplanar spin configuration proposed in the context of the resonating valence bond (RVB) theory of cuprate high temperature superconductors (Lee *et al.*, 2006).

Intrinsic AHE– The concept of an intrinsic AHE, debated for a long time, was brought back to the forefront of the AHE problem because of studies which successfully connected the topological properties of the quantum states of matter and the transport Hall response of a system. In Sec. I.B.1 we have defined σ_{xy}^{AH-int} *both* experimentally and theoretically. From the latter, it is rather straightforward to write σ_{xy}^{AH-int} in terms of the Berry curvature in the $\boldsymbol{k}$-space, from which the topological nature of the intrinsic AHE can be easily recognized immediately. The topological non-perturbative quality of σ_{xy}^{AH-int} is highlighted by the finding that for simple models with spontaneous magnetization and SOI, bands can have nonzero Chern numbers even without an external magnetic field present. This means that expansion with respect to SOI strength is sometimes dangerous since it lifts the degen-

eracy between the up- and down-spin bands, leading to avoided band crossings which can invalidate such expansion.

Even though the interpretations of the AHE in real systems are still subtle and complicated, the view that σ_{xy}^{AH-int} can be the dominant contribution to σ_{xy}^{AH} in certain regimes has been strengthened by recent comparisons of experiment and theory. The intrinsic AHE can be calculated from first-principles calculations or, in the case of semiconductors, using $\boldsymbol{k}\cdot\boldsymbol{p}$ theory. These calculations have been compared to recent experimental measurements for several materials such as $Sr_{1-x}Ca_xRuO_3$ (section II.B), Fe (section II.A), $CuCr_2Se_{4-x}Br_x$ (section II.D), and dilute magnetic semiconductors (section II.C). The calculations and experiments show semi-quantitative agreement. More importantly however, violations of the empirical relation $\sigma_H \propto M$ have been established both theoretically and experimentally. This suggests that the intrinsic contribution has some relevance to the observed AHE. On the other hand, these studies do not always provide a compelling explanation for dominance of the intrinsic mechanism

Fully consistent metallic linear response theories of the AHE – Important progress has been achieved in AHE theory. The semiclassical theory, appropriately modified to account for interband coherence effects, has been shown to be consistent with fully microscopic theories based on Kubo and Keldysh formalisms. All three theories have been shown to be equivalent in the $\varepsilon_F\tau \gg 1$ limit, with each having their advantages and disadvantages (Sec. IV). Much of the debate and confusion in early AHE literature originated from discrepancies and farraginous results from earlier inconsistent application of these linear response theories.

A semiclassical treatment based on the Boltzmann transport equation, but taking into account the Berry curvature and inter-band coherence effects, has been formulated (Sec. IV.A). The physical picture for each process of AHE is now understood reasonably well in the case of elastic impurity scattering.

More rigorous treatments taking into account the multi-band nature of the Green's functions in terms of Kubo and Keldysh formalism have been developed fully (section IV.C). These have been applied to a particular model, *i.e.*, the ferromagnetic Rashba model, with a static impurity potential which produces elastic scattering. The ferromagnetic Rashba model has an avoided crossing which has been identified as a key player in the AHE of any material. These calculations have shown a region of disorder strength over which the anomalous Hall conductivity stays more or less constant as a function of σ_{xx}, corresponding to the intrinsic-dominated regime. The emergence of this regime has been linked to the topological nature of the intrinsic contribution, analogous to the topologically protexted quantized Hall effect.

Emergence of three empirical AHE regimes— Based on the large collections of experimental results and indications from some theoretical calculations, it is now becoming clear that there are at least three different regimes for the behavior of AHE as a function of σ_{xx}: (i) ($\sigma_{xx} > 10^6$ $(\Omega\text{cm})^{-1}$) A high conductivity regime in which $\sigma_{xy}^{AH} \sim \sigma_{xx}$, skew scattering dominates σ_{xy}^{AH}, and the anomalous Hall angle σ_H/σ_{xx} is constant. In this regime however the normal Hall conductivity from the Lorentz force, proportional to $\sigma_{xx}^2 H$, is large even for the small magnetic field H used to align ferromagnetic domains and separating σ_{xy}^{AH} and σ_{xy}^{NH} is therefore challenging. (ii) (10^4 $(\Omega\text{cm})^{-1} < \sigma_{xx} < 10^6$ $(\Omega\text{cm})^{-1}$) An intrinsic or scattering-independent regime in which σ_{xy}^{AH} is roughly independent of σ_{xx}. In this intermediate metallic region, where the comparison between the experiments and band structure calculations have been discussed, the intrinsic mechanism is *assumed* to be dominant as mentioned above. The dominance of the intrinsic mechanism over side-jump is hinted at in some model calculations, but there is no firm understanding of the limits of this simplifying assumption. (iii) ($\sigma_{xx} < 10^4$ $(\Omega\text{cm})^{-1}$) A bad-metal regime in which σ_{xy}^{AH} decreases with decreasing σ_{xx} at a rate faster than linear. In this strong disorder region, a scaling $\sigma_H \propto \sigma_{xx}^n$ with $1.6 < n < 1.7$ has been reported experimentally for a variety of materials discussed in Sec.II. This scaling is primarily observed in insulating materials exhibiting variable range hopping transport and where σ_{xx} is tuned by varying T. The origin of this scaling is not yet understood and is a major challenge for AHE theory in the future. For metallic ultrathin thin films exhibiting this approximate scaling, it is natural that σ_H is suppressed by the strong disorder (excluding weak localization corrections). Simple considerations from the Kubo formula where the energy denominator includes a $(\hbar/\tau)^2$ is that $\sigma_H \propto \tau^{-2}$ when this broadening is larger than the energy splitting between bands due to the SOI. Since in this large broadening regime σ_{xx} is usually no longer linear in τ, an upper limit of $\beta = 2$ for the scaling relation $\sigma_H \propto \sigma_{xx}^\beta$ is expected. The numerical Keldysh studies of the ferromagnetic 2D Rashba model indicates that this power is $\beta \sim 1.6$, close to what is observed in the limited dirty-metallic range considered in the experiments. It is a surprising feature that this scaling seems to hold for both the metallic and insulating samples.

b. Future challenges and perspectives

In the classical Boltzmann transport theory, the resistivity or conductivity at the lowest temperature is simply related to the strength of the disorder. However, quantum interference of the scattered waves gives rise to a quantum correction to the conductivity and eventually leads to the Anderson localization depending on the dimensionality. At finite temperature, inelastic scattering by electron-electon and/or electron-phonon interactions give additional contributions to the resistivity, while suppressing localization effects through a reduction of the phase coherence length. In addition one needs to consider quantum correction due to the electron-electon in-

teraction in the presence of the disorder. These issues, revealed in the 80's, must be considered to scrutinize the microscopic mechanism of σ_{xx} or ρ_{xx} before studying the AHE. This means that it seems unlikely that only $\sigma_{xx}(T)$ characterizes the AHE at each temperature. We can define the Boltzmann transport σ^B_{xx} only when the residual resistivity is well defined at low temperature before the weak localization effect sets in. Therefore, we need to understand first the microscopic origin of the resistivity. Separating the resistivity into elastic and inelastic contributions via Mathhiessen's rule is the first step in this direction.

To advance understanding in this important issue, one needs to develop the theoretical understanding for the effect of inelastic scattering on AHE at finite temperature. This issue has been partly treated in the hopping theory of the AHE described in section II.B where phonon assisted hopping was assumed. However, the effects of inelastic scattering on the intrinsic and extrinsic mechanisms are not clear at the moment. Especially, spin fluctuation at finite T remains the most essential and difficult problem in the theory of magnetism, and usually the mean field approximation breaks down there. The approximate treatment in terms of the temperature dependent exchange splitting, *e.g.*, for $SrRuO_3$ (Sec. II.B), needs to be reexamined by more elaborated method such as the dynamical mean field theory, taking into account the quantum/thermal fluctuation of the ferromagnetic moments. These type of studies of the AHE may shed some light on the nature of the spin fluctuation in ferromagnets. Also the interplay between localization and the AHE should be pursued further in the intermediate and strong disorder regimes. These are all vital issues for quantum transport phenomena in solids in general, as well as for AHE specifically.

Admitting that more work needs to be done, in Fig. 44 we propose a speculative and schematic crossover diagram in the plane of diagonal conductivity σ_{xx} of the Boltzmann transport theory (corresponding to the disorder strength) and the temperature T. Note that a real system should move along the y-axis as temperature is changed, although the observed σ_{xx} changes with T. This phase diagram reflects the empirical fact that inelastic scattering kills off the extrinsic skew scattering contribution more effectively, leaving the intrinsic and side-jump contributions as dominant at finite temperature. We want to help stress that the aim of this figure is to promote further studies of the AHE and to identify the location of each region/system of interest. Of course, the generality of this diagram is not guaranteed and it is possible that the crossover boundaries and even the topology of the phase diagram might depend on the strength of the spin-orbit interaction and other details of the system.

There still remain many other issues to be studied in the future. First-principles band structure calculations for AHE are still limited to a few number of materials, and should be extended to many other ferromagnets. Especially, the heavy fermion systems are an important class of materials to be studied in detail. Concerning this point, a more economical numerical technique is now available (Marzari and Vanderbilt, 1997). This method employs the maximally localized Wannier functions, which can give the best tight-binding model parameters in an energy window of several tens of eV's near the Fermi level. The algorithm for the calculation of σ_{xy} in the Wannier interpolation scheme has also been developed (Wang *et al.*, 2006). Application of these newly developed methods to a large class of materials should be a high priority in the future.

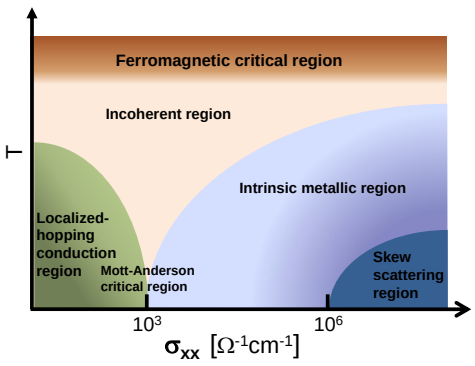


FIG. 44 A speculative and schematic phase diagram for the anomalous Hall effect in the plane of the diagonal conductivity σ_{xx} and the temperature T.

AHE in the dynamical regime is a related interesting problem. The magneto-optical effects such as the Kerr/Faraday rotation have been the standard experimental methods to detect the ferromagnetism. These techniques usually focus, however, on the high energy region such as the visible light. In this case, an atomic or local picture is usually sufficient to interpret the data, and the spectra are not directly connected to the d.c. AHE. Recent studies have revealed that the small energy scale comparable to the spin-orbit interaction is relevant to AHE which is typically $\sim$ 10 meV for 3d transition metal and $\sim$ 100 meV in DMSs (Sinova *et al.*, 2003). This means that the dynamical response, *i.e.*, $\sigma_{xy}(\omega)$, in the THz and infrared region will provide important information on the AHE.

A major challenge for experiments is to find examples of a quantized anomalous Hall effect. There are two candidates at present: (i) a ferromagnetic insulator with a band gap (Liu *et al.*, 2008), and (ii) a disorder induced Anderson insulator with a quantized Hall conductance (Onoda and Nagaosa, 2003). Although theoretically expected, it is an important issue to establish experimentally that the quantized Hall effect can be realized even without an external magentic field. Such a

finding would be the ultimate achievement in identifying an intrinsic AHE. The dissipationless nature of the anomalous Hall current will manifest itself in this quantized AHE; engineering systems using quantum wells or field effect transistors is a promising direction to realize this novel effect.

There are many promising directions for extensions of ideas developed through studies of the AHE. For example, one can consider several kinds of "current" instead of the charge current. An example is the thermal/heat current, which can be also induced in a similar fashion by the anomalous velocity. The thermoelectric effect has been discussed briefly in Sec. II.C, where combining all the measured thermoelectric transport coefficients helped settle the issue of the scaling relation $\sigma_{xy}^{AH} \sim \sigma_{xx}^2$ in metallic DMSs (Pu *et al.*, 2008). Recent studies in Fe alloys doped with Si and Co discussed in Sec. II.A followed a similar strategy (Shiomi *et al.*, 2009). From the temperature dependence of the Lorentz number, they identified the crossover between the intrinsic and extrinsic mechanisms. Further studies of thermal transport will shed some light on the essence of AHE from a different side.

Spin current is also a quantity of recent great interest. A direct generalization of AHE to the spin current is the spin Hall effect (Kato *et al.*, 2004; Murakami *et al.*, 2003; Sinova *et al.*, 2004; Wunderlich *et al.*, 2005), which can be regarded as the two copies of AHE for up and down spins with the opposite sign of σ_{xy}. In this effect, a spin current is produced perpendicular to the charge current. An interesting recent development in spin Hall effect is that the quantum spin Hall effect and topological insulators have been theoretically predicted and experimentally confirmed. We did not include this exciting new and still developing topic in this review article. Interested readers are referred to the original papers and references therein (Bernevig *et al.*, 2006; Kane and Mele, 2005; Koenig *et al.*, 2007).

Acknowledgements

We thank the following people for collaboration and useful discussion. A. Asamitsu, P. Bruno, D. Culcer, V. K. Dugaev, Z. Fang, J. Inoue, T. Jungwirth, M. Kawasaki, S. Murakami, Q. Niu, T. S. Nunner, K. Ohgushi, M. Onoda, Y. Onose, J. Shi, R. Shindou, N. A. Sinitsyn, N. Sugimoto, Y. Tokura, and J. Wunderlich. The work was supported by Grant-in-Aids (No. 15104006, No. 16076205, No. 17105002, No. 19048015, N0. 19048008) and NAREGI Nanoscience Project from the Ministry of Education, Culture, Sports, Science, and Technology of Japan. S. O. acknowledges partial support from Grants-in-Aid for Scientific Research under Grant No. 19840053 from the Japan Society of the Promotion of Science, and under Grant No. 20029006 and No. 20046016 from the MEXT of Japan. J. S. acknoledges partial support from ONR under Grant No. ONR-N000140610122, by NSF under Grant No. DMR-0547875, by SWAN-NRI, by the Cottrell Scholar grant of the Research Corporation. N. P. O. acknowledges partial support from a MRSEC grant from the U. S. National Science Foundation (DMR-0819860). AHM acknowledges support from the Welch Foundation and from the DOE.

References

Adams, E., and E. Blount, 1959, J. Phys. Chem. Solids **10**, 286.

Allen, P. B., H. Berger, O. Chauvet, L. Forro, T. Jarlborg, A. Junod, B. Revaz, and G. Santi, 1996, Phys. Rev. B **53**(8), 4393.

Allen, W., E. G. Gwinn, T. C. Kreutz, and A. C. Gossard, 2004, Phys. Rev. B **70**, 125320.

Baily, S. A., and M. B. Salamon, 2003, J. Appl. Phys. **93**, 8316.

Baily, S. A., and M. B. Salamon, 2005, Phys. Rev. B **71**(10), 104407.

Bastin, A., C. Lewinner, O. Betbeder-Matibet, and P. Nozières, 1971, J. Phys. Chem. Solids **32**, 1811.

Baym, G., and L. P. Kadanoff, 1961, Phys. Rev. **124**, 287.

Berciu, M., and R. N. Bhatt, 2001, Phys. Rev. Lett. **87**, 107203.

Berger, L., 1964, Physica **30**, 1141.

Berger, L., 1970, Phys. Rev. B **2**, 4559.

Bergmann, G., and F. Ye, 1991, Phys. Rev. Lett. **67**, 735.

Bernevig, B. A., T. L. Hughes, and S.-C. Zhang, 2006, Science **314**, 1757.

Berry, M. V., 1984, Proc. Roy. Soc. of London **392**, 45.

Block, T., M. J. Carey, B. A. Gurney, and O. Jepsen, 2004, Phys. Rev. B **70**, 205114.

Bohm, A., A. Mostafazadeh, H. Koizumi, Q. Niu, and J. Zwanziger, 2003, *The Geometric Phase in Quantum Systems* (Springer, Berlin, 2003).

Borunda, M., T. Nunner, T. Luck, N. Sinitsyn, C. Timm, J. Wunderlich, T. Jungwirth, A. H. MacDonald, and J. Sinova, 2007, Phys. Rev. Lett. **99**, 066604.

Burkov, A. A., and L. Balents, 2003, Phys. Rev. Lett. **91**, 057202.

Bychkov, Y. A., and E. I. Rashba, 1984, J. Phys. C **17**, 6039.

Chang, M., and Q. Niu, 1996, Phys. Rev. B. **53**, 7010.

Checkelsky, J. G., M. Lee, E. Morosan, R. J. Cava, and N. P. Ong, 2008, Phys. Rev. **B 77**, 014433.

Chun, S. H., Y. S. Kim, H. K. Choi, I. T. Jeong, W. O. Lee, K. S. Suh, Y. S. Oh, K. H. Kim, Z. G. Khim, J. C. Woo, and Y. D. Park, 2007, Phys. Rev. Lett. **98**, 026601.

Chun, S. H., M. B. Salamon, M. Jaime, R. Suryanarayanan, G. Dhalenne, and A. Revcolevschi, 2000, Physica B **284**, 1442.

Coleman, P., P. W. Anderson, and T. V. Ramakrishnan, 1985, Phys. Rev. Lett. **55**, 414.

Crépieux, A., and P. Bruno, 2001, Phys. Rev. B **64**, 014416.

Culcer, D., A. H. MacDonald, and Q. Niu, 2003, Phys. Rev. **B 68**, 045327.

Dietl, T., H. Ohno, and F. Matsukura, 2001, Phys. Rev. **B 63**, 195205.

Dugaev, V. K., P. Bruno, M. Taillefumier, B. Canals, and C. Lacroix, 2005, Phys. Rev. B **71**, 224423.

Dugaev, V. K., A. Crepieux, and P. Bruno, 2002, J. Mag. and Mag. Mat. **240**, 159.

Edmonds, K. W., K. Y. Wang, R. P. Campion, A. C. Neumann, C. T. Foxon, B. L. Gallagher, and P. C. Main, 2002, Appl. Phys. Lett **81**, 3010.
Fang, Z., N. Nagaosa, K. S. Tahakashi, A. Asamitsu, R. Mathieu, T. Ogasawara, H. Yamada, M. Kawasaki, Y. Tokura, and K. Terakura, 2003, Science **302**, 92.
Feng, J. S.-Y., R. D. Pahsley, and M.-A. Nicolet, 1975, J. Phys. C **8**, 1010.
Fernandez-Pacheco, A., J. M. De Teresa, J. Orna, L. Morellon, P. A. Algarabel, J. A. Pardo, and M. R. Ibarra, 2008, Phys. Rev. B **77**, 004.
Fert, A., A. Friederich, and A. Hamzic, 1981, J. Mag. and Mag. Mat. **24**(3), 231.
Fert, A., and O. Jaoul, 1972, Phys. Rev. Lett. **28**(5), 303.
Fert, A., and P. M. Levy, 1987, Phys. Rev. B **36**(4), 1907.
Fivaz, R. C., 1969, Phys. Rev. **183**, 586.
Fukuyama, H., 1980, J. Phys. Soc. Jap. **49**(2), 644.
Galanakis, I., P. H. Dederichs, and N. Papanikolaou, 2002, Phys. Rev. B **66**, 174429.
Guo, G. Y., and H. Ebert, 1995, Phys. Rev. B. **51**, 12633.
Hadzicleroux, M., A. Hamzic, A. Fert, P. Haen, F. Lapierre, and O. Laborde, 1986, Europhysics Lett. **1**(11), 579.
Haldane, F. D. M., 1988, Phys. Rev. Lett. **61**, 2015.
Haldane, F. D. M., 2004, Phys. Rev. Lett. **93**, 206602.
Hall, E., 1881, Phil. Mag. **12**, 157.
Hall, E. H., 1879, Amer. J. Math. **2**, 287.
Haug, H., and A.-P. Jauho, 1996, *Quantum Kinetics in Transport and Optics of Semiconductors* (Springer, Berlin).
Hewson, A. C., 1993, *The Kondo Problem to Heavy Fermions.* (Cambridge University Press, Cambridge).
Hofstadter, D. R., 1976, Phys. Rev. B **14**(6), 2239.
Holstein, T., 1961, Phys. Rev. **124**(5), 1329.
Hurd, C. M., 1972, *The Hall Effect in Metals and Alloys* (Plenum Press, New York).
Husmann, A., and L. J. Singh, 2006, Phys. Rev. B **73**, 724.
Inoue, J., T. Kato, Y. Ishikawa, H. Itoh, G. E. W. Bauer, and L. W. Molenkamp, 2006, Phys. Rev. Lett. **97**, 046604.
Izumi, M., K. Nakazawa, Y. Bando, Y. Yoneda, and H. Terauchi, 1997, J. Phys. Soc. Jap. **66**, 3893.
Jackiw, R., 1984, Phys. Rev. D **29**, 2375.
Jan, J.-P., 1952, Helv. Phys. Acta **25**, 677.
Jan, J.-P., and J. M. Gijsman, 1952, Physica **18**, 339.
Jones, R. O., and O. Gunnarsson, 1989, Rev. Mod. Phys. **61**, 689.
Jungwirth, T., M. Abolfath, J. Sinova, J. Kučera, and A. H. MacDonald, 2002a, Appl. Phys. Lett. **81**, 4029.
Jungwirth, T., Q. Niu, and A. H. MacDonald, 2002b, Phys. Rev. Lett. **88**, 207208.
Jungwirth, T., J. Sinova, J. Mašek, J. Kučera, and A. H. MacDonald, 2006, Rev. Mod. Phys. **78**, 809.
Jungwirth, T., J. Sinova, K. Y. Wang, K. W. Edmonds, R. P. Campion, B. L. Gallagher, C. T. Foxon, Q. Niu, and A. H. MacDonald, 2003, Appl. Phys. Lett. **83**, 320.
Kadanoff, L. P., and G. Baym, 1962, *Quantum Statistical Mechanics* (Benjamin, Menlo Park).
Kane, C. L., and E. J. Mele, 2005, Phys. Rev. Lett. **95**, 226801.
Karplus, R., and J. M. Luttinger, 1954, Phys. Rev. **95**, 1154.
Kato, T., Y. Ishikawa, H. Itoh, and J. Inoue, 2007, New J. Phys. **9**, 50.
Kato, Y. K., R. C. Myers, A. C. Gossard, and D. D. Awschalom, 2004, Science **306**, 1910.
Kats, Y., I. Genish, L. Klein, J. W. Reiner, and M. R. Beasley, 2004, Phys. Rev. B **70**, 8040.
Katsufuji, T., H. Y. Hwang, and S. W. Cheong, 2000, Phys. Rev. Lett. **84**, 1998.
Kawamura, H., 2007, J. Mag. and Mag. Mat. **310**, 1487.
Keldysh, L. V., 1965, Sov. Phys. JETP **20**, 1018, [Zh. Eksp. Teor. Fiz. **47**, 1515 (1964).].
Kezsmarki, I., S. Onoda, Y. Taguchi, T. Ogasawara, M. Matsubara, S. Iguchi, N. Hanasaki, N. Nagaosa, and Y. Tokura, 2005, Phys. Rev. B **72**, 094427.
Koenig, M., S. Wiedmann, C. Bruene, A. Roth, H. Buhmann, L. W. Molenkamp, X.-L. Qi, and S.-C. Zhang, 2007, Science **318**, 766.
Kohmoto, M., 1985, Ann. Phys. **160**, 343.
Kohn, W., and J. M. Luttinger, 1957, Phys. Rev. **108**, 590.
Kondo, J., 1962, Prog. Theor. Phys. **27**, 772.
Kontani, H., T. Tanaka, and K. Yamada, 2007, Phys. Rev. B **75**, 184416.
Kooi, C., 1954, Phys. Rev. **95**, 843.
Kovalev, A. A., Y. Tserkovnyak, K. Vyborny, and J. Sinova, 2009, unpublished.
Kovalev, A. A., K. Vyborny, and J. Sinova, 2008, Phys. Rev. B **78**, 41305.
Kubo, R., 1957, J. Phys. Soc. Jpn **12**, 570.
Kundt, A., 1893, Wied. Ann. **49**, 257.
Landau, L. D., E. M. Lifshitz, and L. P. Pitaevskii, 1984, *Electrodynamics of Continuous Media* (Oxford), 2nd edition.
Langenfeld, A., and P. Wolfle, 1991, Phys. Rev. Lett. **67**(6), 739.
Lapierre, F., P. Haen, R. Briggs, A. Hamzic, A. Fert, and J. P. Kappler, 1987, J. Mag. and Mag. Mat. **63-4**, 338.
Lavine, J. M., 1961, Phys. Rev. **123**, 1273.
Lee, M., W. Kang, Y. Onose, Y. Tokura, and N. P. Ong, 2008, eprint arXiv:0811.3146.
Lee, M., Y. Onose, Y. Tokura, and N. Ong, 2007, Phys. Rev. B **75**, 172403.
Lee, P. A., N. Nagaosa, and X. G. Wen, 2006, Reviews of Modern Physics **78**(1), 17.
Lee, P. A., and T. V. Ramakrishnan, 1985, Reviews of Modern Physics **57**(2), 287.
Lee, W.-L., S. Watauchi, V. L. Miller, R. J. Cava, and N. P. Ong, 2004, Science **303**, 1647.
Leroux-Hugon, P., and A. Ghazali, 1972, J. Phys. C: Solid State Phys. **5**, 1072.
Liu, C.-X., X.-L. Qi, X. Dai, Z. Fang, and S.-C. Zhang, 2008, Phys. Rev. Lett. **101**, 468.
Luttinger, J. M., 1958, Phys. Rev. **112**, 739.
Luttinger, J. M., and W. Kohn, 1955, Phys. Rev. **97**, 869.
Luttinger, J. M., and W. Kohn, 1958, Phys. Rev. **109**, 1892.
Lyanda-Geller, Y., S. Chun, M. Salamon, P. Goldbart, P. Han, Y. Tomioka, A. Asamitsu, and Y. Tokura, 2001, Phys. Rev. B **63**, 184426.
Lyo, S. K., 1973, Phys. Rev. B **8**, 1185.
MacDonald, A. H., and Q. Niu, 2004, Physics World **53**, 18.
Machida, Y., S. Nakatsuji, Y. Maeno, T. Tayama, and T. Sakakibara, 2007a, J. Mag. and Mag. Mat. **310**, 1079.
Machida, Y., S. Nakatsuji, Y. Maeno, T. Tayama, T. Sakakibara, and S. Onoda, 2007b, Phys. Rev. Lett. **98**, 5720.
MacKinnon, A., and B. Kramer, 1983, Z. Physik. B. **53**, 1.
Mahan, G. D., 1990, *Many-Particle Physics* (Plenum Press, New York), pp. 671–686.
Mainkar, N., D. A. Browne, and J. Callaway, 1996, Phys. Rev. B. **53**, 3692.
Majumdar, A., and L. Berger, 1973, Phys. Rev. B **7**, 4203.
Manyala, N., Y. Sidis, J. F. Ditusa, G. Aeppli, D. P. Young,

and Z. Fisk, 2004, Nature Materials **3**, 255.
Maranzana, F. E., 1967, Phys. Rev. **160**, 421.
Marder, M. P., 2000, *Condensed Matter Physics* (Wiley, New York), eprint Supplementary material by author.
Marzari, N., and D. Vanderbilt, 1997, Phys. Rev. B **56**, 12847.
Mathieu, R., A. Asamitsu, K. Takahashi, H. Yamada, M. Kawasaki, Z. Fang, N. Nagaosa, and Y. Tokura, 2004a, J. Mag. and Mag. Mat. **272**, E785.
Mathieu, R., A. Asamitsu, H. Yamada, K. S. Takahashi, M. Kawasaki, Z. Fang, N. Nagaosa, and Y. Tokura, 2004b, Phys. Rev. Lett. **93**, 1660.
Matl, P., N. P. Ong, Y. F. Yan, Y. Q. Li, D. Studebaker, T. Baum, and G. Doubinina, 1998, Phys. Rev. B **57**, 10248.
Mitra, P., R. Mitra, A. F. Hebard, K. A. Muttalib, and P. Wölfle, 2007, Phys. Rev. Lett. **99**, 046804.
Miyasato, T., N. Abe, T. Fujii, A. Asamitsu, S. Onoda, Y. Onose, N. Nagaosa, and Y. Tokura, 2007, Phys. Rev. Lett. **99**, 086602.
Morosan, E., H. W. Zandbergen, L. Li, M. Lee, J. G. Checkelsky, M. Heinrich, T. Siegrist, N. P. Ong, and R. J. Cava, 2007, Phys. Rev. B **75**, 104401.
Moyal, J. E., 1949, Proc. Cambridge Philos. Soc. **45**, 99.
Murakami, S., N. Nagaosa, and S. C. Zhang, 2003, Science **301**, 1348.
Nagaosa, N., 2006, J. Phys. Soc. Jap. **75**, 420.
Nozieres, P., and C. Lewiner, 1973, J. Phys. (Paris) **34**, 901.
Nunner, T. S., N. A. Sinitsyn, M. F. Borunda, V. K. Dugaev, A. A. Kovalev, A. Abanov, C. Timm, T. Jungwirth, J.-i. Inoue, A. H. MacDonald, and J. Sinova, 2007, Phys. Rev. B **76**, 235312.
Nunner, T. S., G. Zarand, and F. von Oppen, 2008, Phys. Rev. Lett. **100**, 36602.
Oda, K., S. Yoshii, Y. Yasui, M. Ito, T. Ido, Y. Ohno, Y. Kobayashi, and M. Sato, 2001, J. Phys. Soc. Jap. **70**, 2999.
Ohgushi, K., S. Murakami, and N. Nagaosa, 2000, Phys. Rev. B **62**, 6065.
Ohno, H., H. Munekata, T. Penney, S. von Molmar, and L. L. Chang, 1992, Phys. Rev. Lett. **68**, 2664.
Ong, N. P., and W.-L. Lee, 2006, in *Foundations of quantum mechanics in the light of new technology (ISQM Tokyo 2005)*, edited by S. Ishioka and K. Fujikawa (World Scientific), p. 121, eprint arXiv:cond-mat/0508236.
Onoda, M., and N. Nagaosa, 2002, J. Phys. Soc. Jpn. **71**, 19.
Onoda, M., and N. Nagaosa, 2003, Phys. Rev. Lett. **90**, 0660.
Onoda, S., and N. Nagaosa, 2003, Phys. Rev. Lett. **90**, 196602.
Onoda, S., N. Sugimoto, and N. Nagaosa, 2006a, Phys. Rev. Lett. **97**, 126602.
Onoda, S., N. Sugimoto, and N. Nagaosa, 2006b, Prog. Theor. Phys. **116**, 61.
Onoda, S., N. Sugimoto, and N. Nagaosa, 2008, Phys. Rev. B **77**, 165103.
Onose, Y., and Y. Tokura, 2006, Phys. Rev. B **73**, 7442.
Parkin, S. S. P., and R. H. Friend, 1980, Philos. Mag. **41**, 65.
Pfleiderer, C., D. Reznik, L. Pintschovius, H. v. Lohneysen, M. Garst, and A. Rosch, 2004, Nature **427**, 227.
Prange, R. E., and S. M. Girvin (eds.), 1987, *The Quantum Hall Effect* (Springer, Berlin).
Pu, Y., D. Chiba, F. Matsukura, H. Ohno, and J. Shi, 2008, Phys. Rev. Lett. **101**, 172.
Pugh, E. M., 1930, Phys. Rev. **36**, 1503.
Pugh, E. M., and T. W. Lippert, 1932, Phys. Rev. **42**, 709.
Pugh, E. M., and N. Rostoker, 1953, Rev. Mod. Phys. **25**, 151.
Ramaneti, R., J. C. Lodder, and R. Jansen, 2007, Appl. Phys. Lett. **91**, 012502.
Rammer, J., and H. Smith, 1986, Rev. Mod. Phys. **58**, 323.
Ruzmetov, D., J. Scherschligt, D. V. Baxter, T. Wojtowicz, X. Liu, Y. Sasaki, J. K. Furdyna, K. M. Yu, and W. Walukiewicz, 2004, Phys. Rev. **B 69**, 155207.
Samoilov, A. V., G. Beach, C. C. Fu, N. C. Yeh, and R. P. Vasquez, 1998, Phys. Rev. B **57**(22), 14032.
Sangiao, S., L. Morellon, G. Simon, J. M. D. Teresa, J. A. Pardo, J. Arbiol, and M. R. Ibarra, 2009, Phys. Rev. B **79**, 014431.
Schad, R., P. Belien, G. Verbanck, V. V. Moshchalkov, and Y. Bruynseraede, 1998, J. Phys.-Cond. Matt. **10**, 6643.
Schliemann, J., and A. H. MacDonald, 2002, Phys. Rev. Lett. **88**, 137201.
Shen, S., X. Liu, Z. Ge, J. K. Furdyna, M. Dobrowolska, and J. Jaroszynski, 2008, J. Appl. Phys. **103**, 7D13.
Shiomi, Y., Y. Onose, and Y. Tokura, 2009, Phys. Rev. B **79**, 100404, and unpublished data.
Sinitsyn, N. A., 2008, J. Phys.: Condens. Matter **20**, 023201.
Sinitsyn, N. A., A. H. MacDonald, T. Jungwirth, V. K. Dugaev, and J. Sinova, 2007, Phys. Rev. B **75**, 045315.
Sinitsyn, N. A., Q. Niu, and A. H. MacDonald, 2006, Phys. Rev. B **73**, 075318.
Sinitsyn, N. A., Q. Niu, J. Sinova, and K. Nomura, 2005, Phys. Rev. **B 72**, 045346.
Sinova, J., D. Culcer, Q. Niu, N. A. Sinitsyn, T. Jungwirth, and A. H. MacDonald, 2004, Phys. Rev. Lett. **92**, 126603.
Sinova, J., and T. Jungwirth, 2005, in *Frontiers in magnetic materials*, edited by A. V. Narlikar (Springer-Verlag Berlin), p. 185.
Sinova, J., T. Jungwirth, and J. Černe, 2004, Int. J. Mod. Phys. **B 18**, 1083.
Sinova, J., T. Jungwirth, J. Kucera, and A. H. MacDonald, 2003, Phys. Rev. B **67**, 352.
Sinova, J., T. Jungwirth, S. Yang, J. Kucera, and A. H. MacDonald, 2002, Phys. Rev. B **66**, 412.
Smit, J., 1955, Physica **21**, 877.
Smit, J., 1958, Physica **24**, 39.
Smith, A. W., and R. W. Sears, 1929, Phys. Rev. **34**, 1466.
Smrčka, L., and P. Středa, 1977, J. Phys. C: Solid State Phys. **10**, 2153.
Sondhi, S. L., A. Karlhede, S. A. Kivelson, and E. H. Rezayi, 1993, Phys. Rev. B **47**, 16419.
Středa, P., 1982, J. Phys. C: Solid State Phys. **15**, L717.
Sugimoto, N., S. Onoda, and N. Nagaosa, 2007, Prog. Theor. Phys. **117**, 415.
Sundaram, G., and Q. Niu, 1999, Phys. Rev. B **59**, 14915.
Taguchi, Y., Y. Oohara, H. Yoshizawa, N. Nagaosa, T. Sasaki, S. Awaji, Y. Iwasa, T. Tayama, T. Sakakibara, S. Iguchi, K. Ohgushi, T. Ito, *et al.*, 2004, J. Phys.-Cond. Matt. **16**, S599.
Taguchi, Y., Y. Oohara, H. Yoshizawa, N. Nagaosa, and Y. Tokura, 2001, Science **291**, 2573.
Taguchi, Y., T. Sasaki, S. Awaji, Y. Iwasa, T. Tayama, T. Sakakibara, S. Iguchi, T. Ito, and Y. Tokura, 2003, Phys. Rev. Lett. **90**, 257202.
Tatara, G., and H. Kawamura, 2002, J. Phys. Soc. Jpn. **71**, 2613.
Thouless, D. J., M. Kohmoto, M. P. Nightingale, and M. den Nijs, 1982, Phys. Rev. Lett. **49**, 405.
Tokura, Y., and T. Tomioka, 1999, J. Mag. and Mag. Mat. **200**(1-3), 1.

Ueno, K., T. Fukumura, H. Toyosaki, M. Nakano, and M. Kawasaki, 2007, Appl. Phys. Lett. **90**, 072103.

Ueno, K., T. Fukumura, H. Toyosaki, M. Nakano, T. Yamasaki, Y. Yamada, and M. Kawasaki, 2008, J. Appl. Phys. **103**, 7D1.

Venkateshvaran, D., W. Kaiser, A. Boger, M. Althammer, M. S. R. Rao, S. T. B. Goennenwein, M. Opel, and R. Gross, 2008, Phys. Rev. B **78**, 092405.

Wang, X., D. Vanderbilt, J. R. Yates, and I. Souza, 2007, Phys. Rev. B **76**, 195109.

Wang, X., J. R. Yates, I. Souza, and D. Vanderbilt, 2006, Phys. Rev. B **74**, 195118.

Webster, W. L., 1925, Proc. Cambridge Phil. Soc. **23**, 800.

Woelfle, P., and K. A. Muttalib, 2006, Ann. Der Phys. **15**, 508.

Wunderlich, J., B. Kaestner, J. Sinova, and T. Jungwirth, 2005, Phys. Rev. Lett. **94**, 472.

Xiao, D., and Q. Niu, 2009, review in progress to be submitted to Rev. Mod. Phys.

Yanagihara, H., and M. B. Salamon, 2002, Phys. Rev. Lett. **89**, 8720.

Yanagihara, H., and M. B. Salamon, 2007, J. Phys.-Cond. Matt. **19**, 1520.

Yang, S. R. E., J. Sinova, T. Jungwirth, Y. P. Shim, and A. H. MacDonald, 2003, Phys. Rev. **B 67**, 045205.

Yao, Y., L. Kleinman, A. H. MacDonald, J. Sinova, T. Jungwirth, D.-S. Wang, E. Wang, and Q. Niu, 2004, Phys. Rev. Lett. **92**, 037204.

Yao, Y. G., Y. Liang, D. Xiao, Q. Niu, S. Q. Shen, X. Dai, and Z. Fang, 2007, Phys. Rev. B **75**, 020401(R).

Yasui, Y., T. Kageyama, T. Moyoshi, M. Soda, M. Sato, and K. Kakurai, 2006, J. Phys. Soc. Jpn. **75**, 084711.

Yasui, Y., T. Kageyama, T. Moyoshi, M. Soda, M. Sato, and K. Kakurai, 2007, J. Mag. and Mag. Mat. **310**, E544.

Ye, J., Y. B. Kim, A. J. Millis, B. I. Shraiman, P. Majumdar, and Z. Tešanović, 1999, Phys. Rev. Lett. **83**, 3737.

Yoshii, S., S. Iikubo, T. Kageyama, K. Oda, Y. Kondo, K. Murata, and M. Sato, 2000, J. Phys. Soc. Jpn. **69**, 3777.

Zeng, C., Y. Yao, Q. Niu, and H. H. Weitering, 2006, Phys. Rev. Lett. **96**, 037204.

Ziman, J. M., 1967, Adv. in Phys. **16**, 551.